Ref
#3424

Natural Convection in Active and Passive Solar Thermal Systems

REN ANDERSON AND FRANK KREITH

Solar Energy Research Institute, Golden, Colorado 80401

I. Introduction

Recently, architects have successfully built many types of solar-heated buildings, and the solar industry has produced many thousands of reliable and efficient flat-plate collectors (FPCs). In addition, several new types of collectors have been introduced such as the compound parabolic collector (CPC) and the single-axis tracking parabolic trough collector (TPT). Furthermore, central solar receiver power plants with external as well as cavity-type receivers have been placed into operation and their performance has been monitored. In all of these solar thermal systems, natural convection heat transfer occurs. As a result, a large amount of natural convection heat transfer research has been motivated by solar-related applications. The objective of this monograph is to provide a review of those aspects of natural convection research that are applicable to solar system design and analysis. Solar ponds are not included because their convection phenomena are double diffusive and require a different kind of analysis. Double diffusive phenomena have recently been reviewed by Chen and Johnson [1] and Viskanta, Bergman, and Incropera [2].

A. Collector Types and Operating Temperatures

Solar collectors are generally categorized as "active" or "passive." Active collectors depend upon the use of external pumps or fans in order to function properly. Passive collectors depend entirely upon natural convection to transport energy from the point of collection to the point of use.

There are three basic types of thermal collectors [3]:

1. Nonconcentrating and stationary (solar buildings, active and passive flat-plate collectors, and solar ponds) for low temperatures.
2. Slightly concentrating, with or without periodic adjustments (CPCs and V-troughs) for intermediate temperatures.
3. Concentrating, with either one- or two-axis tracking for intermediate and high temperatures.

Figure 1 shows schematic diagrams of the most common types of active solar-thermal collectors. Figure 2 shows the approximate operating tem-

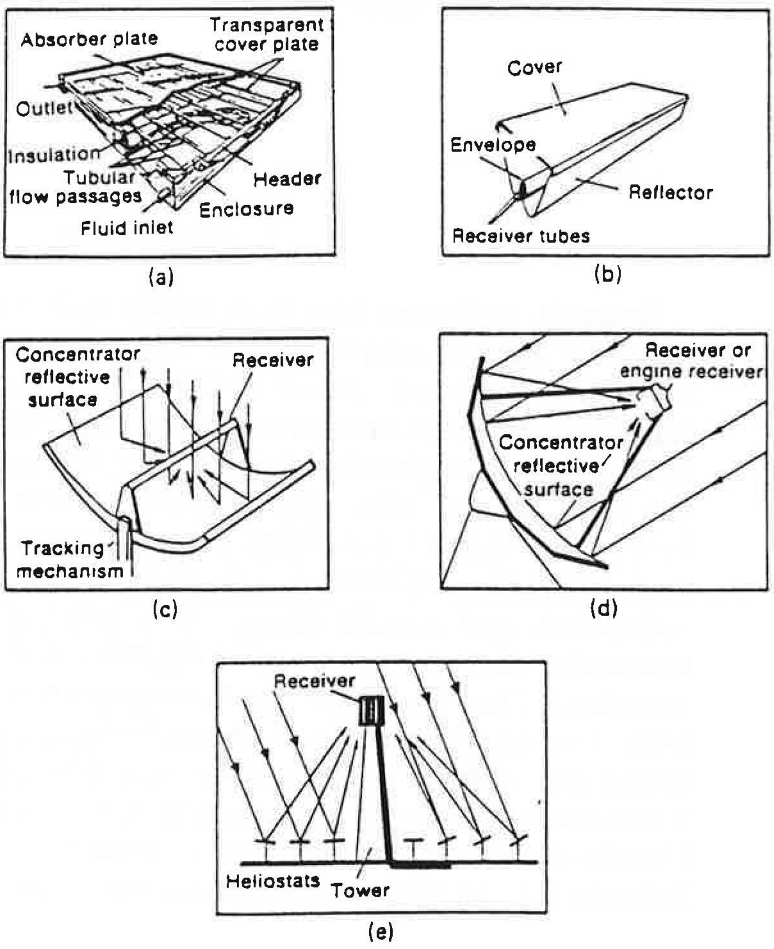

FIG. 1. Schematic diagrams of common types of active solar thermal collectors: (a) flat plate-statinary (b) compound parabolic collector (CPC), (c) single-axis-tracking parabolic trough, (d) dual-axis-tracking, paraboloid dish, (e) central receiver system with dual-axis-tracking heliostats.

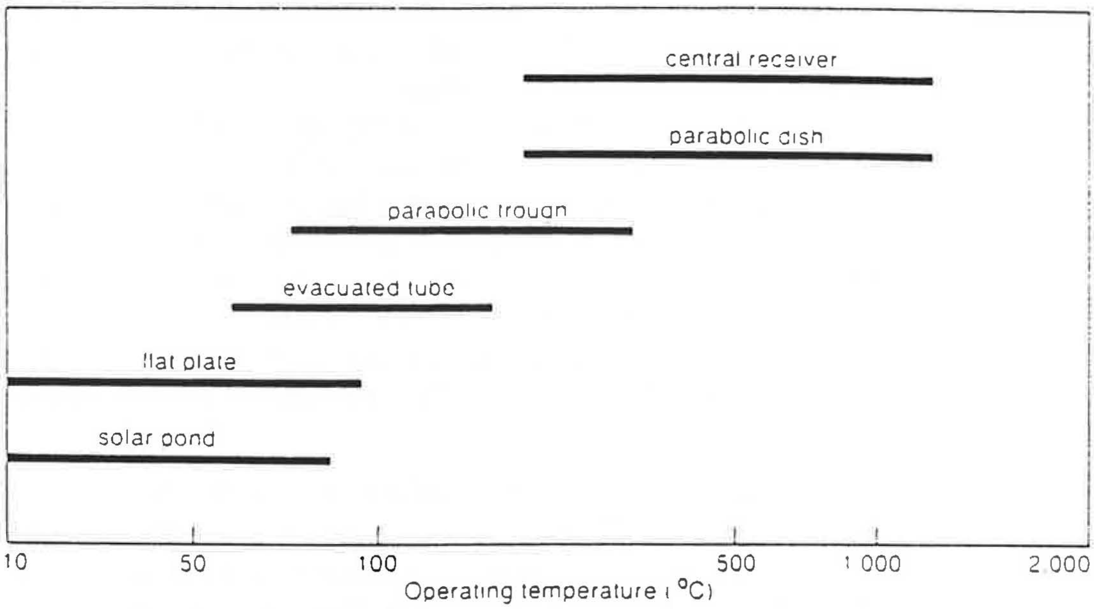

FIG. 2. Approximate operating temperatures of active solar collectors.

perature ranges for each type of active collector [4]. Flat-plate collectors are suitable for supplying hot water or hot air at temperatures up to 80°C with relatively good efficiency. They require no moving parts, have good durability, and can collect both direct and diffuse radiation. The key elements for a flat-plate collector are a frame, one or two transparent covers, a receiver or "absorber" plate with flow channels connected to inlet and outlet headers through which a working fluid passes, and some back-side insulation. The cover, usually of glass or a plastic, is transparent to solar radiation but opaque to infrared radiation from the receiver plate. Thus, the receiver plate absorbs solar radiation, heats up, and transfers heat to the working fluid, usually water or air. One of the most cost-effective applications of flat-plate collectors is domestic hot water heating.

To heat a fluid to temperatures above 80°C with good efficiency, solar energy must be concentrated on the receiver. The concentration ratio C is defined as [5]

$$C = A_a/A_r \tag{1}$$

where A_a is the aperture area and A_r is the receiver area.

Concentration reduces the size and surface area of the solar receiver and, therefore, reduces the heat losses, which are proportional to the surface area. The reduction in heat losses contributes to higher temperature capability. Concentration can be achieved by refraction or reflection, but reflection is used in most solar applications. Compound parabolic concentrators (CPC) can concentrate without tracking and utilize the beam as well as the diffuse radiation within the acceptance angle of the collector. They can achieve a concentration ratio of about two without adjustment and up to five with periodic tilt adjustment [5].

Tracking increases the complexity of the collector system and limits collection to the beam part of solar radiation. Line-focus collectors that track the sun in one direction can achieve concentration ratios of the order of 50 and deliver temperatures up to about 350°C. To heat a fluid to temperatures above 350°C with good efficiency requires a concentration ratio of 200 or more. Such a concentration ratio can only be achieved by means of dual-axis (azimuth and altitude) tracking of the sun by point-focus receiver systems. Basically two designs are available for high solar concentrations:

1. Central receiver systems (CRS) in which radiation is reflected from tracking mirrors (heliostats) onto a stationary receiver that can have the configuration of a cylinder with vertical flow tubes (external type) or a cavity lined with flow tubes (cavity type) as shown in Fig. 3.

2. Dual-axis-tracking paraboloid dish systems (PDS) with point-focus receivers in which the reflector as well as the receiver move to track the sun;

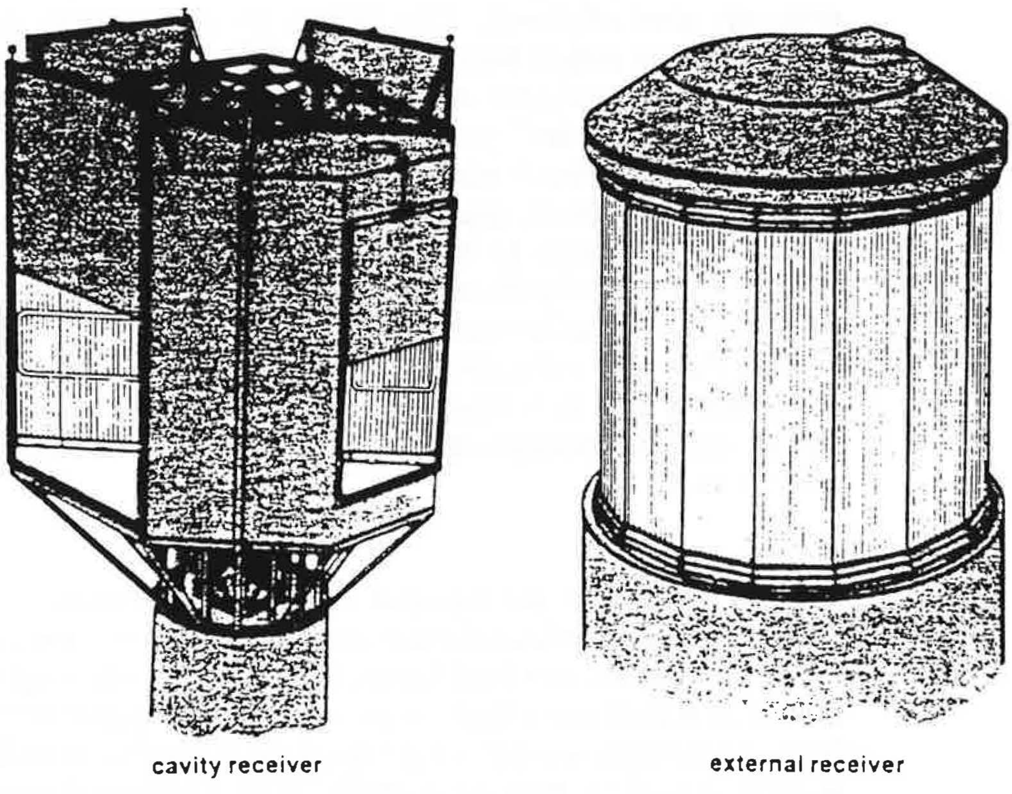

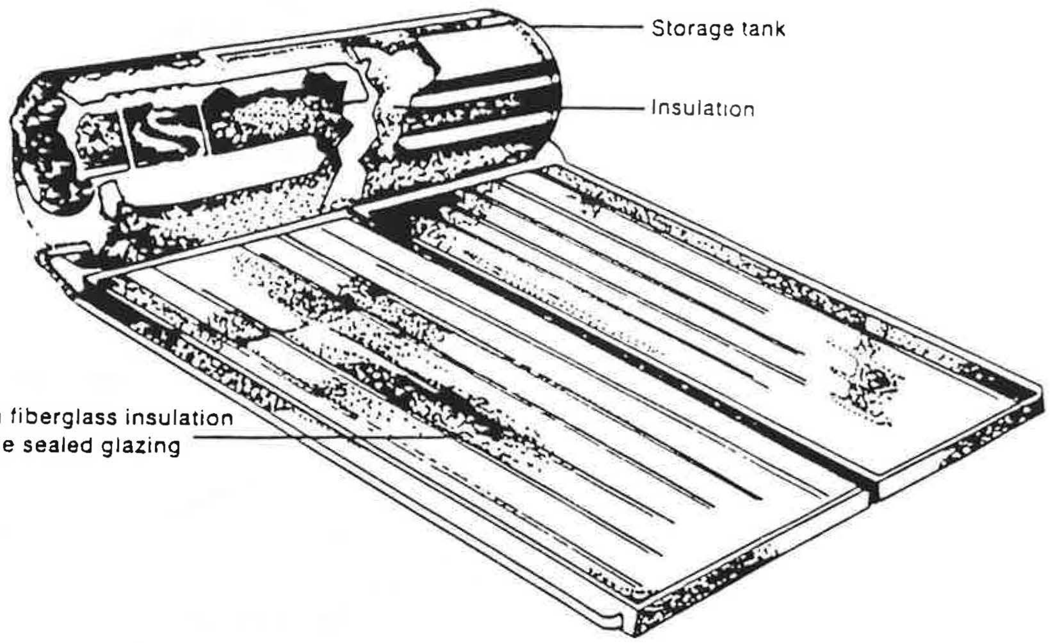

FIG. 4. Schematic diagram of a flat-plate thermosiphon collector.

Collectors for passive solar thermal applications range from small flat-plate thermosiphon units (Fig. 4) to various types of solar building components. The most common types of solar building components are the Trombe wall, the atrium or sunspace, and direct gain windows. Solar buildings can also incorporate vents or windows for ventilation cooling. In a solar building, natural convection is the major heat distribution mechanism between building zones.

From an examination of the diagrams of the main types of solar buildings in Fig. 5, it is apparent that their geometries and thermal boundary conditions can vary widely. In addition, buildings often are complicated by the presence of furniture, draperies, and nonrectangular wall intersections.

The enclosure aspect ratio (room height/room length) in building applications can be large or small. The Trombe wall is a large aspect ratio configuration with parallel flat plates in a vertical position. Other types of solar building configurations (sunspace, direct gain) have aspect ratios close to one.

The Rayleigh numbers in building applications are on the order of 1×10^{10}, indicating that the natural convection flow next to heated and cooled surfaces will have a boundary-layer structure. Depending upon the specific application, this natural convection flow may be laminar, partially turbulent, or fully turbulent. Because of the complexity of the problem, it is important to carefully integrate results from laboratory experiments with results from measurements in full-scale buildings. This integration process

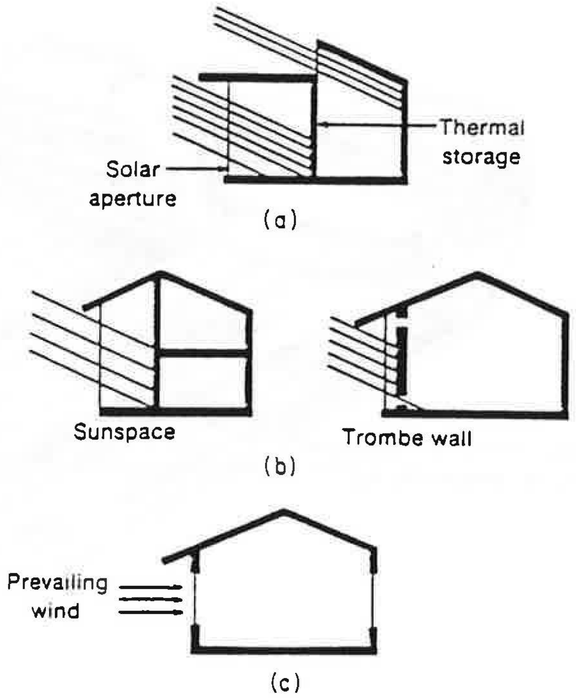

FIG. 5. Schematic diagrams of various types of passive heated and cooled solar buildings: (a) direct gain, (b) indirect gain, (c) ventilation cooling.

is summarized in Table I. Results gained from laboratory research must be reduced to reliable design information before they become useful tools to builders and architects.

B. EFFICIENCY AND OVERALL HEAT-LOSS COEFFICIENTS OF ACTIVE COLLECTORS

The useful heat output q_u of a thermal collector using a liquid or gaseous working fluid is proportional to the rate of increase of the temperature of the working fluid [3]:

$$q_u = \dot{m}c_p(T_{out} - T_{in}) \tag{2}$$

where $\dot{m}$ is the working fluid mass flow rate through the collector, c_p is the specific heat at constant pressure, T_{in} is the inlet temperature of the working fluid, and T_{out} is the outlet temperature.

It should be noted that the heat transferred to the working fluid in the collector does not equal the useful energy delivered by the solar system. Heat losses from connecting pipes and valves and transient effects at start-up in the morning and after insolation has been interrupted by clouds decrease system heat delivery [4].

The instantaneous thermal efficiency η for a thermal collector is given by the relation [3]

$$\eta = q_u/A_a I_c = \eta_o - U(T_H - T_{amb})/I_c C \tag{3}$$

where η_o is the optical efficiency, T_H the average receiver surface temperature in degrees Kelvin, T_{amb} the ambient temperature in degrees Kelvin, U the total heat-transfer (or thermal loss) coefficient between the collector surface and the surrounding in watts per square meter per degree Kelvin, based on the receiver area A_r and average surface temperature T_r, and I_c the solar irradiance (or insolation) on the collector aperture area in watts per square meter.

The insolation I_c comprises different elements of the solar radiation, depending on the type of solar collector [5].

1. For flat-plate collectors, I_c is the total hemispherical irradiation, $I_b + I_d$.
2. For tracking collectors with low concentration ($C < 10$), I_c is the radiation within the acceptance angle $[I_b + (I_d/C)]$.
3. For tracking collectors with high concentration ($C > 10$), I_c is the solar beam radiation I_b.

Here I_d is the diffuse insolation and I_b is the solar beam radiation.

TABLE I

INTEGRATION OF LABORATORY-SCALE AND FULL-SCALE RESEARCH RESULTS

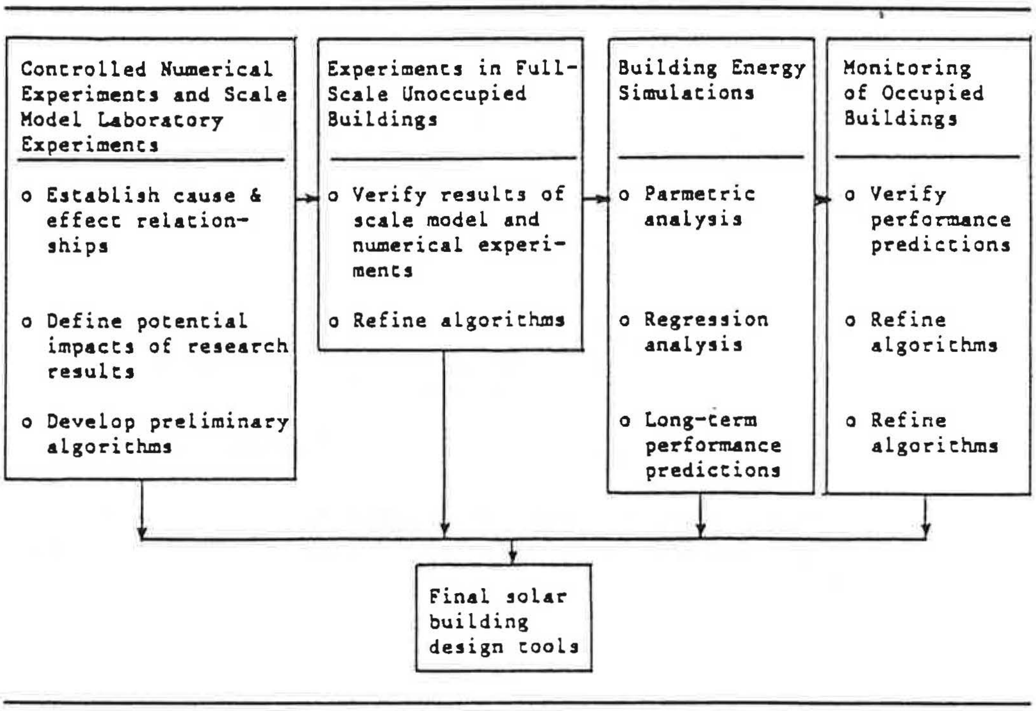

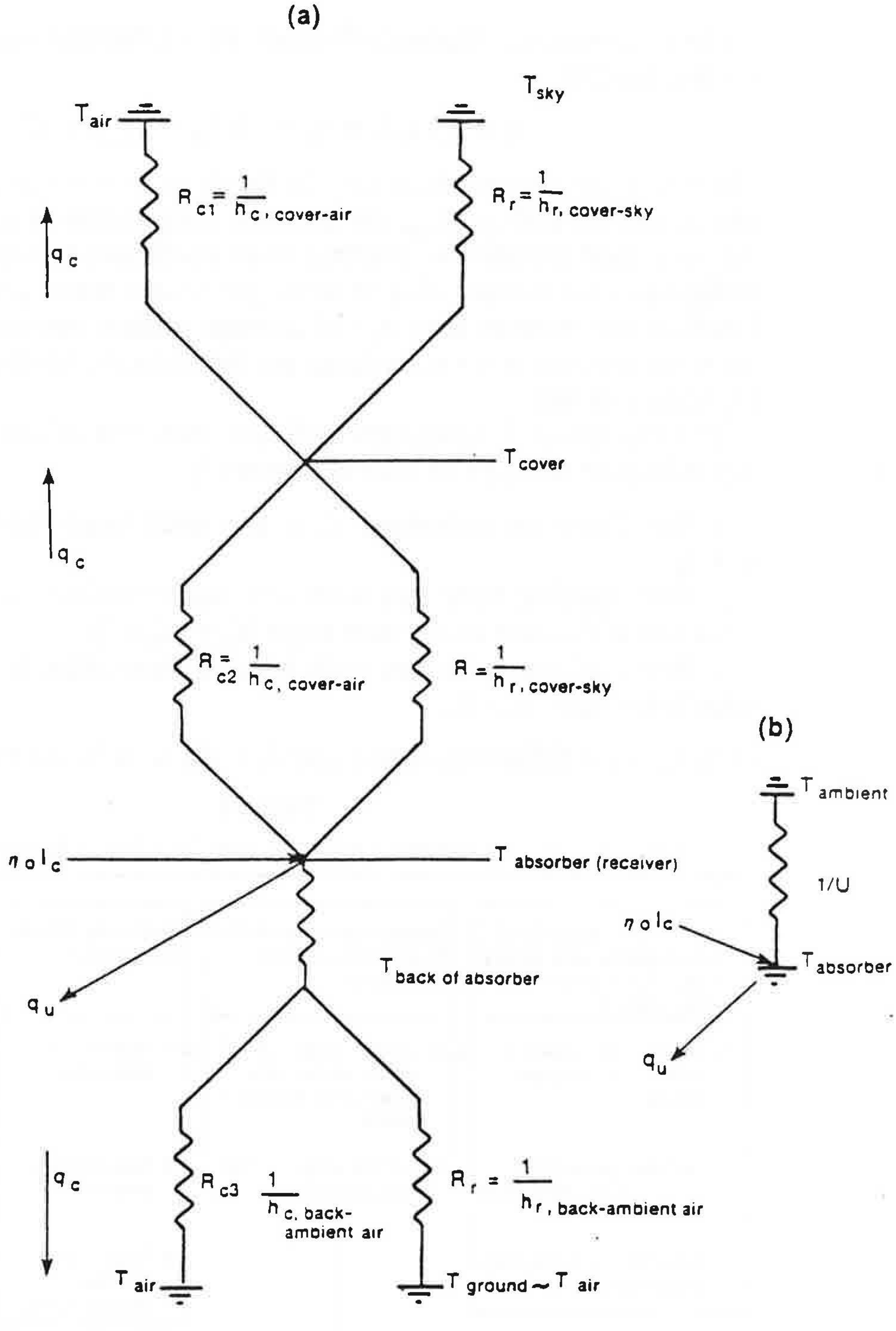

FIG. 6. Thermal network for the overall heat-loss coefficient U, from a receiver with a single transparent cover. (a) Detailed network for convection and radiation. (b) Simplified network.

The efficiency analysis, Eq. (3), shows that the three most important factors affecting the efficiency of solar thermal conversion for a given temperature output and insolation are the concentration ratio, the optical efficiency, and the overall heat-loss coefficient of the absorber. Of these three, the overall heat-loss coefficient is critically dependent upon natural convection phenomena.

The overall heat-loss coefficient is a simplified concept since the heat loss from a solar absorber occurs by complex interactions between radiation and convection. Figure 6a shows a thermal network for the heat loss from a collector with a single cover that is transparent to solar radiation, but opaque in the infrared. The overall heat-transfer loss coefficient U can be obtained from a detailed thermal analysis if the individual convection heat transfer coefficients and the radiation exchange coefficients are known. Such an analysis leads to the simplified circuit with U as the loss coefficient used in the efficiency equations (Fig. 6b). The radiation exchange coefficient can be calculated from available information with relatively good accuracy [3, 5, 6], but the free convection heat-transfer coefficient requires knowledge of the operating conditions and geometry. Figure 7 shows in simplified fashion the various heat-flow resistances for calculating heat-transfer coefficients for flat-plate collectors, compound parabolic collectors, and single-axis-tracking parabolic troughs. The schematic diagrams in Fig. 3 show the geometries applicable for a central receiver with an external

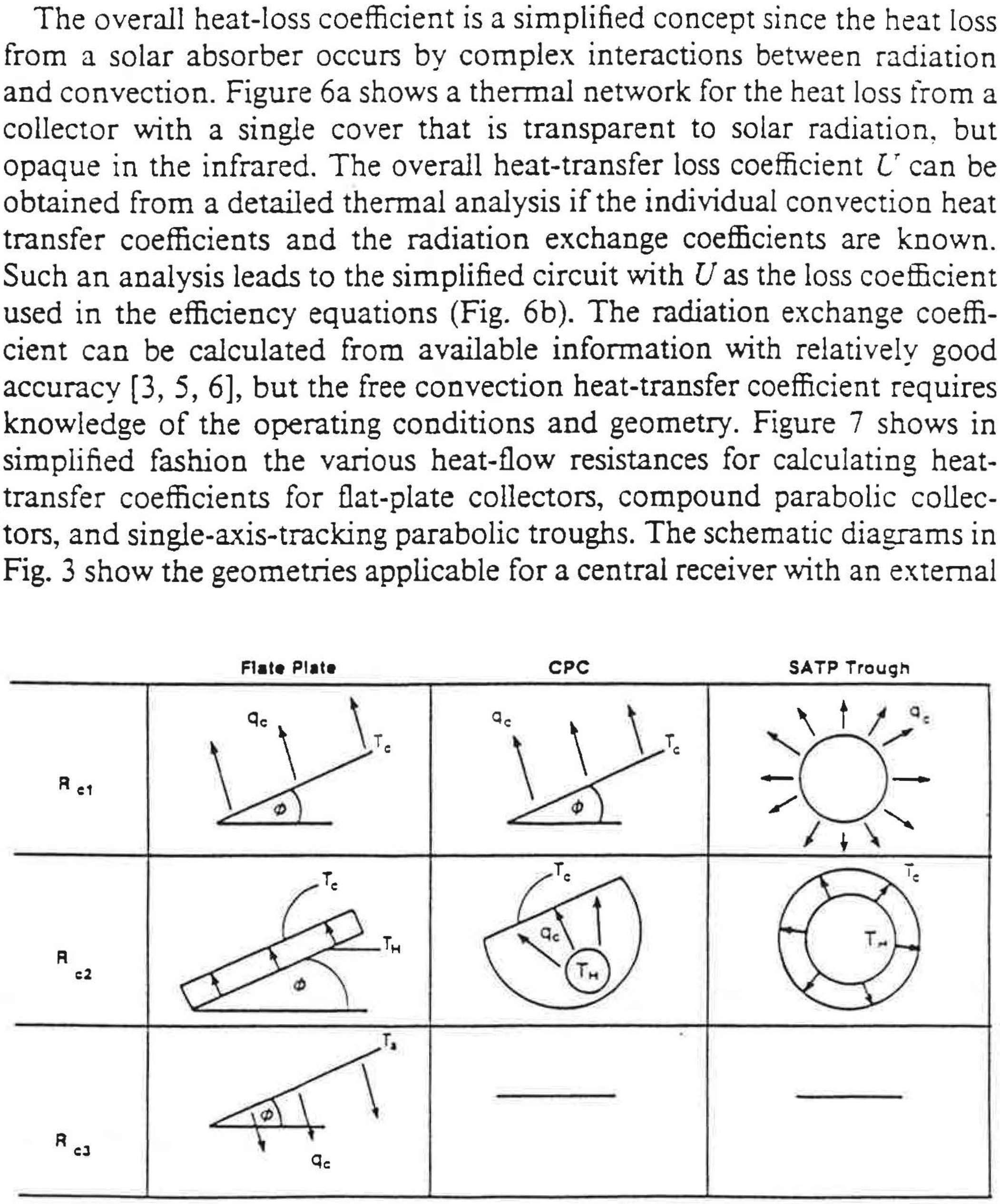

FIG. 7. Geometries and orientation for natural convection losses from flat plate collectors, compound parabolic collectors, and single-axis-tracking parabolic troughs; R_{c1}, R_{c2}, and R_{c3} as in Fig. 6.

or cavity design. In all of these cases, free convection plays an important role. In Section II we will present the available information about free convection heat transfer for the geometries relevant to all of these active solar systems.

C. Thermal Design Characteristics of Solar Buildings

Buildings rank with transportation and industry as one of the three main users of energy in the U.S. economy. Building energy consumption can be reduced by designing buildings to use solar energy for a portion of their heating and cooling needs.

In heating applications, solar buildings can be categorized depending on whether the solar energy that enters through the windows is used directly in the building zone in which it is absorbed (direct gain) or is transported from the direct gain zone to another building zone (indirect gain) (Fig. 5).

In cooling applications, prevailing winds are used in combination with stack driven ventilation to move cool outside air through the building. These types of solar applications have come to be known as passive solar to distinguish them from the active solar applications that have been discussed in the previous section.

A passive system has been defined by Balcolmb [7] as "one in which the thermal energy flow is by natural means." Most passive designs use south-facing glass in the building as the solar collection element and structural mass in the building as the thermal storage element. A successful passive design requires integration of the solar collection, thermal storage, and heat distribution functions into the architecture of the building. Obviously, a thorough understanding of natural convection in enclosed spaces is absolutely necessary to successfully achieve this integration without sacrificing the comfort standard of conventional heating systems.

In practice, solar buildings can consist of any combination of direct gain, indirect gain and ventilation cooling components. A fundamental understanding of the heat-transfer aspects of each of these generic configurations is necessary if they are to be successfully integrated into an overall building design. In Section III we present available information about free convection relevant to the design of passive solar systems.

II. Natural Convection in Active System Configurations

As mentioned previously, natural convection is important for the performance of solar collectors because it directly affects the thermal losses between the absorber surface and its surroundings.

A. FLAT-PLATE COLLECTORS

The natural convection losses from flat-plate collectors have commonly been analyzed by modeling the collector as a large-aspect-ratio, two-dimensional air gap with isothermal hot and cold walls (Fig. 8). This air gap may exist between the absorber and the transparent cover as well as between two transparent covers above the absorber if a double-glazed collector design is used. In both cases free convection occurs jointly with radiation. Flat-plate collectors usually operate without concentration and are inclined to the horizontal by an angle ϕ. There have been a number of reviews in recent years, including those by Buchberg [8], Catton [9], and Ostrach [10, 11] that cover various aspects of convection in enclosures. The reviews that most directly deal with the relation of enclosure research to heat losses from solar collectors are those of Buchberg *et al.* [8] and Catton [9].

A large fraction of the energy losses from flat-plate solar collectors is due to a recirculating convective cell that forms in the cavity between the hot absorber surface and transparent cover plate. The magnitude of the heat leak produced by the buoyant circulation cell between the absorber and cover plates of the collector is proportional to the overall temperature difference between the absorber and cover. It also depends upon cavity geometry, thermal boundary conditions, and physical properties of the cavity fluid.

The structure of the natural convection flow in a flat-plate collector is a strong function of the tilt angle of the collector. As the collector tilt angle

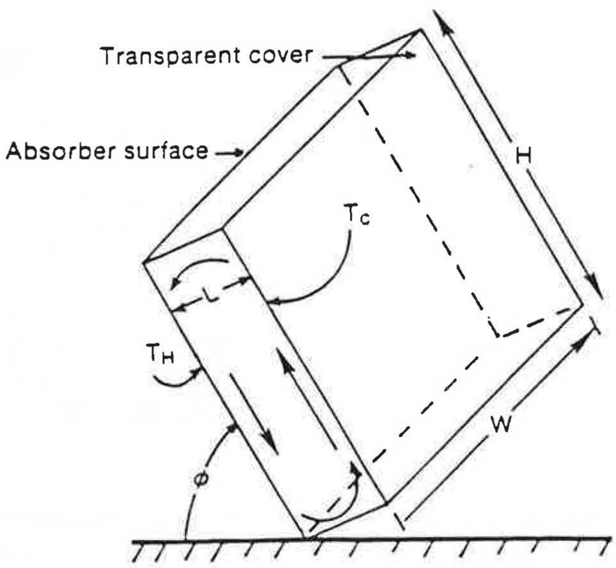

FIG. 8. Schematic diagram of gap in a flat-plate collector with a single transparent cover.

decreases from vertical ($\phi = 90°$) to horizontal ($\phi = 0°$) the flow changes from convection in a vertical slot with differentially heated side walls to Benard convection in a horizontal fluid layer heated from below and cooled from above. Hart [12] observed that for $0 \leq \phi \leq 80°$ thermal instabilities lead to the formation of longitudinal rolls with the axis of each roll oriented up the slope, and superimposed upon the primary flow. For near vertical orientations ($80 \leq \phi \leq 90$) secondary instabilities take the form of transverse rolls with axes oriented across the slope. The secondary flows cause an increase in convective heat transfer across the collector air gap.

Additional experimental studies of this phenomenon have been conducted by Ozoe *et al.* [13], Ruth *et al.* [14], Linthorst *et al.* [15], Inaba [16], and Goldstein and Wang [17]. Three-dimensional numerical calculations have been carried out by Ozoe *et al.* [18]. Schematic drawings visualizing natural convection in flat-plate collector geometries are shown in Fig. 9. Linthorst *et al.* [15] report that the characteristics of natural convective flow in an inclined rectangular cavity are a strong function of the aspect ratio of the cavity. Their experimentally derived curves for transition from stationary to nonstationary and two-dimensional to three-dimensional flow are shown in Fig. 10 as a function of aspect ratio and Rayleigh number Ra. For large values of the aspect ratio (AR), the flow quickly

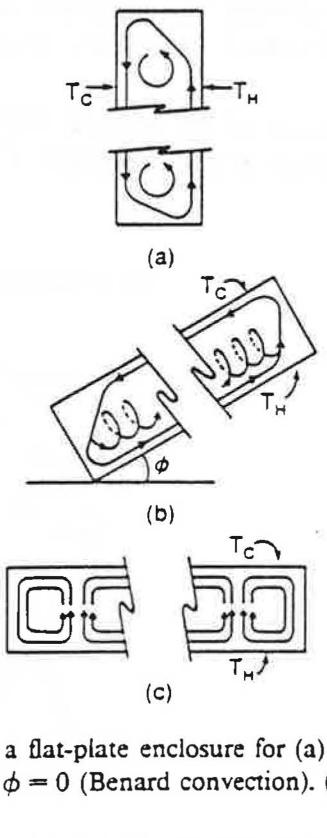

FIG. 9. Flow structure inside a flat-plate enclosure for (a) $\phi = 90°$ (transverse rolls), (b) $\phi = 30°$ (longitudinal rolls), (c) $\phi = 0$ (Benard convection). (Adapted from Linthorst *et al.* [15].)

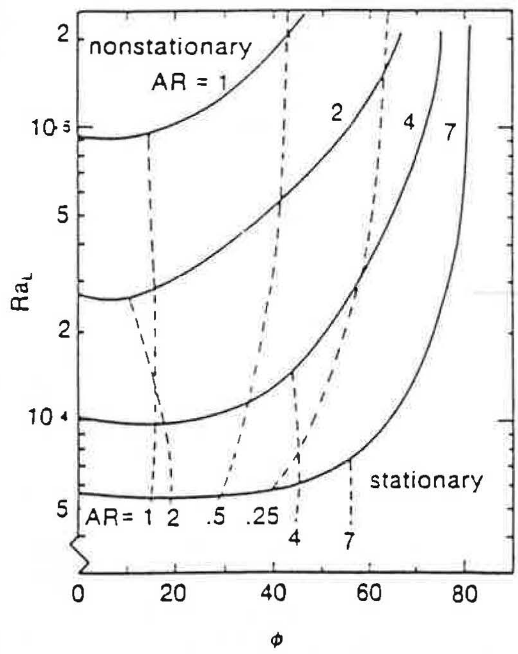

FIG. 10. Stability diagram showing transition from stationary to nonstationary (———) and from two-dimensional to three-dimensional flow (———). (From Linthorst *et al.* [15])

becomes nonstationary and/or three dimensional for inclined orientations. For AR = 7 and $0° \le \phi \le 60°$, the critical Rayleigh number for transition to nonstationary three-dimensional flow is about 6,000. This means that for conditions representative of a flat-plate solar collector (AR $\gg$ 1 and $\mathrm{Ra}_L \sim 2 \times 10^5$) the flow is always strongly three dimensional and nonstationary.

ElSherbiny *et al.* [19] conducted a comprehensive experimental investigation of the heat transfer in air-filled, high-aspect-ratio enclosures with isothermal walls, covering the ranges

$$10^2 \le \mathrm{Ra}_L \le 2 \times 10^7, \qquad 5 \le H/L = \mathrm{AR} \le 110, \qquad \text{and} \qquad 0° \le \phi \le 90°$$

where $\mathrm{Ra}_L = g\beta L^3\, \Delta T/\nu\alpha$ and ΔT is the temperature difference between the lower and upper surface of the air gap. A comparison of the ranges of these parameters with previous experimental studies is shown in Fig. 11 [19a–19d].

ElSherbiny *et al.* found that the transition from the conduction to convection regime in vertical enclosures is a strong function of the aspect ratio when AR < 40. The following heat-transfer correlations are recommended:

1. For vertical layers ($\phi = 90°$):

$$\overline{\mathrm{Nu}_L} = [\overline{\mathrm{Nu}_1}, \overline{\mathrm{Nu}_2}, \overline{\mathrm{Nu}_3}]_{\max} \tag{4}$$

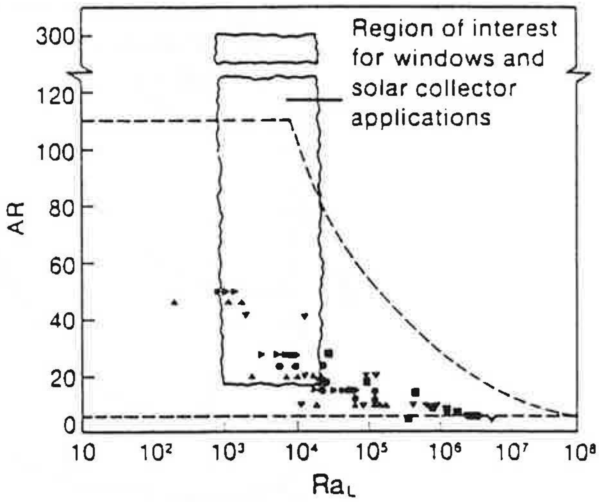

FIG. 11. Summary of experimental investigations of natural convection in high-aspect-ratio enclosures. ▶, Degraaf and Van der Held [19a]; ▲, Eckert and Carlson [19b]; ■, Schinkel and Hoogendoorn [19c]; ●, Randall, Mitchell and El-Wakil [19d], ———, ElSherbiny, Raithby, and Hollands [19] (adapted from ElSherbiny, Raithby, and Hollands [19].)

where

$$\overline{Nu_1} = 0.0605\ Ra_L^{1/3} \tag{5}$$

$$\overline{Nu_2} = [1 + \{0.104\ Ra_L^{0.293}/(1 + (6310/Ra_L)^{1.36})\}^3]^{1/3} \tag{6}$$

$$\overline{Nu_3} = 0.242(Ra_L/AR)^{0.272} \tag{7}$$

2. For inclined layers ($\phi = 60°$):

$$\overline{Nu_L} = [\overline{Nu_1}, \overline{Nu_2}]_{max} \tag{8}$$

where

$$\overline{Nu_1} = [1 + \{0.0936\ Ra_L^{0.314}/(1 + G)\}^7]^{1/7} \tag{9}$$

$$G = 0.5/[1 + (Ra_L/3160)^{20.6}]^{0.1} \tag{10}$$

$$\overline{Nu_2} = (0.104 + 0.175/AR)Ra_L^{0.283} \tag{11}$$

The notation in Eqs. (4) and (8) indicates that the maximum value of the average Nusselt number calculated from the correlations for Nu_i (where $i = 1$ to 3) should be used.

For tilt angles between 60° and 90° ElSherbiny *et al.* [19] suggest a linear interpolation between the limiting correlations given above:

$$\overline{Nu_\phi} = [(90° - \phi)\ Nu_{60} + (\phi - 60°)\ Nu_{90}]/30° \tag{12}$$

Extrapolating these equations beyond the experimental range of variables is not recommended.

For tilt angles between 0° and 75°, Hollands *et al.* [20] recommend the following correlation for the average Nusselt number:

$$\overline{\mathrm{Nu}} = 1 + 1.44\left(1 - \frac{1708}{\mathrm{Ra}\cos\phi}\right)^{\bullet}\left[1 - \frac{1708\,(\sin 1.8\phi)^{1.6}}{\mathrm{Ra}\cos\phi}\right] + \left[\left(\frac{\mathrm{Ra}\cos\phi}{5830}\right)^{1/3} - 1\right]^{\bullet} \tag{13}$$

where L is the distance between the plates at temperatures T_{H} and T_{C}, respectively, and the Rayleigh number Ra is given by

$$\mathrm{Ra} = \frac{2g(T_{\mathrm{H}} - T_{\mathrm{C}})L^3}{\nu^2(T_{\mathrm{H}} + T_{\mathrm{C}})}$$

A dot to the right of a bracket denotes that $[\chi]^{\bullet} = (|\chi| + \chi)/2$. Thus when $\mathrm{Ra} < (1708)/(\cos\phi)$ the Nusselt number in Eq. (13) is exactly equal to unity. The condition $\mathrm{Nu} = 1$ implies that the heat transfer across the air cavity is by pure conduction.

The natural convection circulation in the cavity between the cover plate and the absorber can be suppressed by making the aspect ratio of the collector very large or very small. The former approach is used in the design of double-pane windows. The latter approach is used in the design of various types of internal partitions (honeycombs, horizontal slats, vertical slats) that are placed in the collector cavity (Fig. 12). A summary of the aspect ratio dependence of natural convection in vertical rectangular enclosures as reported by Bejan [94] is shown in Fig. 13. The Nusselt number reaches a peak for values of the aspect ratio between 0.1 and 1.0, and drops rapidly in value for very large and very small values of the aspect ratio.

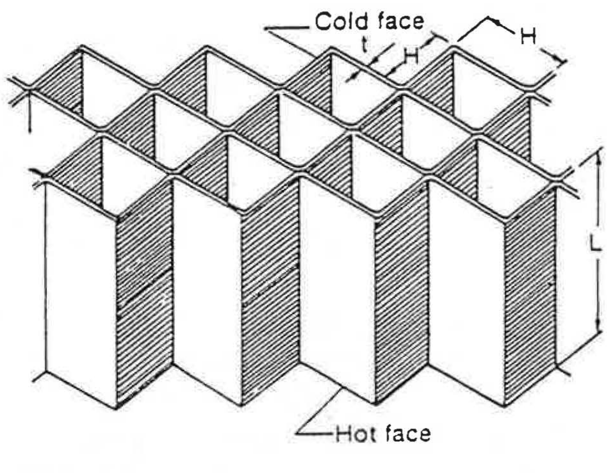

FIG. 12. Schematic diagram of honeycomb structure used to suppress convection.

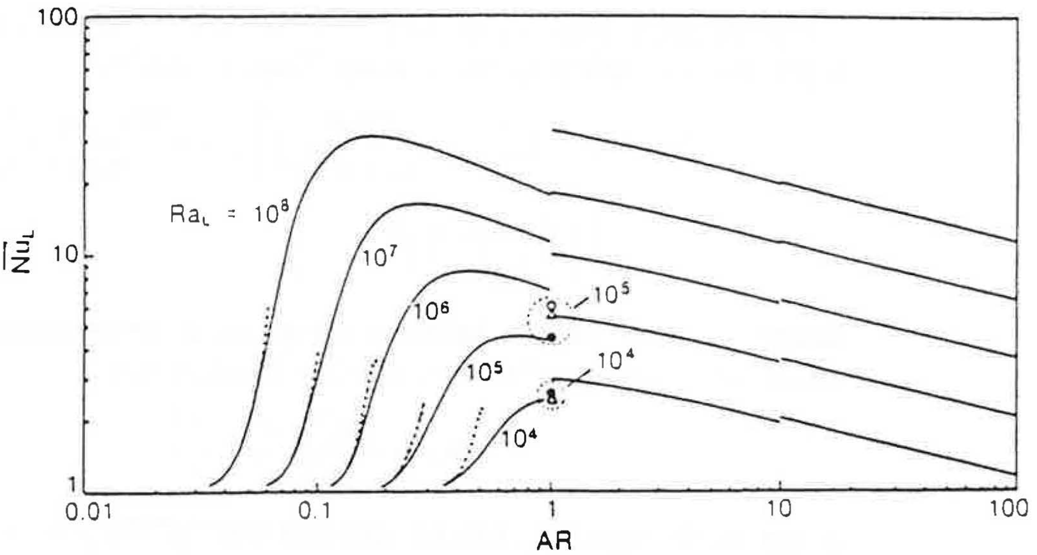

FIG. 13. Aspect ratio dependence of heat-transfer coefficient (from Bejan [92]).

A review of the theory and application of honeycombs for suppressing natural convection in flat-plate solar collectors is given by Buchberg *et al.* [21, 22] and by Hollands [23]. For an inclined, square honeycomb, the Nusselt number depends on the Rayleigh number, the inclination, and the AR of the honeycomb. For the range $0 < \mathrm{Ra} < [6000\ \mathrm{AR}^4]$, $30° < \phi < 90°$, and $1/\mathrm{AR} = 3$, 4, or 5, the Nusselt number for air is given by Cane *et al.* [24] in the form

$$\overline{\mathrm{Nu}_L} = \frac{\bar{h}_c L}{k} = 1 + 0.89 \cos(\phi - 60°) \times \left(\frac{\mathrm{Ra}_L\, \mathrm{AR}^4}{2420}\right)^{(2.88 - 1.64 \sin \phi)} \tag{14}$$

For minimum heat loss the honeycomb should be designed to give a Nusselt number of 1.2, according to Hollands *et al.* [25]. For air at atmospheric pressure and moderate temperatures, $370\ \mathrm{K} > T_m > 280\ \mathrm{K}$, the aspect ratio for minimum heat loss can be found from

$$\frac{1}{\mathrm{AR}} = C(\phi)\left(1 + \frac{200}{T_m}\right)^{1/2}\left(\frac{100}{T_m}\right)(T_H - T_C)^{1/4} L^{3/4} \tag{15}$$

where L is the thickness of the honeycomb in centimeters, T_m is the average of the coverplate and absorber temperature in degrees Kelvin, and the function $C(\phi)$ is plotted in Fig. 14.

Hollands *et al.* [26] and Hoogendoorn [27] independently calculated total heat transfer in honeycomb structures including radiation effects.

They found that conduction heating of the honeycomb increases the radiative losses from the collector and reduces the benefits associated with the convection suppression that is provided by the honeycomb if the honeycomb is allowed to come into direct contact with the hot absorber plate. Hollands and Iynkaran [28] recommend that a 10-mm air gap be left between the honeycomb and the absorber plate to reduce conductive heating of the honeycomb structure.

Two-dimensional slats are an alternative method of convection suppression. These slats can be oriented horizontally (forming transverse slots) or vertically (forming longitudinal slots). Transverse slats have been investigated by Arnold *et al.* [29, 30], Meyer *et al.* [31], and Smart *et al.* [32]. These studies demonstrate that for transverse rectangular cell aspect ratios less than 0.1, convection is suppressed for Ra_L up to 4×10^5 for a tilt angle of 60°. Meyer *et al.* [31] found that heat transfer increased, compared to an enclosure without transverse slats, for transverse rectangular cell aspect ratios in the range $0.5 \le Ar \le 4$. Symons and Peck [33] and Symons [34] have investigated the reduction in convective heat transfer produced by longitudinal slats. Symons and Peck [33] compared the heat transfer across a transverse slot with $AR = 0.17$ to the heat transfer across a longitudinal slot with the same cross-sectional dimensions. They found that the heat transfer across the longitudinal slot was less than the heat transfer across the transverse slot for tilt angles in the range $24° \le \phi \le 75°$. For tilt angles in the range $0° \le \phi \le 24°$, the heat transfer was the same, regardless of slot orientation. For tilt angles in the range $75° \le \phi \le 90°$, the heat transfer across the transverse slot was less than the heat transfer across the longitudinal slot. The effectiveness of longitudinal slots appears to be related to their ability to damp out the longitudinal convection cells that form when the collector is tilted from the vertical.

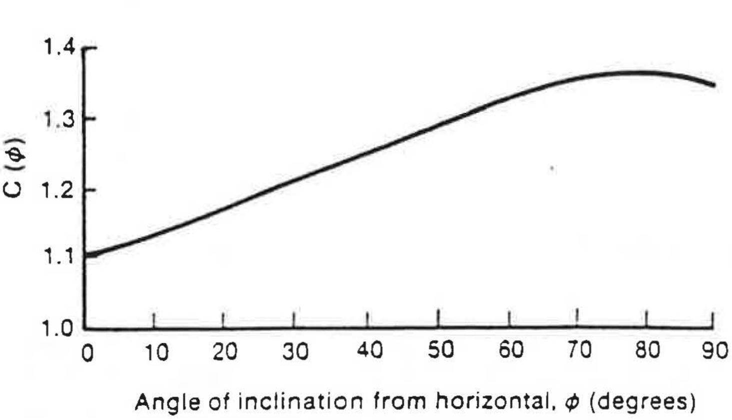

FIG. 14. Plot of $C(\phi)$ versus ϕ for use in Eq. 15 (from Hollands *et al.* [25]).

Some aspects of heat transfer in flat-plate solar collectors require more sophisticated models than those based on enclosures with isothermal walls. Balvanz and Kuehn [35] have shown that the effect of finite wall conductivity can be significant, particularly for a constant-flux boundary condition where wall conduction can reduce the wall-temperature gradient and produce a corresponding decrease in heat transfer from the wall. Figure 15a shows the wall temperature profile measured by Anderson and Bohn [36] in an enclosure with a finite conductivity wall. Figure 15b shows the corresponding decrease in heat transfer predicted by Balvanz and Kuehn [35]. MacGregor and Emery [37] calculated natural convection flow in a vertical enclosure while varying thermal boundary conditions at the heated wall. They found 30% higher convective losses for a constant flux condition than for an isothermal condition. In their work the average temperature difference between the hot and cold walls was used in the definition of the Nusselt number for the constant flux surface. Schinkel and Hoogendoorn [38] repeated the calculations of MacGregor and Emery for $Ra_L = 5.8 \times 10^4$ and found the Nusselt number for a constant flux surface to be more than 20% more than for an isothermal surface. This prediction was found to agree with experiments in air. Schinkel and Hoogendoorn also

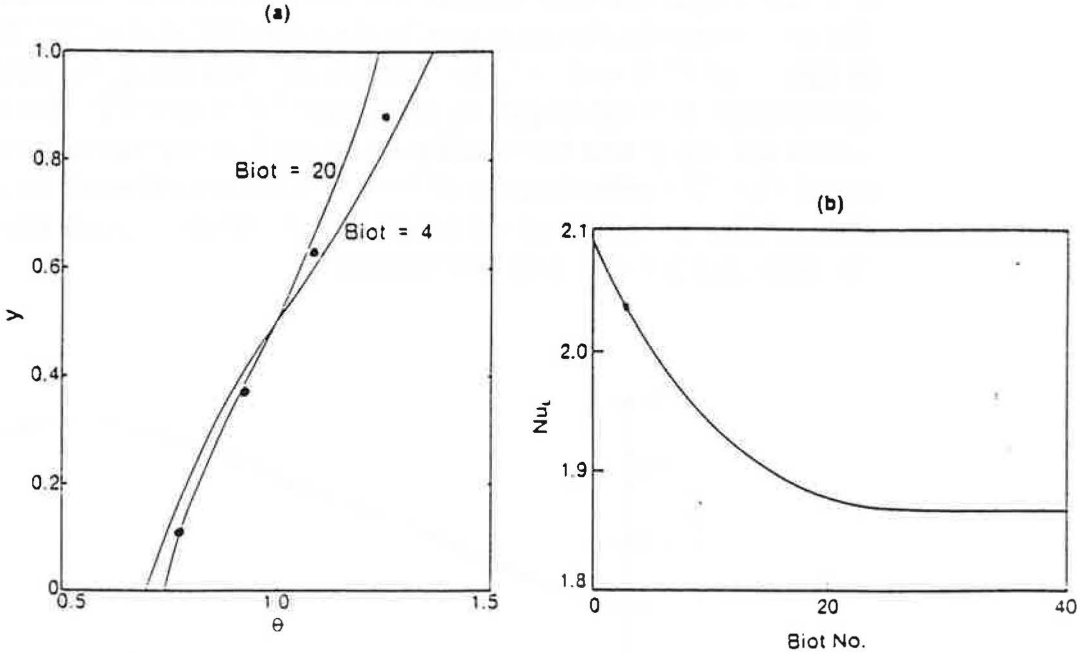

FIG. 15. (a) Experimental measurements of wall surface temperature by Anderson and Bohn, ●, Bi = 10 [36] for finite wall conductance compared to theoretical predictions by Balvanz and Kuehn [35]; Bi $= K_w t/K_f H$. $\theta = (T - T_C)/(T'_H - T_C)$. (b) Effect of finite Bi on overall Nusselt number (after Balvanz and Kuehn [35]).

did experimental comparisons at $\phi = 60°$, $40°$, and $20°$ and found increases of 14%, 11%, and 9%, respectively.

In an actual flat-plate collector, the absorber will be at some condition in between an isothermal and a constant-flux surface. This overlapping state is caused by the coupling between the free-convective flow in the cavity separating the absorber and cover and the forced-convective flow of the heat transfer fluid through tubes in the absorber plate. Chao *et al.* [39] numerically analyzed the effect of spatial sawtooth variations in the temperature of an inclined enclosure with AR = 2. They found that surface-temperature variations produced a stronger circulation and a higher overall Nusselt number than did a uniform temperature. The sawtooth variation in surface temperature studied by Chao *et al.* [39] is particularly relevant to liquid collectors, where heat-exchanger tubes are connected at regular intervals along the surface of the absorber plate.

The thermal boundary condition at the cover plate results from the interaction of internal and external convection and thus is not known *a priori* as in the case of the isothermal wall model. A number of researchers have looked at cases where a free-convection boundary layer exists on the outside surface as well as on the inside surface of the cover plate. Such a condition would exist when the external wind velocity is zero. Lock and Ko [40] demonstrated that the resulting interaction produces a nearly constant-flux surface with a linear temperature profile except for regions near the top and bottom of the plate. Anderson and Bejan [41, 42] extended the analysis of Lock and Ko to wider range of plate thermal resistance and included the effects of thermal stratification in the fluid on either side of the plate. Viskanta and Lankford [43] conducted experiments in an air-filled enclosure that was separated into two zones by a conducting partition. Sparrow and Prakash [44] conducted a numerical investigation of an enclosure with $H/L = 1$ which was coupled via a conductive wall to an external natural convection flow.

B. LINE FOCUSING COLLECTORS

Line-focus collectors have recently received a great deal of attention for industrial heat applications at intermediate temperatures [44, 45]. There are two commercial types of line focusing collectors: the compound parabolic trough and the tracking parabolic trough. Both are usually deployed in a horizontal position. The parabolic trough collector must track the sun continuously. The optical design of the compound parabolic type requires no tracking at concentration ratios below 2 and only biyearly tilt adjustment at concentration ratios below 5.

1. *Compound Parabolic Collector*

Compound parabolic collectors have been studied by Winston [46], Rabl [47], and O'Gallager *et al.* [48]. In a CPC, heat loss is by natural convection from the cylindrical receiver surface in the space formed by the aperture cover and the reflector. Typical CPC configurations are shown in Fig. 16a. Generalizing the shape of CPC cavities and receivers is difficult because the detailed geometry of these designs depends upon the manner that the CPC shape is designed.

There are two approaches to the calculation of natural convection losses from CPC collectors. The losses can be approximated by replacing the collector with an equivalent eccentric cylindrical annulus, or the losses can be calculated directly. Examination of the shapes presented by Rabl [47], O'Gallager *et al.* [48], and Ortabasi and Fehlner [49] shows that with concentration ratios between 1.6 and 3.0 the heat loss and flow can be approximated by natural convection in an eccentric cylindrical annulus.

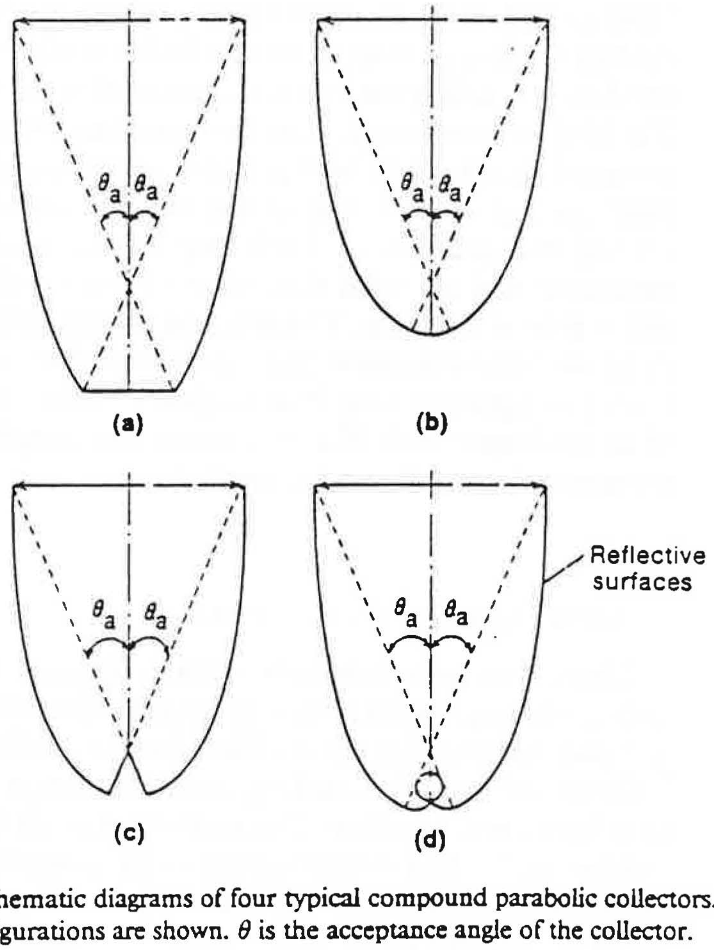

FIG. 16. Schematic diagrams of four typical compound parabolic collectors. Four possible absorber configurations are shown. θ is the acceptance angle of the collector.

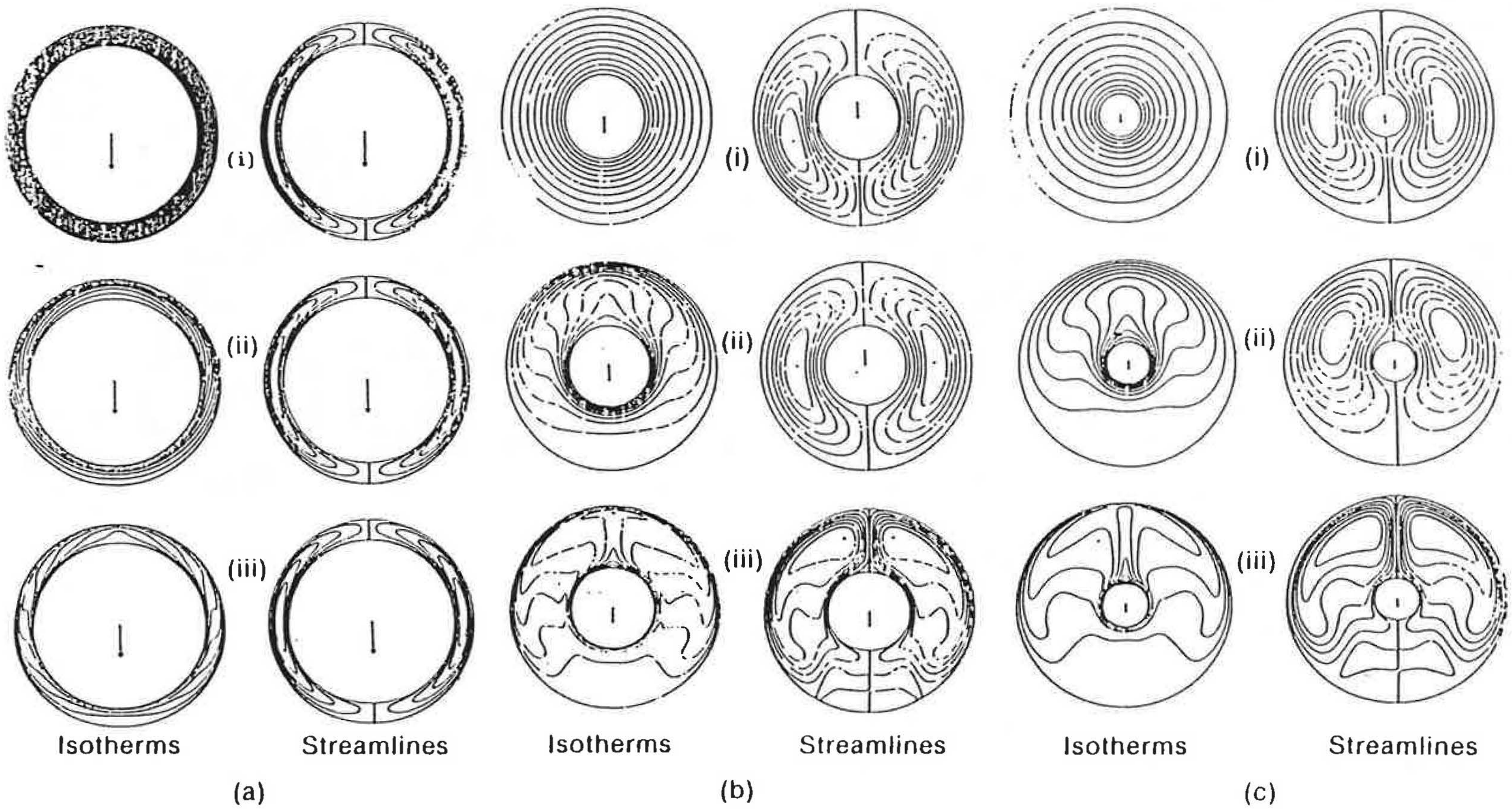

FIG. 17. Isotherms and streamlines for concentric cylinders with (i) $Ra = 10^2$, (ii) $Ra = 10^4$, and (iii) $Ra = 10^6$ and radius ratios of (a) 1.25, (b) 2.6, and (c) 5.0. Ra is calculated based upon the average gap between cylinders. (From Lee *et al.* [50]).

Correlations for the evaluation of the heat loss in an eccentric cylindrical annulus geometry are given by Lee *et al.* [50]. These authors determined, both experimentally and numerically, the characteristics of natural convection heat transfer in concentric as well as eccentric cylindrical annuli. The results cover a range of inner-to-outer diameter ratios from 1.25 to 5.0 and eccentricity ratios up to ± 0.9 for air ($Pr = 0.7$). Figure 17 shows the isotherms and streamlines for concentric cylinders for D_i/D_o ratios of 1.25, 2.6, and 5.0 at Ra of 10^2, 10^4, and 10^6. Figure 18 shows the isotherms and streamlines at eccentricity ratios e of -0.9, 0.67, 0.9 for $Ra = 5 \times 10^5$ and D_i/D_o of 2.6. Figure 19 shows the results for the average convection heat-transfer coefficient between the inner and outer surface versus Ra for eccentricity ratios of 0, -0.67, 0.67, and 0.33. Lee *et al.* based their definition of Rayleigh number on the average size of the gap between cylinders.

A CPC collector configuration, representative of commercial designs, has been studied by Hsieh [51] and Hsieh and Mei [52]. His configuration (see Fig. 20) can be approximated by an annular space between the receiver envelope and the surface formed by the reflector and the transparent aperture cover at the top. When the outer surface of the structure is treated

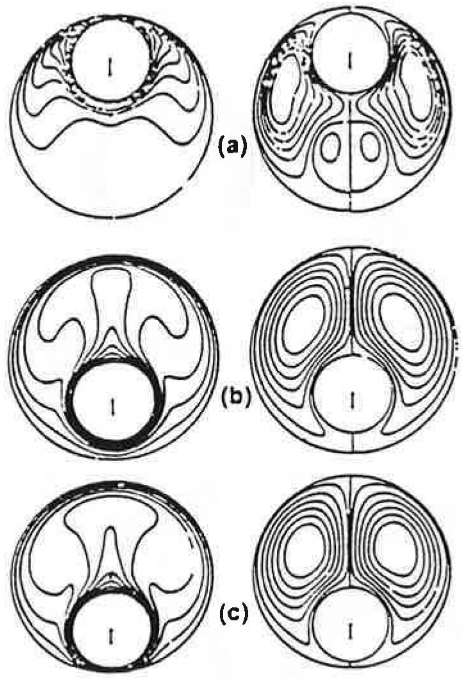

FIG. 18. Isotherms and streamlines at eccentricity ratios of (a) -0.9, (b) $\frac{2}{3}$, (c) 0.9, for $Ra = 5 \times 10^5$ and radius ratio of 2.6. The Rayleigh number is calculated from the average gap between cylinders. (From Lee *et al.* [50]).

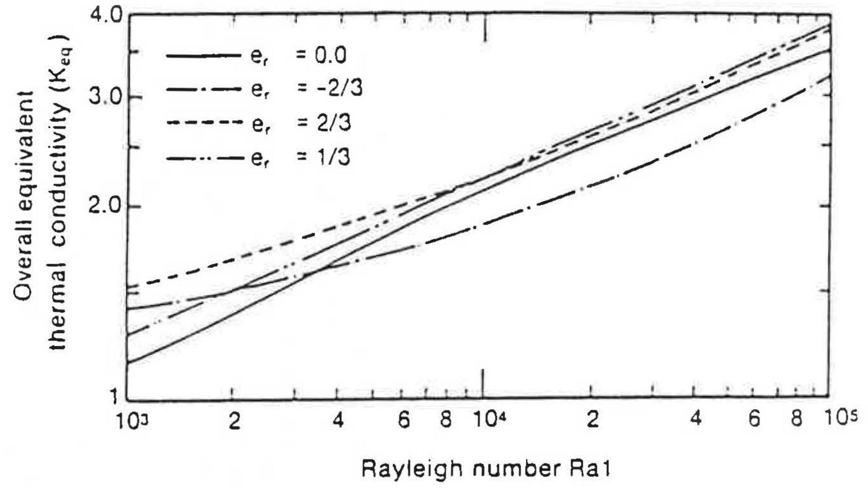

FIG. 19. Overall heat-transfer coefficient versus Rayleigh number for radius ratio of 5. Rayleigh numbers are calculated from the average gap between cylinders. Here, $K_{eq} = q_c \ln(S)/2\pi k\, \Delta T$, where

$$S = \frac{\sqrt{(r_o + r_i)^2 - e^2} + \sqrt{(r_o - r_i)^2 - e^2}}{\sqrt{(r_o + r_i)^2 - e^2} - \sqrt{(r_o - r_i)^2 - e^2}}$$

(From Lee *et al.* [50].)

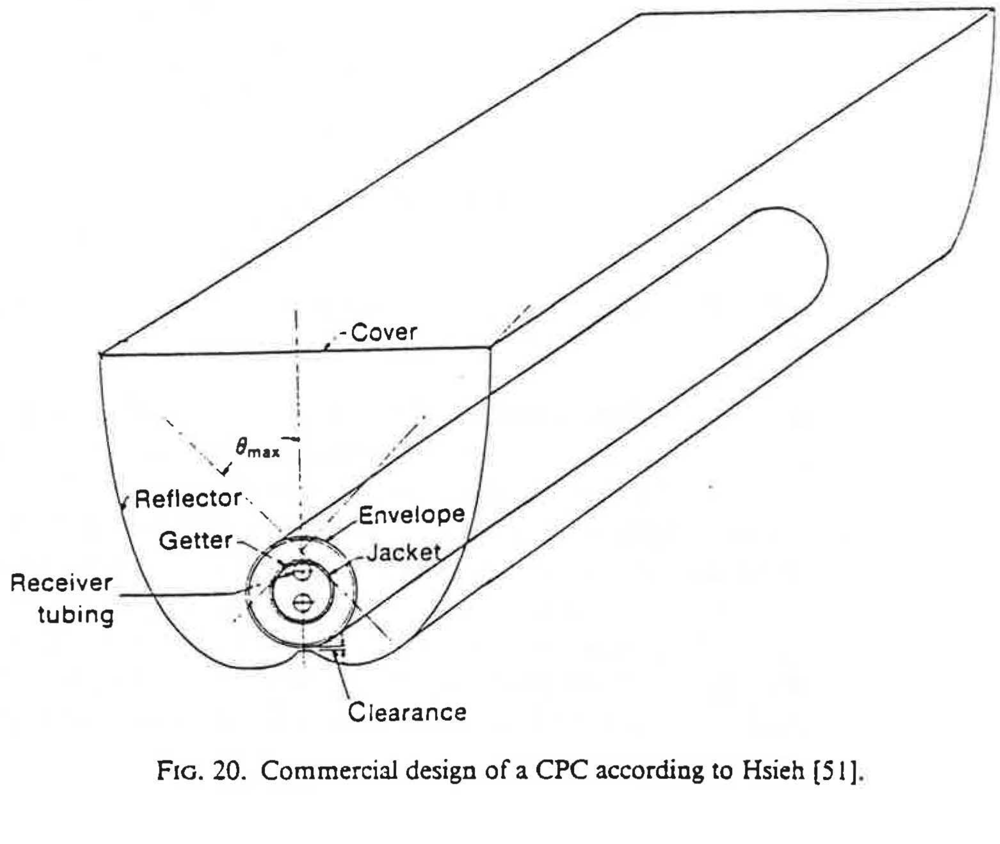

FIG. 20. Commercial design of a CPC according to Hsieh [51].

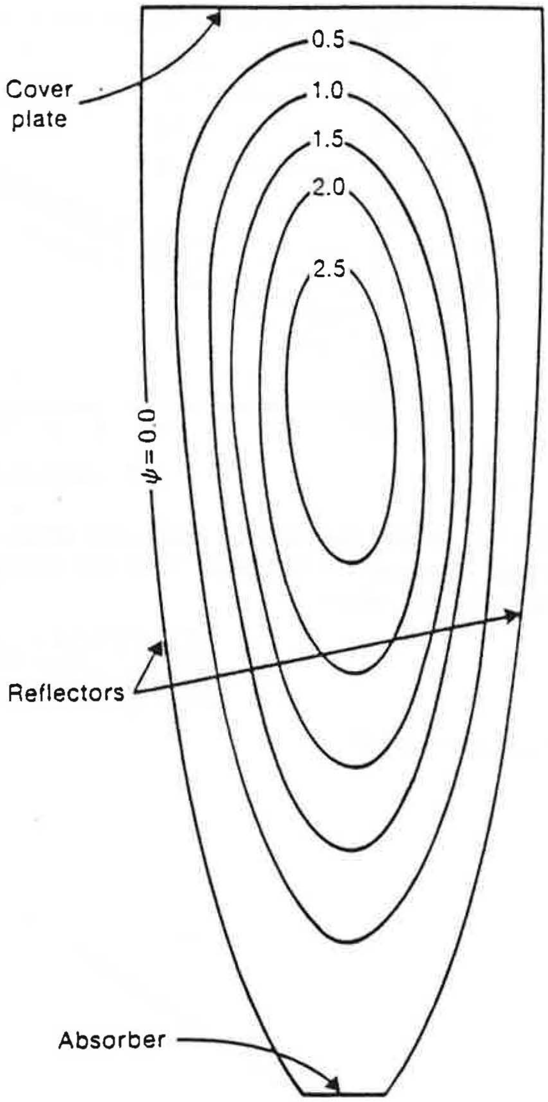

FIG. 21. Convective pattern in a compound parabolic collector with a coverplate and planar absorber (from Abdel-Khalik *et al.* [53]).

as an equivalent cylinder, the heat-loss mechanism from the receiver can be approximated as natural convection through an annulus with a diameter ratio of about 3 and an eccentricity e of about 0.75.

Abdel-Khalik *et al.* [53] carried out a finite-element analysis of a CPC collector with its axis oriented horizontally and developed heat-loss equations for concentration ratios of 2 to 10 and Rayleigh numbers, based upon cavity thickness, of 2×10^3 to 1.3×10^6. The convection pattern in this Rayleigh number range was found to be unicellular (Fig. 21). The reflector walls were assumed to be adiabatic while the absorber and cover plate were isothermal.

Meyer *et al.* [54] determined the losses from a V-trough collector as a function of Rayleigh number and tilt angle. Their collector had straight rather than parabolic sides, but it approximated closely the behavior of a CPC collector. They found that the collector tilt affects heat transfer similarly to that for rectangular enclosures.

Convective losses from a CPC collector can be reduced when the absorber is cylindrical by surrounding the absorber with a concentric glass tube. Collares Pereira *et al.* [55] and Woo [56] have conducted experiments with glass tubes surrounding the CPC collectors. The available experimental and analytic results, for the overall loss coefficient in CPC collectors with and without a transparent cylindrical cover over the receiver, are summarized in Table II [56a–56c]. The overall loss coefficients found in experimental tests of various CPC designs are in reasonably good agreement with each other and they indicate that surrounding the absorber with a transparent cylinder reduces losses by about a factor of two.

TABLE II

SUMMARY OF HEAT LOSSES IN NONEVACUATED CPC COLLECTORS[a]

Reference	Heat-loss coefficient Normalized to collector aperture (W/m² °C)	Geometric concentration	Heat-loss coefficient normalized to absorber (W/m² °C)	Remarks
I. No envelope				
Rabl *et al.* [56a]	1.85 ± 0.1	5.2	9.6 ± 0.5	Tube absorber
	2.7 ± 0.2	3.0	8.1 ± 0.6	Fin absorber
Meyer *et al.* [54]	1.8–2.5	2–3	3.6–7.5	Flat absorber, measured experimentally
II. Tube with Glass Envelope				
Rabl *et al.* [56a]	2.2	1.5	3.3	Calculated
Patton [56b]	1.82	1.6	2.9	Measured experimentally
Woo [56]	2.8 ± 0.1	1.65	4.6 ± 0.2	Measured experimentally
Collares Pereira *et al.* [55]	2.64	1.5	4.0	Measured experimentally
Prapas *et al.* [56c]	—	—	4.4	Calculated for absorber only

[a] Well-designed CPCs with selective absorber coating, and absorber thermally isolated from mirrors so that losses are dominated by convection.

2. *Single-Axis-Tracking Parabolic Trough Collectors*

In a single-axis-tracking parabolic trough concentrator, which operates at concentration ratios from 25 to 50, the incident solar radiation is reflected onto a planar or a cylindrical absorber, as shown in Fig. 22. This absorber generally has a transparent cover to reduce heat losses from its surfaces. Unless the space surrounding the absorber is evacuated, the convection heat loss is by natural convection in the space between flat plates or between concentric tubes in conjunction with radiation. When the absorber has a selective surface, natural convection is the dominant mechanism. Rabl, Bendt, and Gaul [57] have shown that for conventional, unevacuated line-focusing parabolic trough collectors with tubular receivers, the ratio of outer to inner diameter (D_o/D_i) varies typically from 1.5 to 2.6.

Natural convection flow and heat transfer under geometric conditions similar to those encountered in the tubular receivers of single-axis-tracking line-focusing collectors have been studied by several investigators, most recently by Kuehn and Goldstein [58–61] and Lee *et al.* [50]. Equations for heat transfer by natural convection between isothermal long concentric horizontal circular cylinders have been developed by Kuehn and Goldstein and compared with experimental data obtained by various investigators. They recommend for the average Nusselt number between isothermal concentric cylinders with inner and outer surface temperatures T_i and T_o,

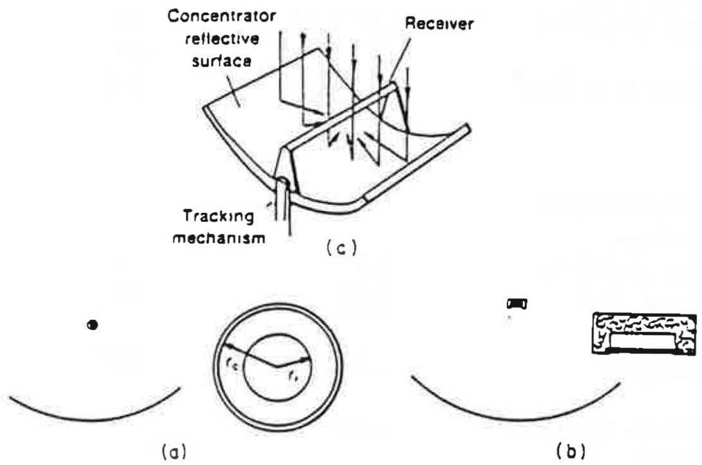

FIG. 22. (a) Schematic front view of parabolic trough concentrating collector with (a) cylindrical and (b) planar receiver. (c) Three dimensional schematic view of a paraboloid trough collector.

respectively, the relation

$$\overline{\mathrm{Nu}_{D_i}} = \frac{2}{\ln\{(1 + 2/E^{1/15})/(1 - 2/F^{1/15})\}} \tag{16}$$

where

$$E = [0.518\ \mathrm{Ra}_{D_i}^{1/4}\,(1 + (0.559/\mathrm{Pr})^{3/5})^{-5/12}]^{15} + (0.1\ \mathrm{Ra}_{D_i}^{1/3})^{15} \tag{17}$$

$$F = \left(\left[\left(\frac{2}{1 - e^{-0.25}}\right)^{5/3} + G^{5/3}(0.587\ \mathrm{Ra}_{D_o}^{1/4})^{5/3}\right]^{3/5}\right)^{15} + (0.1\ \mathrm{Ra}_{D_o}^{1/3})^{15} \tag{18}$$

$$G = \left[\left(1 + \frac{0.6}{\mathrm{Pr}^{0.7}}\right)^{-5} + (0.4 + 2.6\ \mathrm{Pr}^{0.7})^{-5}\right]^{-1/5} \tag{19}$$

and

$$\overline{\mathrm{Nu}_{D_i}} = \bar{h}_c D_i/k \tag{20}$$

$$\bar{h}_c = \frac{q_c}{\pi D_i L(T_i - T_o)} \tag{21}$$

$$\mathrm{Ra}_{D_i} = g\beta D_i^3(T_i - T_o)/\nu\alpha, \qquad \mathrm{Ra}_{D_o} = g\beta D_o^3(T_i - T_o)/\nu\alpha \tag{22}$$

Equation (16) correlates available experimental data over the ranges of Rayleigh numbers from 10^2 to 10^{10} and Prandtl number between 0.01 and 1,000 as shown in Fig. 23.

Evaluation of T_i in the above relations requires iteration. To avoid this, Kuehn and Goldstein [61] suggest the simple relation, valid for $\mathrm{Pr} = 0.71$ and laminar flow,

$$\mathrm{Nu}_{D_i,\mathrm{conv}} = \frac{2}{(1 + 2/0.4\ \mathrm{Ra}_{D_i}^{1/4})/(1 - 2/0.587\ \mathrm{Ra}_{D_o}^{1/4})} \tag{23}$$

The above correlation is considered satisfactory for horizontal trough collectors with cylindrical receivers, although it does not take into account the nonuniform temperature of the receiver surface and is therefore subject to an unknown error under practical operation conditions in the sun.

C. POINT-FOCUSING SYSTEMS

The earliest reported application of a point-focusing system was Archimedes' use of reflecting mirrors in 212 B.C. to set the ships of the invading Romans on fire at Syracuse. Many inventors, alchemists, and scientists have proposed point focusing of solar radiation as a means of achieving

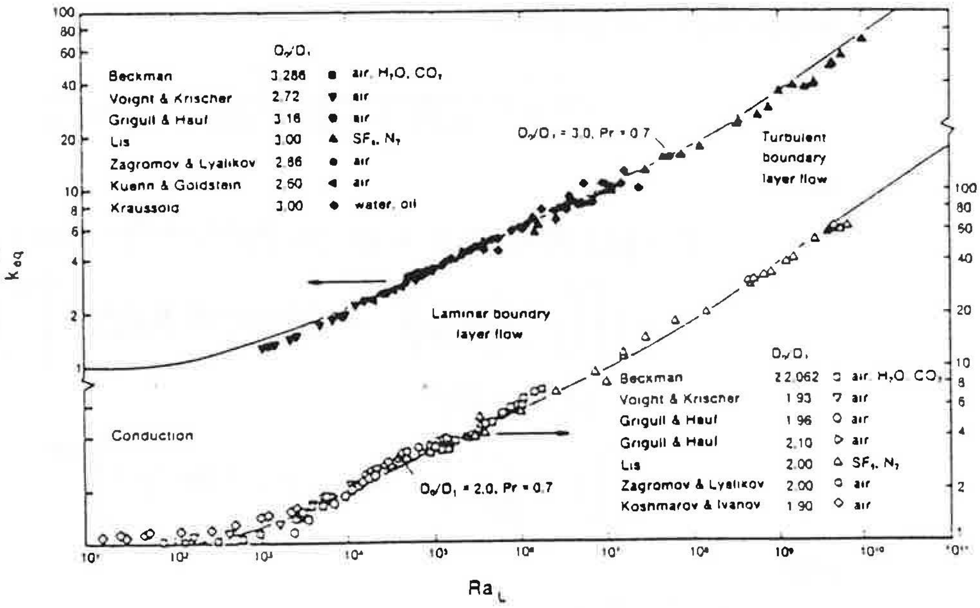

FIG. 23. Comparison of correlating equations with experimental results for natural convection between horizontal concentric cylinders; $\overline{K}_{eq} = \mathrm{Nu}_{D_i} \cosh^{-1}[D_i^2 + D_o^2 - 4\varepsilon^2/2D_iD_o]/2$, where ε is the normalized distance that the inner cylinder is displaced from concentricity. The Rayleigh number is based on the average gap width. (From Kuhn and Goldstein [60]).

extremely high temperatures for many applications [62]. But use of point focusing for large-scale installations has only taken place within the past decade. Since 1980 several central receiver systems in sizes up to 10 mW electric capacity have been built for electric power production and industrial heat and dual-axis-tracking paraboloid concentrators have been employed for heat and electric power generation. The distributed total energy system at Shenandoah, Georgia is shown in Fig. 24. The collector field for this paraboloid dish system (PDS) consists of 114 parabolic dishes; each of them is 7 m in rim diameter with a cavity receiver located at the focus as shown schematically in Fig. 1b. Paraboloid dishes are generally less than 10 or 20 m in diameter because larger dishes are difficult to build and are subject to excessive wind loading. Hence, receivers for dish systems are relatively small. Natural convection for this type of receiver will be discussed in Section II,C,3.

Figure 1e is a simple diagram of a central receiver solar power system. Dual-axis-tracking heliostats concentrate direct solar radiation onto a tower-mounted central receiver, which can be a cavity or external design. There the radiant energy is used to heat a working fluid to high temperatures for piping to the bottom of the tower and subsequent use as a high-temperature heat source for industrial processes, operating a turbine, or storing for future use (63).

Central receivers generally are large and have high surface temperatures and complex geometries. Heat transfer and fluid flow occur in regimes for which experimental data are scant and predictive methods are uncertain. The lack of steady flow in atmospheric boundary layers further complicates analysis in the case of the external receiver. Abrams [64] developed a map of available natural convection data in the Grashof number versus Reynolds number regimes as well as the operating regime of typical solar central receivers (Fig. 25). Progress has been made in providing information upon which the convective losses of central receivers can be based, but uncertainties remain in understanding and predicting convection losses from central receivers.

To predict the efficiency of any receiver in a point-focusing system, it is necessary to calculate the amount of incident solar radiation that is intercepted, reflected, and emitted by the receiver and the losses by convection and conduction. In many cases, natural convection is a dominant factor, and in this section we will summarize the available information for the three industrially most important receiver types: external and cavity receivers for CRS applications and cavity receivers for PDS applications.

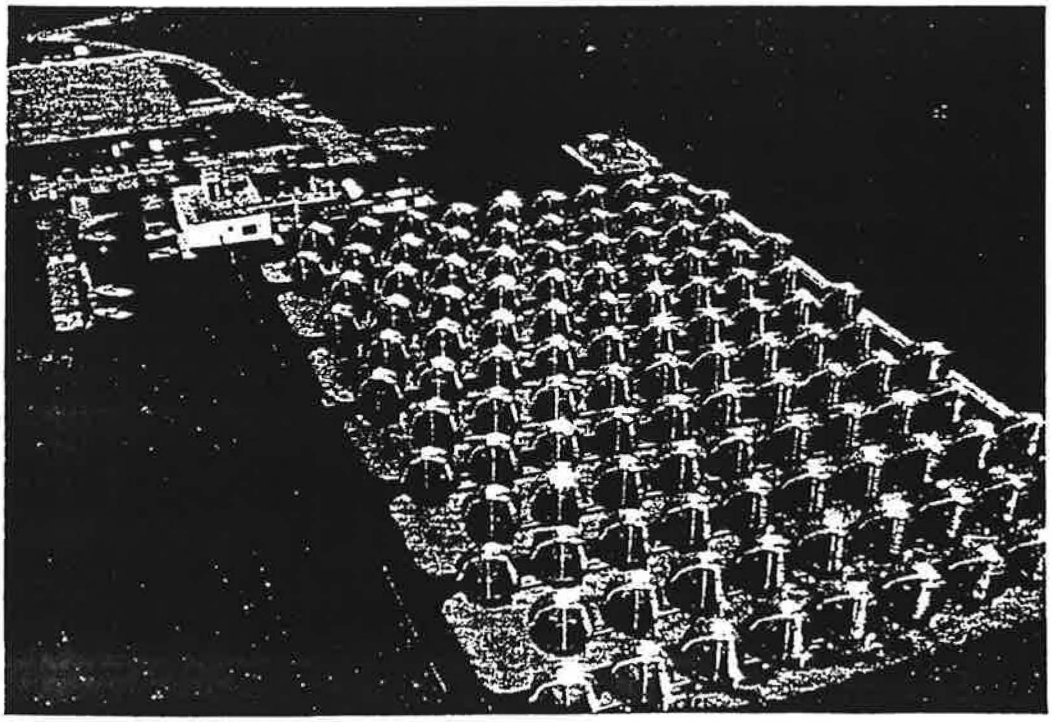

FIG. 24. Two-axis-tracking parabolic dish collectors in Shenandoah Field (courtesy of Sandia National Labortories).

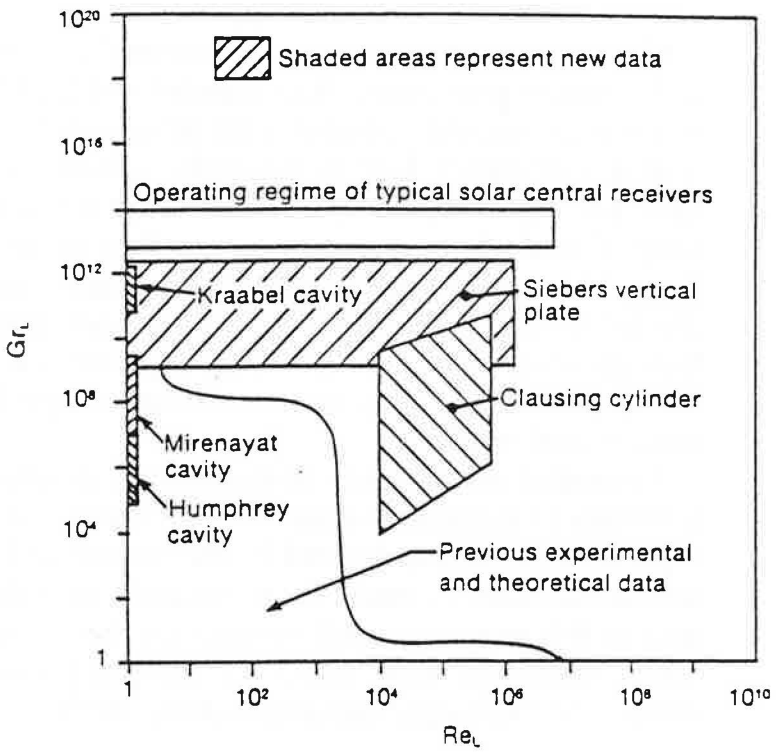

FIG. 25. Range of scaling variables for which convection data are available for solar central receivers (from Abrams [64]).

1. *External Receivers—Central Receiver Systems*

An external receiver essentially is a cylinder formed of vertical flow tubes. The solar radiation reflected from the heliostat field falls on tubes arranged outside the cylinder. The working fluid passes through the radiatively heated tubes. The receiver for the 10-MW Solar 1 prototype solar power plant in Barstow, California is a once-through boiler located atop a 76-m-tall tower that is 7 m in diameter and 12.5 m high (Fig. 26). The average outside temperature of this receiver is approximately 600°C, and wind velocities perpendicular to this receiver range between 0 and 25 m/sec. For these conditions and cylinder diameter, Reynolds numbers are between 0 and 10^8 and Grashof numbers between 10^{12} and 10^{14}.

Heat-transfer experiments simulating these conditions have been performed by Siebers *et al.* [65] using a 3 m by 3 m electrically heated plate located in a wind tunnel. Air velocities ranged from 0 to 6 m/sec and plate temperatures went to 600°C under conditions of forced, natural, and mixed convection. In these experiments the wind was parallel to the plate, whereas in a cylindrical central receiver, winds were perpendicular as well as parallel to the surface. Experimental data were obtained in the range of

Grashof numbers between 1×10^9 and 2×10^{12} and Reynolds numbers between 0 and 2×10^6 for plate-to-ambient absolute temperature ratios in the range of 1 to 2.7. The local Nusselt number, based on the vertical distance from the bottom y and obtained from natural convection experiments, are given by Eqs. (24) and (25).

1. For turbulent natural convection

$$\mathrm{Nu}_y = 0.098\ \mathrm{Gr}_y^{1/3}(T_s/T_{\mathrm{amb}})^{-0.14} \qquad \text{for} \quad 10^9 < \mathrm{Gr}_y < 2 \times 10^{12} \tag{24}$$

2. For laminar natural convection

$$\mathrm{Nu}_y = 0.404\ \mathrm{Gr}_y^{1/4} \qquad \text{for} \quad \mathrm{Gr}_y < 10^9 \tag{25}$$

Equation (24) applies when either the wall temperature or the heat flux is uniform, whereas Eq. (25) applies only when the heat flux is uniform. Transition from laminar to turbulent flow occurs over a range of Grashof numbers, which depends on the temperature ratio (T_s/T_∞) [65]. The experimental results are compared with Eqs. (24) and (25) in Fig. 27.

For conditions with forced convection dominant and the free-stream velocity parallel to the plate the following equations apply.

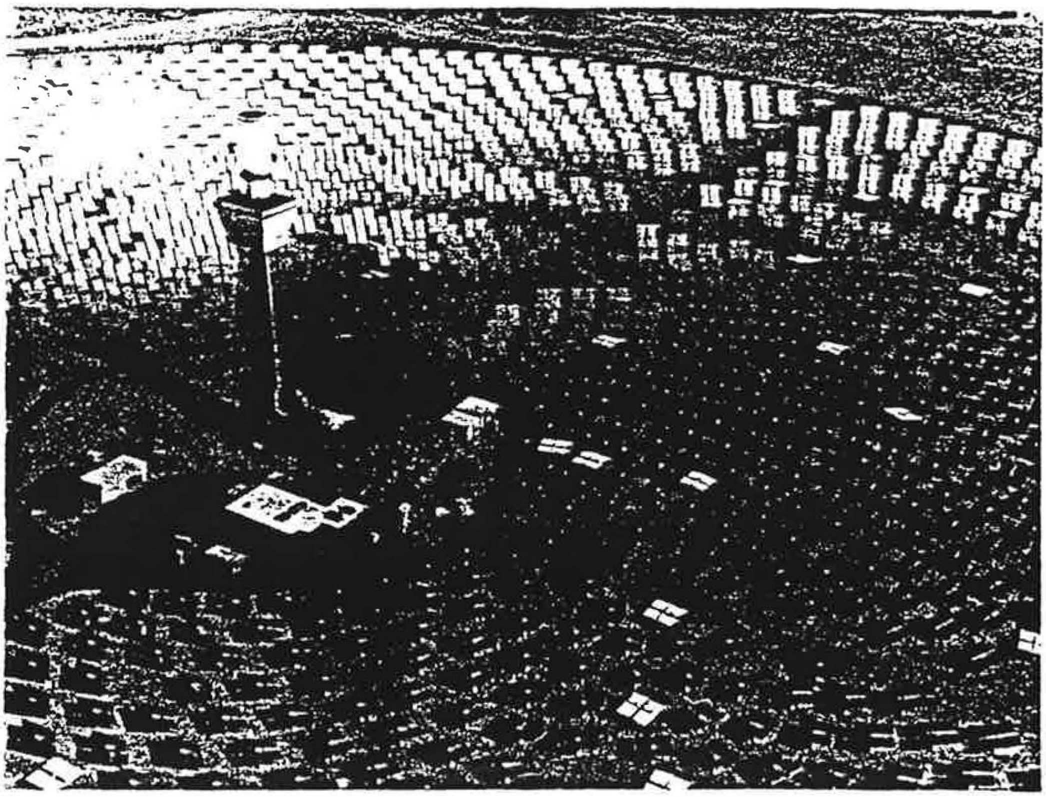

FIG. 26. Photograph of Solar 1, prototype solar power plant at Barstow, California.

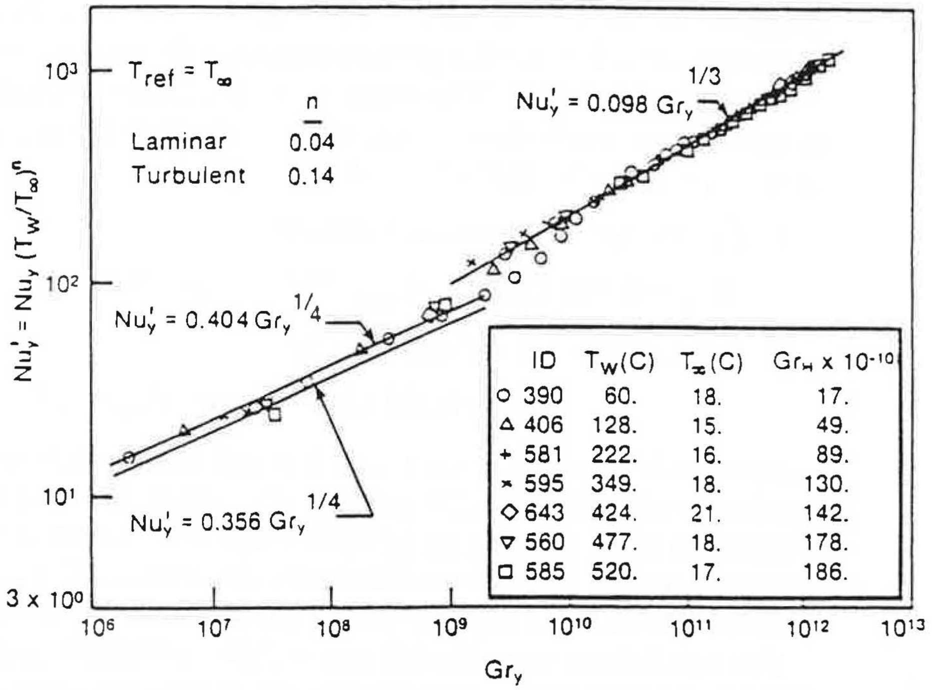

FIG. 27. Correlation of effects of variable properties on natural convection from a vertical surface in air (from Siebers *et al.* [65]).

1. For laminar forced convection

$$Nu_x = 0.453\ Re_x^{1/2}\ Pr^{1/3} \qquad \text{for} \quad Re_x < 2 \times 10^5 \tag{26}$$

2. For turbulent forced convection

$$Nu_x = 0.307\ Re_x^{-0.8}\ Pr^{0.6}(T_s/T_{amb})^{-0.4} \qquad \text{for} \quad Re_x > 2 \times 10^5 \tag{27}$$

In Eqs. (26) and (27), x is the distance from the leading edge of the plate. All fluid properties in Eqs. (24) to (27) should be evaluated at the ambient temperature T_{amb}.

The length-averaged heat-transfer coefficient for natural convection $\bar{h}_{nat}$ is determined from Eqs. (24) and (25). The length-averaged heat-transfer coefficient for forced convection $\bar{h}_{for}$ is determined from Eqs. (26) and (27). For $Gr/Re^2 > 10.0$, the heat transfer should be determined from the equations for natural convection while for $Gr/Re^2 < 0.7$, the forced convection equations are applicable. It is important to note that these equations have been validated only with ambient wind parallel to the plate and orthogonal to the buoyant natural convective flow. Errors resulting from the application of these equations to external receivers not meeting these conditions are not known.

For mixed-convection in the flow regime defined by $0.7 \leq Gr/$

$Re^2 \leq 10.0$, heat-transfer coefficients are calculable to within $\pm 10\%$ by

$$\bar{h}_{mix} = (\bar{h}^3_{nat} + \bar{h}^3_{for})^{1/3} \tag{28}$$

Analysis of the experimental data [65] showed some scatter in the transition region (Fig. 28). A correlation for the average location of transition is

$$Re_{crit} = \frac{4 \times 10^5}{1 + 6.4(Gr_x/Re_x^2)^{1.5}} \tag{29}$$

Because it is difficult to achieve high Grashof numbers in air, Clausing [66] built a cryogenic wind tunnel and used nitrogen at 80 K as the working fluid. The setup achieved simultaneously values of $Gr \approx 3 \times 10^{10}$ and $Re \approx 3 \times 10^6$. Abrams [64] expressed concern about the forced-convection data obtained in the tunnel because turbulence is intense and the velocity distribution is asymmetric, with variations being approximately 23%. But the natural convection correlations proposed by Clausing [67] and Siebers *et al.* [65] agree within 20%.

Natural convection data obtained in the cryogenic tunnel wind a 14-cm-diameter, 28-cm-tall cylinder [67] yielded the following empirical correlations for the average-Nusselt-number base on the height H:

$$Nu_H = 0.082\ Ra_H^{1/3} \times f(T_s/T_{amb}) \quad \text{for} \quad 1.6 \times 10^9 < Ra_L < 10^{12} \tag{30}$$

where $f(T_s/T_{amb}) = -0.9 + 2.4\ (T_s/T_{amb}) - 0.5(T_s/T_{amb})^2$ for $1 < (T_s/$

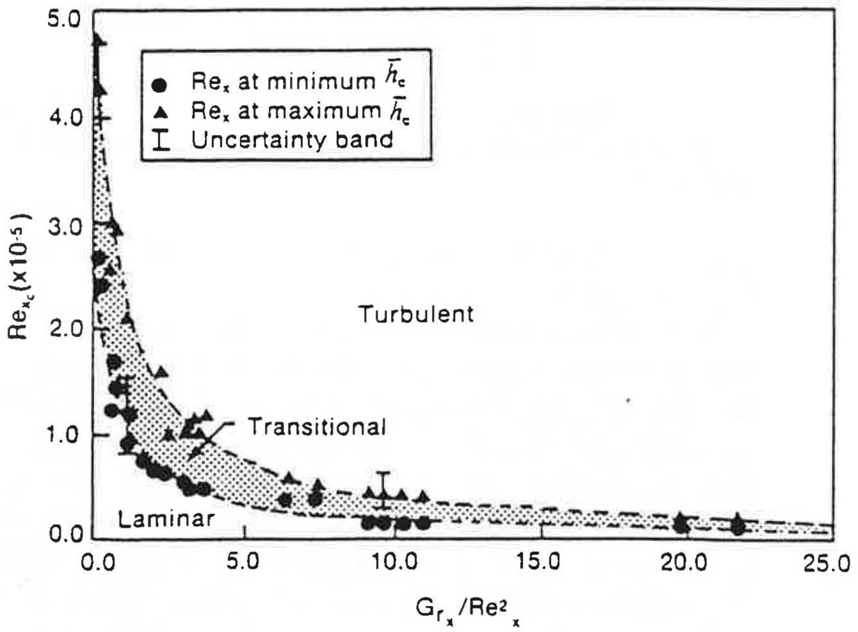

FIG. 28. Effect of Re and Gr on transition in mixed convection from a vertical heated surface (from Siebers *et al.* [65]).

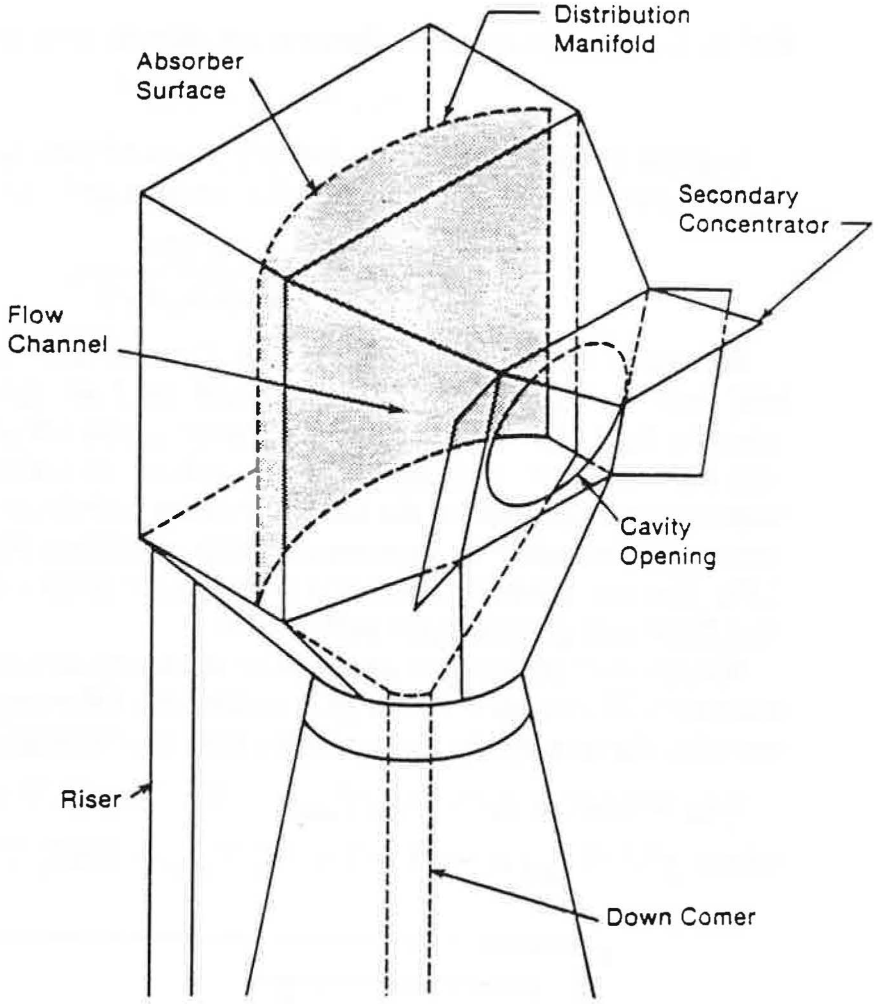

FIG. 29. High-temperature direct absorption receiver cross section for a falling-film molten salt system. The shaded region indicates the location of falling film. From Wang and Copeland [69a]).

$T_{amb}) < 2.6$. In Eq. (30) properties are based on the average temperature $(T_s + T_{amb})/2$.

A computer code to predict the heat loss from external receivers in a steady ambient wind has been developed at Sandia National Laboratory for the cylindrical receiver of Solar 1 [68]. The code can determine the laminar and turbulent mixed-convection heat-transfer coefficient on an external receiver up to the line of separation. Availability of heat-transfer data in the wake region is scant, but measurements in pure forced convection from cylinders [69] have shown that between 30 and 50% of the total convective losses can occur in the wake region. Atmospheric turbulence differs from that in a wind tunnel. The effect of the wake region as well as of atmospheric turbulence on the convection loss has not yet been investigated.

2. *Cavity Receivers—Central Receiver Systems*

In a cavity-type receiver, solar radiation passes through an aperture into the interior. In current designs the interior is lined with flow passages in which the working fluid is heated, but direct contact heat exchangers have also been proposed for use in cavity receivers. Figure 29 shows an advanced design currently under development at the Solar Energy Research Institute (SERI), using direct radiation absorption [69a]. In this design radiation is absorbed by a thin layer of molten salt that flows down an inclined absorber surface. Another direct absorption concept under development at Sandia makes us of solid particles falling through the cavity receiver to directly absorb incoming solar radiation.

The analysis and interpretation of experimental data on the convection heat loss from cavity receivers are more complex than those for external receivers. Clausing [67] postulated a convective flow pattern for cavity receivers and devised a network representation of the loss mechanism. Although the analytic model is oversimplified, it does cover some of the key elements that govern convective losses from cavity receivers. The density of the air entering a cavity solar receiver is typically a factor of three or four larger than the density of the air at the temperature of the refractory surfaces inside the receiver. If the aperture is in the lower portion of the cavity, the air inside the cavity will be stratified and relatively stagnant in the upper region. Thus it is reasonable to divide the volume into a convective and a stagnant zone (Fig. 30). The convective heat loss from a cavity receiver depends on two factors: (1) the ability of buoyancy to transfer mass and energy across the aperture and (2) flow across the aperture because of wind. Preliminary experimental results indicate that the thermal resistance between the interior cavity walls and the air inside the cavity

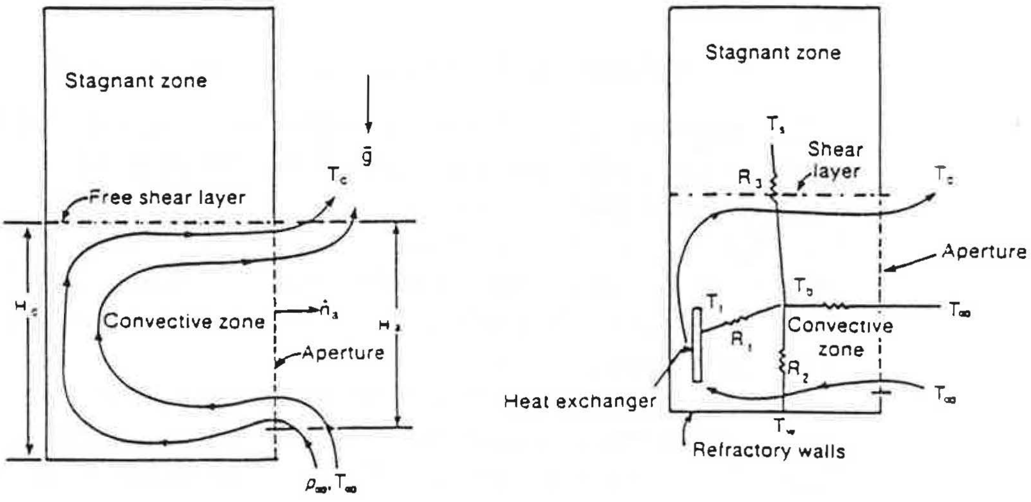

FIG. 30. Postulated flow pattern for cavity-type receiver (from Clausing [67]).

controls the convective heat loss and that the external wind has relatively little effect. By performing a simple energy balance on the flow through the aperture of the receiver, the convective loss q_c can be expressed as

$$q_c = \dot{m}c_p(T_c - T_{amb}) = (\rho_\infty V_a A_a)c_p\,\Delta T \tag{31}$$

In Eq. (31) T_c is the average gas temperature inside the cavity, A_a the aperture area, and V_a the average velocity of the inflow, which can be expressed according to Clausing [67] by

$$V_a = \frac{1}{2}\left[V_b^2 + \left(\frac{V_{wind}}{2}\right)^2\right]^{1/2} \tag{32}$$

where

$$V_b = [g\beta(T_c - T_{amb})H]^{1/2} \tag{33}$$

and L equals the projected vertical aperture height.

Another expression for q_c, derived from the thermal network model in Fig. 30, is

$$q_c = \bar{h}_t A_t(T_t - T_b) + \bar{h}_w A_w(T_w - T_b) + \bar{h}_s A_s(T_s - T_b) \tag{34}$$

The subscripts t, w, and s refer to the heat exchanger surface, wall, and stagnation region, respectively (Fig. 30).

The average heat-transfer coefficients between the inner surfaces and the air can be estimated from the semiempirical relation given by Clausing [67],

$$\overline{\mathrm{Nu}_H} = 0.082\ \mathrm{Ra}_H^{1/3}\,[-0.9 + 2.4\,(T_s/T_{amb}) - 0.5(T_s/T_{amb})^2]\,f(\phi) \tag{35}$$

where

$$f(\phi) = 1 \qquad \text{for} \quad 0^\circ < \phi < 135^\circ$$

and (36)

$$f(\phi) = 0.66\,[1 + (\sin\phi)/\sqrt{2}] \qquad \text{for} \quad \phi > 135^\circ$$

The angle ϕ in Eq. (35) is the zenith angle between the normal to the heat-transfer surface and the zenith. For a heated downward facing surface $\phi = 180^\circ$ and $f(\phi) = 0.66$. Equation (35) holds for $\mathrm{Ra}_H > 1.6 \times 10^9$ and $1 < (T_s/T_{amb}) < 2.6$. The above predictions by Clausing [67] were found to be in close agreement with experimental data obtained by McMordie [70] on a full-scale cavity receiver and Mirenayat [71] in a laboratory scale electrically heated cavity.

Experimental studies of natural convection in two-dimensional open cavities have been conducted by Sernas and Kyriakidas [72], Chen and Tien [73], Hess and Henze [74], and Humphrey *et al.* [75] and in a three-dimensional cavity by Kraabel [76]. Sernas and Kyriakidas, Chen and Tien, and Hess and Henze studied convection from cavities in which only the back wall was heated. Sernas and Kyriakidas and Chen and Tien found that the heat transfer from a heated back wall of height H approached that for the heat transfer from a heated vertical plate of similar height in a semi-infinite medium for $\mathrm{Ra}_H > 10^7$. Hess and Henze examined the effect of baffles on the heat transfer from an open cavity in the Rayleigh range $3 \times 10^9 \leq \mathrm{Ra}_H \leq 3 \times 10^{11}$. The baffles were placed at the top and bottom of the cavity aperture and extended one quarter of the height of the cavity. Even though the baffles reduced the effective aperture area of the cavity by 50%, the heat transfer from the cavity was only reduced by 10%. Humphrey, Sherman, and Chen conducted experiments in a cavity in which the floor and back wall of the cavity were both heated. Their experiments were conducted for $\mathrm{Ra}_H = 2.9 \times 10^7$ and included studies of the effects of cavity tilt angle, external forced convection flow, and cavity aspect ratio. They found the natural convection flow to be unsteady with periodic oscillations at frequencies of 2–5.5 Hz.

Kraabel [76] conducted his experiments using a 2.2 m cubical cavity with electrical heating elements on all of the interior surfaces of the cavity. The aperture was vertical and was one face of the cube. Automatically positioned probes in the aperture plane measured velocity and temperature distributions. The convective loss was determined by (1) integrating the product of the temperature and velocity distributions and by (2) calculating the difference between the electric power input and the power radiated from the cavity. The two results were in good agreement. The second method, being more rapid, was used for most of the convective loss determinations. The cavity wall temperature was varied from 90° to 750°C, corresponding to Grashof number variations in the range from 9.4×10^{10} to 1.2×10^{12}. Flow visualization revealed secondary flow patterns characterized by a pair of counter-rotating vortices that fully occupied the upper half of the cavity. The total convective losses were correlated by

$$\overline{\mathrm{Nu}_L} = 0.088\ \mathrm{Gr}_L^{1/3}(T_s/T_{\mathrm{amb}})^{0.18} \tag{37}$$

where the physical properties in the Nusselt and Grashof numbers are evaluated at the ambient temperature. Kraabel found that Eq. (37) also fitted Mirenayat's [71] measurements of the convective losses from 0.2-m and 0.6-m cavities, thus being valid to Gr_L as low as 5×10^7. In Eq. (37), the appropriate heat-transfer area to calculate convective loss is the entire interior surface area of the cavity. Kraabel's experiments were conducted with the cavity protected from environmental winds by large curtains. However, on occasion winds arose during tests without discernible effect upon the convective loss. This finding is consistent with McMordie's

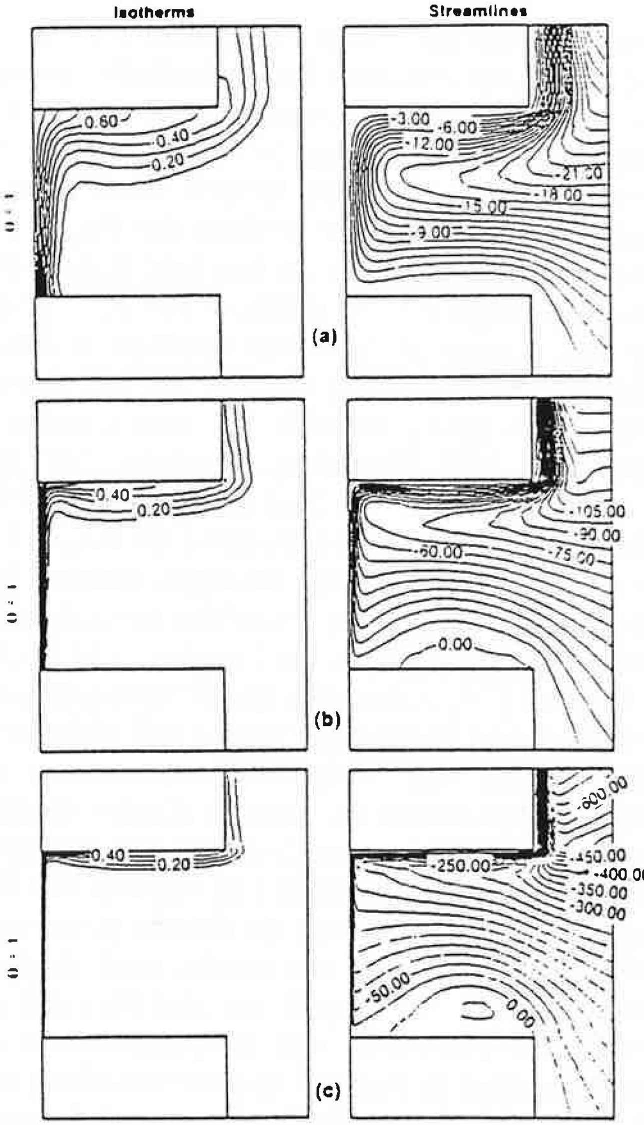

FIG. 31. Calculated flow pattern in an open cavity: (a) $Ra_H = 10^5$, (b) $Ra_H = 10^7$, (c) $Ra_H = 10^9$ (from Chen and Tien [78]).

experience at the Central Receiver Test Facility [70]. But so far, there are not sufficient measurements to conclude that cavity convective losses are unaffected by ambient wind.

A computer model that predicts laminar natural convection heat loss from two dimensional cavities has been developed by LeQuere *et al.* [77]. They found that the flow in a bottom heated cavity was unsteady for $Ra_H > 10^6$. Calculations have also been performed by Chen and Tien [78] for a two-dimensional cavity with a heated back wall in laminar flow. They calculated the steady flow characteristics over the range $1 \times 10^3 \leq Ra_H \leq 1 \times 10^9$.

Humphrey, Sherman, and To [79] extended the work of LeQuere, Humphrey, and Sherman to turbulent flow and compared their calculations with the experimental measurements from a small air-filled cavity. Good agreement was found between measurements and predictions of the velocity and temperature fields. Calculated results that show the flow patterns in the cavity studied by Chen and Tien [78] are shown in Fig. 31.

Boehm [80] summarized and evaluated available data of thermal losses from central receivers and also recommended Eq. (37) to predict the natural convection heat loss from cavity receivers, for the range $10^5 <$ Gr $< 10^{12}$ with the height of the cavity as the significant length and with fluid properties based on the ambient temperature T_∞. Boehm [80] also reported that Kraabel compiled natural convection results in air for flat plates, vertical cylinders, and cavities whose apertures are equal in height to the inner back panels and recommended the equation

$$\overline{\mathrm{Nu}_H} = 0.052\,\mathrm{Gr}_H^{0.36} \tag{38}$$

with properties evaluated at T_∞. Available experimental data are compared with Eq. (38) in Fig. 32. A comparison of the correlation given by Eq. (38) with experimental field data from cavity receivers is shown in Fig. 33. Data for the molten salt alternative central receiver (ACR), the molten salt electric equipment (MSEE), and the sodium-cooled cavity receiver (SCCR) are shown in Fig. 33. The maximum estimated wind effects are shown by an error bar. A similar comparison of Eq. (38) with available data from external receivers is shown in Fig. 34. Here are shown data for the Advanced Sodium Receiver (ASR) of the International Energy Agency (IEA).

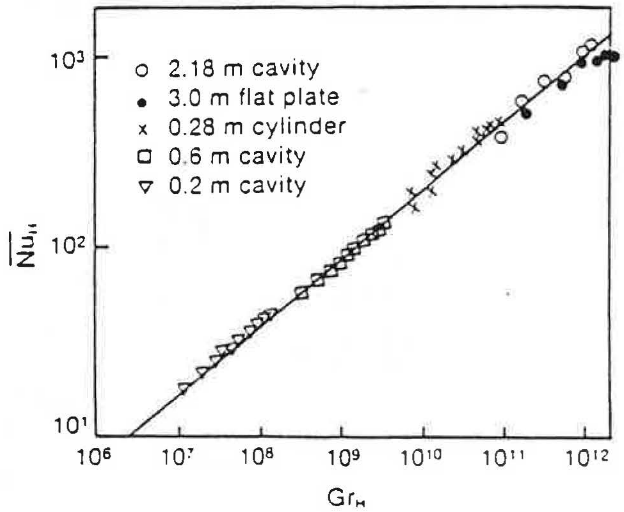

FIG. 32. Results of natural convection studies in air for length scale, H, measured significant length in vertical direction and fluid properties evaluated at ambient temperature (from Boehm [80]).

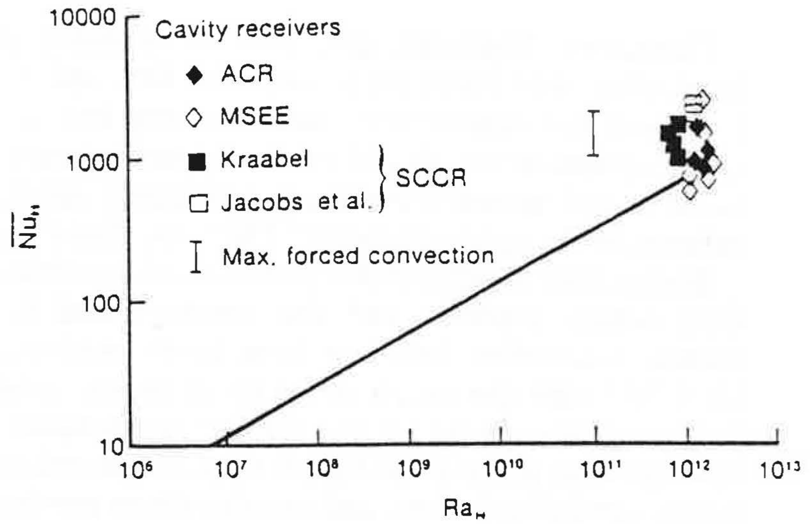

FIG. 33. Experimental convective loss results for cavity receivers (from Boehm [80]).

The relative importance of natural convective losses from cavity receivers can be reduced by operating the receivers at high flux levels. Anderson [81] has examined convective heat and mass transfer in a high-flux receiver with a falling-film on the absorber panel (Fig. 29). The performance characteristics of a carbonate molten-salt film with $(T_i + T_o)/2 = 700°C$ are shown in Fig. 35. The temperature difference between the falling film and the heated wall is plotted as a function of film Reynolds number and solar flux in Fig. 35a, and the relative importance of natural convective losses from the surface of the film is plotted in Fig. 35b. As the level of the solar flux falling on the film is increased i.e., as the film

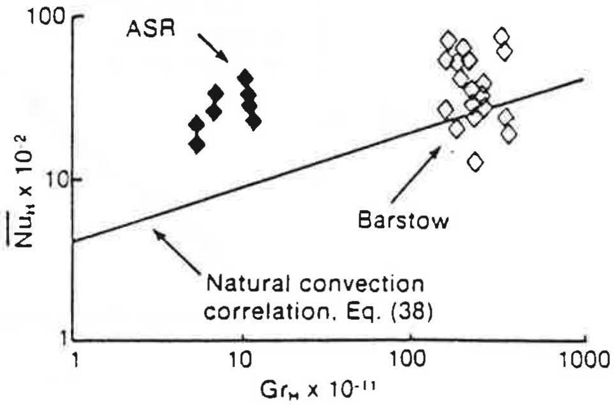

FIG. 34. Existing convective loss results for external receivers (from Boehm [80]).

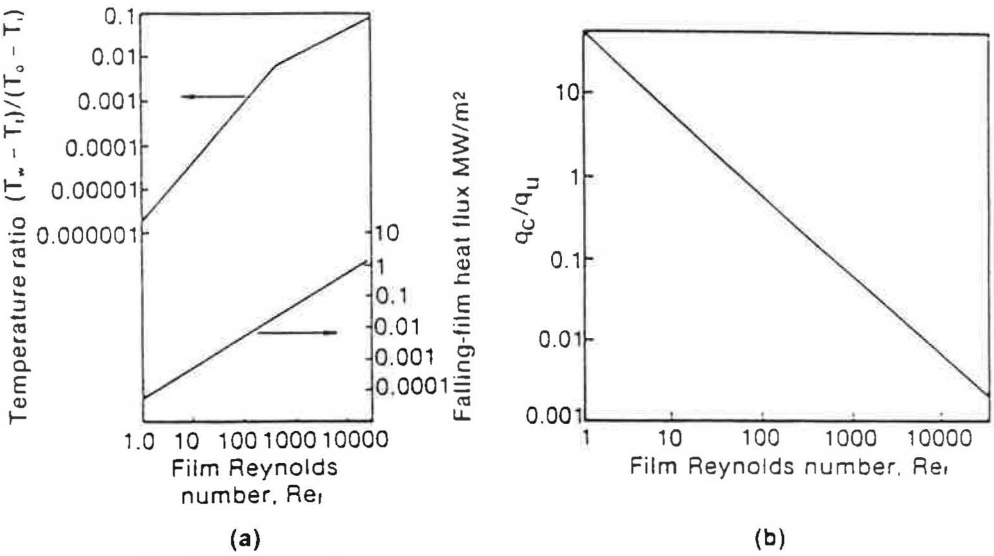

FIG. 35. Temperature distribution and heat flux in a falling-film receiver with Pr = 1 and $(T_o - T_i) = 400°C$. (a) Film temperature and heat flux versus Reynolds number Re_f. (b) Convective-to-nonconvective loss ratio versus Reynolds number Re_f (from Anderson [81]).

Reynolds number is increased) the relative importance of natural convection losses decreases substantially.

An interesting concept for suppressing natural convection into and out of a central receiver has been proposed by Taussig [82]. Called the aerowindow, it injects a transparent gas stream across the receiver aperture, thereby insulating the cavity from the surroundings. Aerowindows generate a vortex inside the receiver when Gr/Re^2 is between 1 and 10. In this regime both natural and forced convection are important, but no experimental data are available. A numerical analysis of the laminar regime by Humphrey and Jacobs [83] suggests that small downward flows are more effective in reducing thermal loss than comparable upward flows.

3. *Cavity Receivers — Parabolic Dish Systems*

In contrast to central receiver systems, which focus the energy collected by a large heliostat field upon a single receiver, distributed solar energy collection systems utilize many small receivers connected together to collect the energy delivered from each focusing reflector. The convective transport process in distributed collection systems is more complicated than in central receiver systems because the orientation of each receiver changes as the collector tracks the sun throughout the day. The Shenandoah project, located at Shenandoah, Georgia consists of a field with 120 parabolic dishes, each with a cavity-type receiver [84]. The basic configuration of the parabolic dish/receiver system is shown in Fig. 36. A detail of the cavity receiver design for the Shenandoah project is shown in Fig. 37. The interior wall of the cavity is covered by an elliptical coil assembly. The outer portion of the cavity is shrouded by a wind shield to reduce convective losses. Kugath *et al.* [85] measured thermal losses from this receiver by pumping hot fluid through the receiver when the collector was not tracking the sun. Conduction losses were determined by blocking the aperture opening, and radiative losses were calculated based upon the cavity geometry and temperature distribution. Natural convection losses were determined by subtracting conduction and radiative losses from the total losses measured during the test. Natural convection losses from the receiver are shown as a function of the receiver declination angle in Fig. 38. The minimum losses occur when the cavity is pointing directly downward with a declination angle of 90°. Kugath *et al.* [85] also measured the effects of a 10 mph wind upon receiver losses and found that the total heat loss was strongly dependent upon cavity orientation. The maximum heat losses occurred when the forced flow was directed at the aperture of the cavity and were four times the magnitude of the pure natural convection losses that were measured in the absence of any wind. The following empirical correlation for free-convection loss from a cavity as a function of cavity

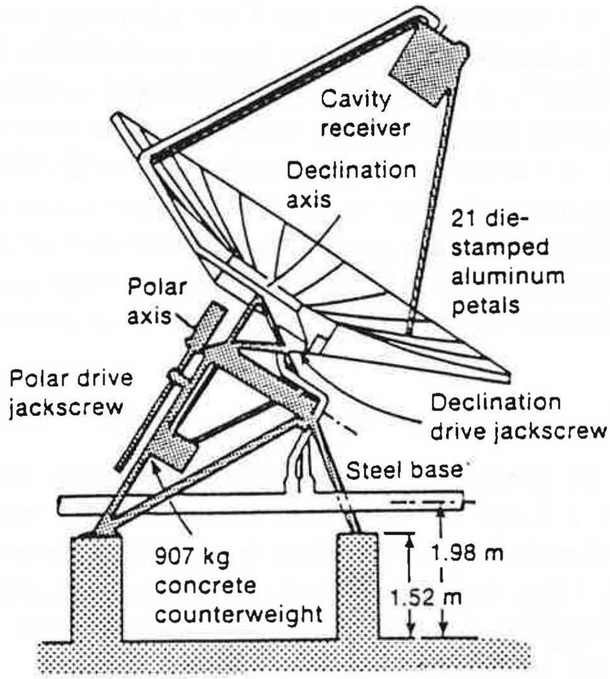

FIG. 36. Schematic diagram showing receiver and parabolic dish in use in the solar thermal cogeneration project at Shenandoah, Georgia.

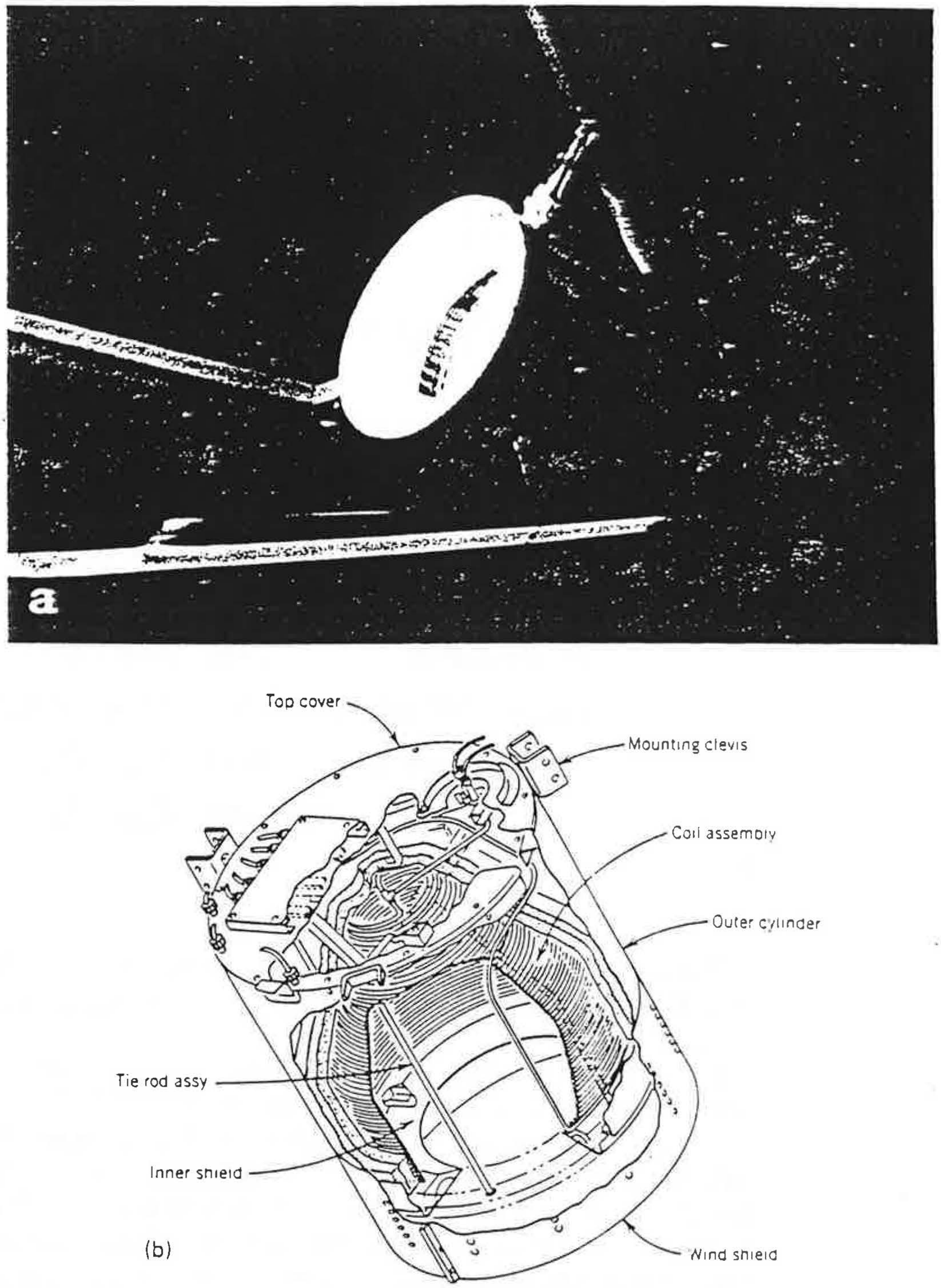

FIG. 37. Cutaway view of a cavity (focal plane) receiver (courtesy of Sandia National Laboratories).

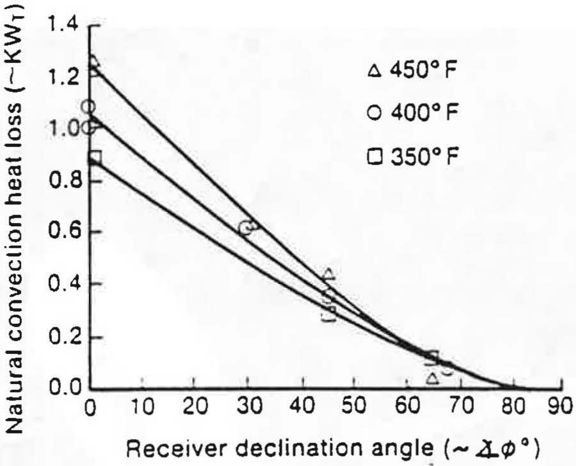

FIG. 38. Curves of natural convection losses versus receiver declination angle (from Kugath *et al.* [85]).

orientation has been proposed by Koenig and Marvin [86]:

$$\overline{\mathrm{Nu}_L} = 0.52P(\phi)K^{1.75}\,\mathrm{Ra}_L^{0.25} \tag{39}$$

$$P(\phi) = \cos^{3.2}\phi \qquad \text{when} \quad 0° \le \phi \le 45° \tag{40}$$

$$P(\phi) = 0.707\cos^{2.2}\phi \qquad \text{when} \quad 45° \le \phi \le 90°$$

$$K = R_{\mathrm{aper}}/R_{\mathrm{cav}} \qquad \text{when} \quad R_{\mathrm{aper}} \le R_{\mathrm{cav}} \tag{41}$$

$$K = 1, \qquad \text{when} \quad R_{\mathrm{aper}} = R_{\mathrm{cav}}$$

and

$$L = \sqrt{2}R_{\mathrm{cav}} \tag{42}$$

The characteristic length used in the evaluation of the Nusselt number and Rayleigh number in (39) is $\sqrt{2}R_{\mathrm{cav}}$, where R_{cav} is the radius of the cavity.

Harris and Lenz [87] calculated the performance of distributed dish cavity receivers as a function of cavity geometry. Cavity geometries considered in their study are shown in Fig. 39. Natural convection losses were calculated by using Eq. (39). They found cavity losses to be 12% of the energy entering the cavity. For a cavity temperature of 550°C these cavity losses were due to equal contributions from radiation and natural convection. It was also found that, for the same cavity aperture and insulation thickness, cavity geometry had almost no effect on system efficiency.

Because of the complexity of the convective heat transfer process in open cavities, Somerscales and Kassemi [88] have suggested the use of an electrochemical technique that measures mass transfer rather than heat transfer to determine the convective-loss characteristics of the cavity. Somerscales *et al.* suggest the use of the electrochemical technique because it has the potential to be simpler, cheaper and faster than heat transfer measurements. Heat transfer can then be inferred based upon the analogy between mass and heat transfer. Somerscales and Kassemi [88] examined mass transfer in nine cylindrical cavities with diameter to height ratios in the range $\frac{1}{2} \leq D/H \leq 2$. They found that the comparison of their mass transfer results with heat transfer results was not entirely satisfactory because:

1. There was a considerable difference in the range of values of D/H used in the heat-transfer and mass-transfer experiments that were compared in their study. The heat-transfer measurements were made with deep cavities (D/H small), whereas in the mass-transfer tests the cavities were shallow (D/H large).
2. The Schmidt number of the fluids was many times greater than the Prandtl number of the fluids used in the heat-transfer tests.
3. It was not certain that comparable flow regimes were being considered.

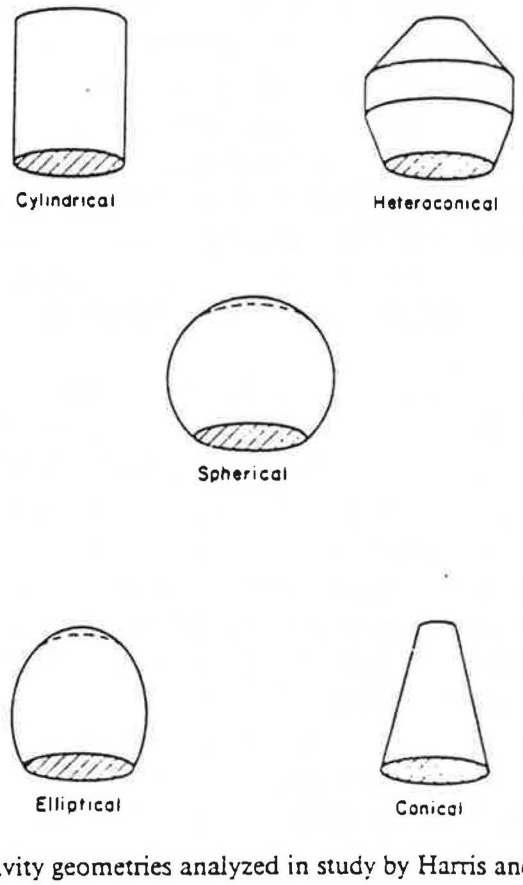

FIG. 39. Cavity geometries analyzed in study by Harris and Lenz [87].

Additional research is necessary to clarify their results and provide correlations for natural convection losses from cavity-type receivers with changing orientation relative to the force field.

III. Natural Convection in Solar Buildings

Solar energy can be used to provide a large fraction of a buildings energy requirements by designing buildings to act as efficient solar collectors, (Balcomb *et al.* [89], Jones, and McFarland [90]). In heating applications, sunshine enters south facing windows and strikes absorbing surfaces, which heat up and warm the air in the adjacent room. This warm air is then moved largely by natural convection to the remainder of the house where it is either used immediately for heating or stored for later use. In ventilation cooling applications, the direction of heat transfer is essentially reversed. Cold night air is introduced through open windows or vents and used to remove heat from the interior of the building. Natural convection plays an important role in the transport of energy within the building, in both heating and cooling applications. Thermal network models for solar buildings are similar to those for flat-plate collectors with the exception that horizontal surfaces play an important role in determining the heat-transfer characteristics of the building. In addition, a successful design for a solar building includes a unique performance criterion that is not required of active solar energy systems. A solar building should not only provide a high level of thermal efficiency, it must also provide for the thermal comfort of the occupants of the building. A fundamental understanding of natural convection in enclosures with complicated geometries and complicated thermal boundary conditions is important to designing efficient and comfortable solar buildings.

Common types of solar building components have been described previously (Fig. 5) and include direct gain, indirect gain and ventilation cooling applications. Simple thermal models for these configurations are shown in Fig. 40. In direct gain applications, one must predict thermal stratification, temperature distributions, and heat transfer in a single zone enclosure as a function of the location (horizontal or vertical wall) at which heating or cooling occurs. In indirect gain applications, one would like to know how the geometry of openings affects the transport of energy between building zones. Finally, in ventilation cooling applications one would like to know how opening geometry affects the transport of energy between the interior and exterior of the building. An understanding of these transport processes is necessary for the sizing and orientation of

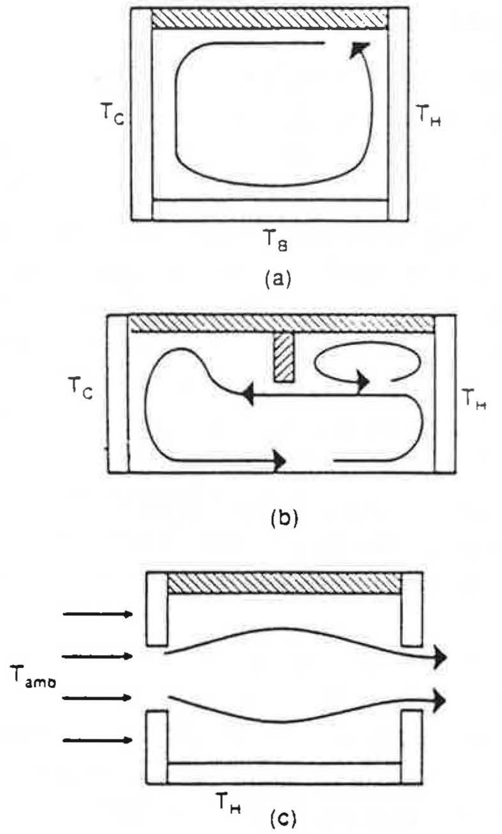

FIG. 40. Simple thermal models for solar building applications; see also Fig. 3. (a) Direct gain, (b) indirect gain, (c) ventilation cooling.

thermal storage and apertures that maximize the performance of the building. In this section we will examine the contribution of natural convection to heat transfer through the building envelope, heat transfer within a single zone, and heat transfer between zones in solar buildings. Infiltration, and forced convection heat transfer also are important in many building applications but are not considered here.

A. BUILDING ENVELOPE

The envelope of a building consists mostly of planar surfaces such as walls and windows. The total heat loss under given climatic conditions depends on infiltration rates, heat losses through walls and their insulation, and heat losses and gains through windows. Natural convection plays an important role in all these loss mechanisms.

1. *Single-Pane Windows*

Single-pane windows constitute one of the largest sources of heat loss from buildings, especially when they face north. A single-pane window can be idealized as a vertical surface between two air reservoirs.

Lock and Ko [40], Anderson and Bejan [41], and Viskanta and Lankford [43] have examined combined natural convection/conduction heat transfer through a vertical plate separating two semi-infinite fluid reservoirs. Sparrow and Prakash [44] conducted a numerical analysis of an enclosure with AR = 1, which was coupled through one conductive wall to an external natural convection flow. The results of these studies can be used to develop a general description of heat transfer through a single-pane window. Figure 41 compares the relative importance of radiation losses to internal convection heat losses through a single pane window as a function of external wind velocity. It can be seen that the radiation and convection heat losses are of the same order of magnitude in many building applications.

The natural convection heat-transfer coefficient used in Fig. 41 for zero external wind is based upon the conjugate conductive/convective analysis of Anderson and Bejan [41]. The natural convection heat-transfer coefficient for high external wind is based upon the boundary layer analysis of Gill [91] and Bejan [92], assuming that the window's surface temperature approaches the external air temperature. The gradual decrease of $\bar{h}_{rad}/\bar{h}_{conv}$ with increasing temperature difference results from the dependence of h_{conv} upon $(T_H - T_C)^{1/4}$. The shift in the two curves for different wind velocities also results from the dependence of $\bar{h}_{conv}$ upon temperature difference.

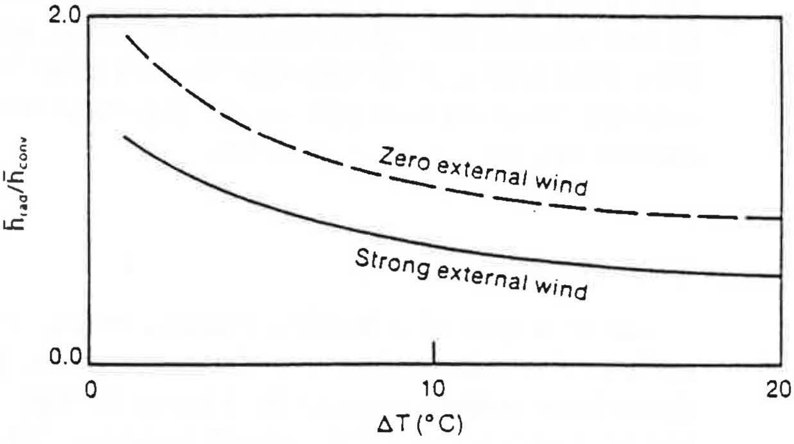

FIG. 41. Relative contributions of convective and radiative heat transfer through a single-pane window: $\bar{h}_{rad} = \sigma(T_H^4 - \bar{T}_{window}^4)/(T_H - T_C)$, $T_C = 0$°C.

2. *Double-Pane Windows*

Most new buildings in the U.S. have double pane windows because of their superior insulating qualities. Korpela *et al.* [93] carried out a series of numerical experiments on high-aspect-ratio enclosures with the specific application of double-pane windows in mind. Their primary goal was to determine the optimum spacing between panes for minimum heat loss. They found that as the AR was increased at constant window height, the flow in the cavity exhibited, in succession, a conduction-dominated unicellular flow, a multicellular flow, and finally reversion to a unicellular flow. The final unicellular flow was not a boundary-layer flow but was in the transition regime between conduction- and convection-dominated heat transfer. The minimum heat transfer was found at the onset of multicellular flow. Korpela *et al.* [93] suggest the following formula for calculating the optimum AR for minimum heat transfer as a function of Gr_H:

$$\mathrm{AR}^3 + 5\,\mathrm{AR}^2 = 1.25 \times 10^{-4}\,\mathrm{Gr}_H \tag{43}$$

where Gr_H is the Grashof number and equals $g\beta H^3\,\Delta T/\nu^2$ and H is the height of the cavity. ElSherbiny *et al.* [19] conducted an extensive series of experiments in large aspect ratio enclosures. They found that for AR > 40, the transition between conduction and convection dominated heat transfer is independent of AR. Therefore, the optimum spacing for large AR, double-pane windows depends only on the temperature difference across the window and is independent of the height of the window. For large AR Eq. (43) reduces to

$$L_{\mathrm{opt}} = 20(\nu\alpha/g\beta\,\Delta T)^{1/3} \tag{44}$$

It is important to note that the (constant H/variable L) case considered by Korpela, Lee, and Drummond [93] is different from the (constant L/variable H) case previously considered by Bejan [94]. Bejan's analysis assumes boundary-layer flow and considers the dependence of Nu_L on AR with fixed plate spacing L and variable height H. Korpela *et al.* limited their study to Gr_H numbers in the transitional region between conduction- and boundary-layer dominated heat transfer and considered the dependence of Nu_H upon AR with fixed H and variable L. The analysis by Korpela *et al.* predicts the combination of Gr_H and AR that produces minimum heat transfer at fixed H, whereas the analysis by Bejan gives the combination of Gr_L and AR that produces maximum heat transfer at fixed L.

B. SINGLE-BUILDING ZONES

An understanding of the impact of complicated boundary conditions upon the natural convection pattern in enclosures resembling a room (i.e., enclosures with aspect ratios of the order of one) is important to predict natural convection heat transfer within a building. In building applications one commonly encounters nonrectangular geometries with nonuniform thermal boundary conditions with surfaces that are often not perfectly smooth or straight. Flow patterns can be complicated by the presence of internal obstructions such as wall hangings, window coverings, and furniture. The thermal boundary conditions in building applications are generally three dimensional and can involve heating and cooling of several surfaces. In comparison with a flat-plate collector that has only one heated surface at the bottom and one cooled surface at the top, any building surface can be thermally active, regardless of its orientation.

Heating and cooling of vertical surfaces produce an overall circulation pattern similar to that seen in vertical flat-plate collectors (Fig. 9a). Floor heating generates unstable vertical temperature gradients that can lead to the formation of thermal plumes or Benard circulation similar to that found in a horizontal flat-plate collector (Fig. 9c). In buildings, combinations of horizontal and vertical temperature gradients can occur within a single building zone. The flows generated by these two types of temperature gradients compete with each other and their combined action determines the heat transfer, temperature distributions, and thermal stratification levels in the buildings.

1. *Triangular Spaces*

Most studies of single-zone building heat transfer have been for rectangular enclosures, whereas many building applications include nonrectangular spaces. Notable exceptions to the rectangular studies are experimental studies of triangular enclosures by Flack *et al.* [95], Flack [96], and Poulikakos and Bejan [97]. In addition, Akinsete and Coleman [98] and Poulikakos and Bejan [99] conducted numerical studies of natural convection in triangular enclosures. Triangular spaces occur in A-frames, attics, and rooms with cathedral ceilings or clerestories (Fig. 5). Flack *et al.* [95] measured the heat transfer in an air-filled horizontal isosceles triangular enclosure by using a Wollaston prism/Schlieren interferometer. The base of the enclosure was insulated and the upper enclosure had one isothermal heated side and one isothermal cooled side. Their experiments showed that the average Nusselt number was within 20% of that for a rectangular enclosure, if the heated side of the triangle is used as the characteristic length dimension. However, a strong conduction-dominated region formed near the apex of the enclosure due to the physical proximity of the hot and cold surfaces in that region. This conduction-dominated region resulted in a sharp increase in heat transfer on the hot wall near the apex.

Flack [96] used the same apparatus previously used by Flack *et al.* [95] to examine the case when both upper sides of the enclosure were at the same temperature, while the floor of the enclosure was maintained at a different temperature. For stable heating (hot ceiling, cold floor) the heat transfer varied at most by 10% from a pure conduction solution. Four horizontally aligned Bernard cells formed along the axis of the enclosure during unstable heating (hot base, cold sides). The axis of rotation of the Benard cells was perpendicular to the long axis of the enclosure. Poulikakos and Bejan [97] considered natural convection in an air- or water-filled unstably heated right-triangular enclosure. The flow was found to be turbulent during the water experiments because of the high Rayleigh numbers ($\mathrm{Ra}_H \sim 10^8$) that were reached during the water experiments. Poulikakos and Bejan [97] report the following correlation for their air experiments

$$\overline{\mathrm{Nu}}_H = 0.345\ \mathrm{Ra}_H^{0.3} \quad \text{for} \quad H/L = 0.207 \quad \text{and} \quad 10^6 \geq \mathrm{Ra}_H \geq 10^7 \qquad (45)$$

Akinsete and Coleman [98] conducted a numerical study on a stably heated right-triangular enclosure with $800 < \mathrm{Gr}_L < 6400$, $0.0625 < \mathrm{AR} \leq 1$ and $\mathrm{Pr} = 0.733$. Like Flack [96], they determined that heat transfer was conduction dominated for high-aspect-ratio enclosures, indicated by a drastic drop in heat transfer as AR was increased. Poulikakos and Bejan [99] conducted a two-dimensional transient numerical study of an isosceles triangular enclosure with cold upper sides and a warm base. They assumed that the fluid in the enclosure was initially isothermal at the base temperature T_H, and at time $t = 0$ the upper sides of the enclosure were suddenly cooled to T_G. For large AR enclosures, the transient Nusselt numbers initially overshot their steady state values. This numerical solution assumed the presence of two symmetrical axially oriented rolls in contrast to the transversely oriented rolls observed by Flack [96].

2. *Heating and Cooling of Vertical Surfaces in Enclosures*

The thermal boundary conditions in buildings heated by direct solar gain are generally three dimensional, involve both horizontally and vertically imposed temperature gradients, and include local and uniformly distributed heat sources. Adjacent surfaces at different temperatures can produce interactive flows. One recent study by Sparrow and Azevedo [100] investigated whether heat transfer from a vertical plate would be different if the edges were unshrouded (permitting possible lateral inflow of fluid toward the plate) or if they were shrouded (thereby blocking the possible inflow). Figure 42 illustrates the four lateral-edge configurations investigated as well as the basic vertical flat-plate assembly. Configuration I corresponds to the case of unshrouded and insulated lateral edges, configu-

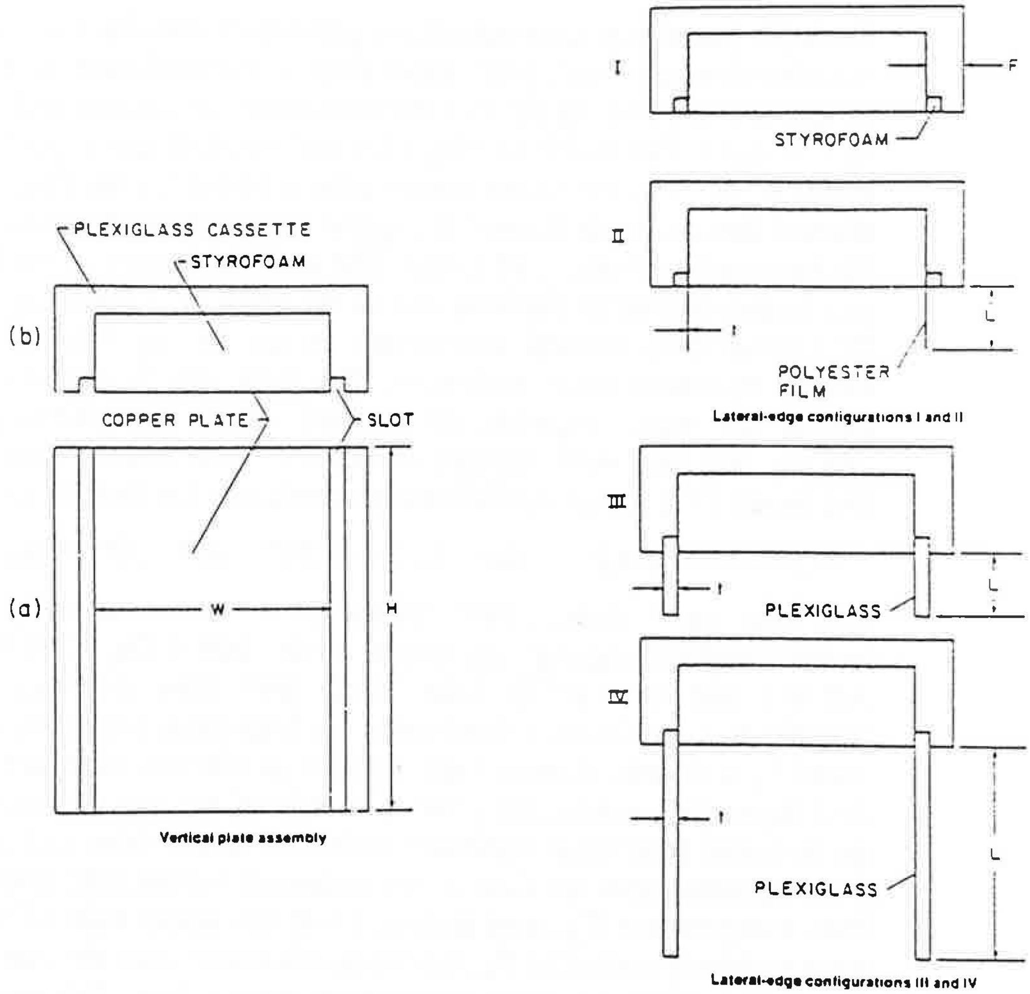

FIG. 42. Lateral-edge configurations used by Sparrow and Azevedo [100].

ration II corresponds to a hydrodynamic blockage with low thermal mass, while configurations III and IV are similar to II but with a different material. The dimensions defining the lateral-edge configurations are displayed in Table III, corresponding to the symbols in Fig. 42.

Experiments were performed under conditions corresponding to Rayleigh numbers from about 8.5×10^7 to 10^9 with Prandtl numbers essentially constant at about 5. The results of this study are plotted in Fig. 43; the data are correlated by the equation

$$\overline{\mathrm{Nu}}_H = 0.623\ \mathrm{Ra}_H^{1/4} \tag{46}$$

where the pertinent length dimension in the Rayleigh number is the height of the plate H. The key conclusion drawn by the authors is that lateral-edge effects are negligible for plates with ratios of height to width of less than 1.5

TABLE III

DIMENSIONS DEFINING THE LATERAL-EDGE CONFIGURATIONS[a]

Case	L	t	F
I	—	—	1.4
II	2.54	0.011	1.4
III	2.54	0.635	1.4
IV	8.50	0.635	1.4

[a] All dimensions are in centimeters.

and insensitivity to lateral-edge effects may be extrapolated to a height to width ratio of as much as 4.

Bohn *et al.* [101] examined heat transfer in a cubical enclosure with three-dimensionally heated and cooled vertical walls and found that the temperature in the middle of the enclosure was a strong function of the temperature distribution on the vertical walls of the enclosure. By using the area-weighted bulk-temperature difference defined by

$$\Delta T_b = T_H - T_b, \qquad T_b = \sum_i T_i A_i / \sum_i A_i \tag{47}$$

in the definition of the heat-transfer coefficient it was possible to express the heat-transfer results for any combination of hot and cold vertical walls by a single correlation. Bohn and Anderson [102] subsequently found that the bulk temperature defined by Eq. (47) closely predicted the average core temperature in a cubical enclosure with three-dimensional thermal bound-

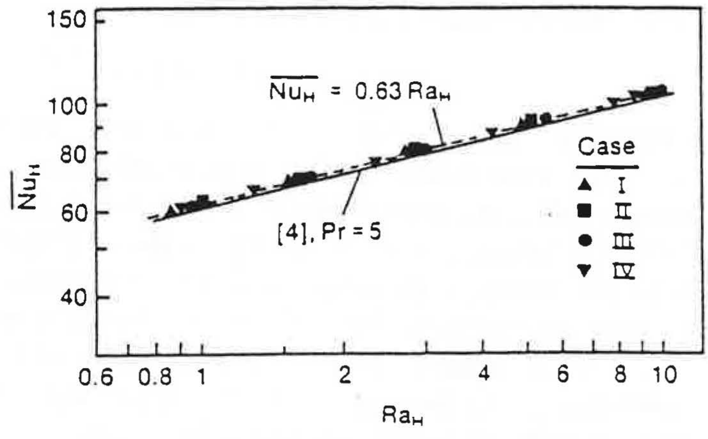

FIG. 43. Nusselt number results for the various lateral-edge configurations (from Sparrow and Azevedo [100]).

ary conditions on its vertical walls. This bulk-temperature-difference scaling demonstrates that the heat transfer in the boundary-layer regime of an enclosure with complicated thermal boundary conditions on vertical surfaces is driven by the temperature difference between a given surface and the bulk fluid temperature in the core of the enclosure. If this scaling is not observed, the heat transfer from a vertical surface in an enclosure with complicated thermal boundary conditions on the vertical walls can appear to be drastically different than that in an enclosure where one surface is uniformly heated and one surface is uniformly cooled.

This point can be demonstrated by considering the example of an enclosure with three heated vertical walls and one cooled vertical wall. For this case, the bulk temperature difference is

$$\Delta T_b = (T_H - T_C)/4 \tag{48}$$

and since $T_H - T_C = \Delta T$, $\Delta T/\Delta T_b = 4$.

Because the overall heat transfer to the cold surface for this example has to be the same regardless of the temperature difference used to define the heat-transfer coefficient, this implies

$$\bar{h}_b \, \Delta T_b = \bar{h} \, \Delta T \qquad \text{or} \qquad \bar{h}/\bar{h}_b = \tfrac{1}{4} \tag{49}$$

Thus, the heat-transfer coefficient based upon ΔT will be one-quarter that of the heat-transfer coefficient based upon ΔT_b for the three-heated- and one-cooled-wall geometry described above. This apparent discrepancy results from the choice of the temperature difference used to define the heat-transfer coefficient; it does not indicate a change in the convective heat-transfer mechanism. If ΔT_b is used rather than ΔT, the heat-transfer coefficient remains constant regardless of the thermal boundary conditions at the vertical walls of the enclosure. Bohn *et al.* [101] recommend the following correlation for natural convection heat transfer in enclosures with multiple heated and cooled vertical walls

$$\bar{h}_b L/k = 0.62 \; \mathrm{Ra}_H^{0.250} \tag{50}$$

Depending upon window location, direct solar gain may produce many localized, heated areas rather than a uniformly heated wall. Jaluria [103] conducted a numerical study of the interaction of multiple horizontal heated strips on a vertical surface in the boundary layer regime. He found that the velocity increased and the temperature decreased as the fluid moved downstream from the region being heated. Downstream heaters experienced heat-transfer enhancement provided they were far enough downstream to benefit from the added velocity induced by upstream heaters, without being exposed to hot fluid.

A majority of experiments with Rayleigh numbers in the range corresponding to full-scale buildings' interior spaces ($\sim 10^{10}$) have been performed with water and Freon using small-scale laboratory test cells. Workers at Los Alamos National Laboratory (see Yamaguchi [104]) have used freon in small-scale tests so that high Rayleigh numbers can be achieved in small enclosures. Small-scale testing can be simpler, quicker, and cheaper to accomplish than equivalent full-scale testing, but there is always some uncertainty regarding the degree to which the small-scale test actually models the full-scale situation. Olsen *et al.* [105] recently attempted to answer this question by conducting simultaneous small-scale and full-scale experiments over the range $1 \times 10^{10} \leq \mathrm{Ra}_H \leq 5 \times 10^{10}$. Olsen *et al.* [105] used Freon® 114 gas in the scale model. The physical capabilities of the full-scale and small-scale experiments are shown in Table IV. A comparison between temperature measurements in the full-scale and small-scale experiment is shown in Figs. 44 and 45. Figure 44 shows a comparison of vertical temperature profiles taken midway between the hot and cold vertical walls, and Fig. 45 shows a comparison of horizontal temperature profiles taken near the heated vertical wall.

Olsen *et al.* performed flow visualization experiments by injecting a neutrally buoyant smoke tracer. The vertical boundary layers on the heated and cooled surfaces were turbulent, characterized visibly by random eddy motion. Once the hot boundary layer reached the ceiling, it turned the corner and flowed along the ceiling toward the cold wall looking like a turbulent jet. When it reached the top of the cold wall, some of the

TABLE IV

CHARACTERISTICS OF FULL-SCALE AND SMALL-SCALE EXPERIMENTS[a]

	Full scale	Small scale
Dimensions		
Height, H	2.6 m	49 cm
Width, W	3.9 m	69 cm
Length, L	7.9 m	136 cm
Aspect ratios		
Height/length AR_L	0.33	0.36
Height/width AR_W	0.67	0.71
Prandtl number, Pr	0.7	0.8
Grashoff number, Gr_H	$1-5 \times 10^{10}$	$1-5 \times 10^{10}$
Typical hot-wall temperatures	25–40°C	25–50°C
Typical cold-wall temperatures	5–10°C	5–10°C
Emissivity of heating and cooling surfaces	low	low
Emissivity of floor and ceiling	high	high
Emissivity of side walls	high	low

[a] Experiments done by Olsen *et al.* [105].

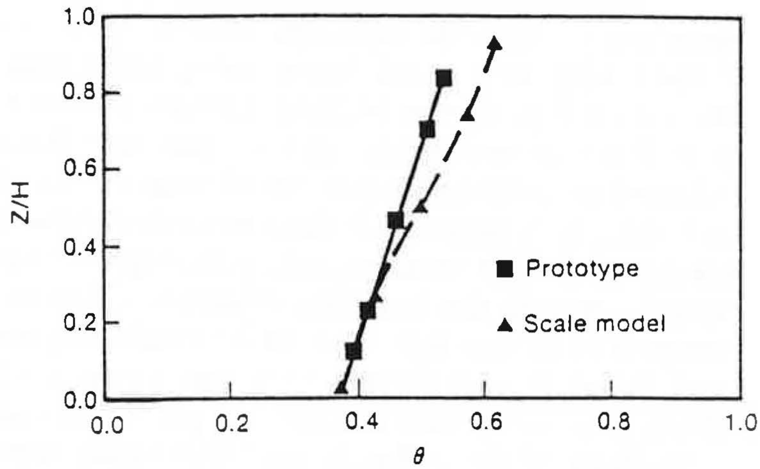

FIG. 44. Comparison of temperature versus height for the prototype and scale model midway between the hot and cold walls (from Olsen *et al.* [105]).

flow reversed direction, proceeding all the way back to the hot wall directly beneath the ceiling jet. A similar two-layer structure occurs near the floor, driven by the cold wall boundary layer. Although there were some differences in the magnitude of the core vertical temperature profiles (see Fig. 44), which were apparently a result of different thermal boundary conditions on the floor and ceiling in the small and large test cells, these differences did not affect the flow patterns or turbulent nature of the vertical boundary layers. The temperature measurements taken near the heated wall show qualitative agreement between the full and small scale.

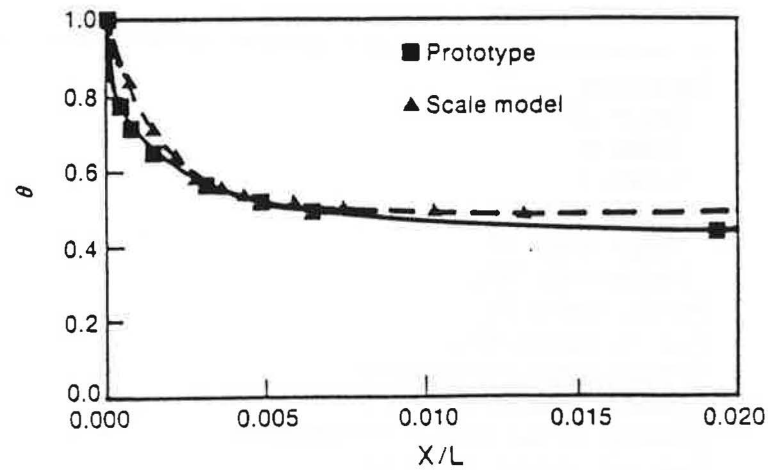

FIG. 45. Comparison of dimensionless temperature versus distance from the wall for the prototype and scale model hot-wall boundary layers (from Olsen *et al.* [105]).

There are a number of advantages associated with the use of liquids rather than gases in scale model studies. Fluids generally have higher thermal conductivities than gases, making it easier to approach adiabatic conditions on insulated walls. Also, the high density of liquids makes it relatively easy to suspend neutrally buoyant particles for use in flow visualization experiments or local velocity measurements. Direct application of the results from experiments that use fluids to buildings is based on the observation that, at high Rayleigh numbers, the Prandtl number effect on average heat transfer is largely accounted for by the Rayleigh number ($Ra_H = Gr_H \times Pr$).

Churchill and Chu [106] have successfully correlated experimental data for average natural convection heat transfer from a vertical plate in an unconfined medium for both laminar and turbulent regimes. Their correlation has the form

$$\overline{Nu}_H^{1/2} = 0.825 + 0.387\, Ra_H^{1/6}/\Psi(Pr) \tag{51}$$

with

$$\Psi(Pr) = [1 + 0.492/Pr^{9/16}]^{8/27} \tag{52}$$

The weak dependence of $\Psi(Pr)$ upon the Prandtl number tends to support the conclusion that average heat-transfer results are only weakly dependent upon the Prandtl number, provided that the Nusselt number is correlated as a function of the Rayleigh number. Numerical and experimental studies of natural convection in enclosures also exhibit only a weak dependence upon Prandtl number; however, experimental data for transitional and turbulent flows in enclosures are somewhat limited at the present time. Additional studies are required to fully determine the errors associated with the use of liquids to model transitional and turbulent natural convection in buildings.

3. *Heating and Cooling of Vertical and Horizontal Surfaces in Enclosures*

In solar buildings the hot and cold surfaces result from the presence of windows, thermal storage walls, auxiliary heating systems or solar illumination. In many cases of interest, both horizontal and vertical surfaces will be thermally active. A summary of natural convection studies for heat transfer to and/or from horizontal and vertical surfaces in single zone enclosures is shown in Table V. In all of these studies, two of the vertical walls on opposite sides of the enclosures were adiabatic. In our discussion we will use a shorthand notation consisting of four letters to specify the thermal boundary conditions on the remaining four walls of the enclosures, with H signifying an isothermal heated wall, C signifying an isother-

TABLE V

SUMMARY OF ENCLOSURE CONVECTION STUDIES WITH VERTICAL AND HORIZONTAL HEAT FLUXES

Configuration	Parameters	Reference
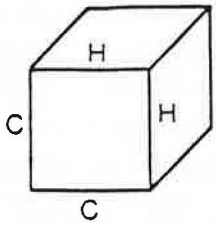	$Pr = 1.8 \times 10^4, 8.8 \times 10^4$ $4.0 \times 10^4 \leq Ra \leq 5.1 \times 10^4$ $A = 1, 3$ $0 \leq \Omega \leq 176.7$	Ostrach and Raghavan [107]
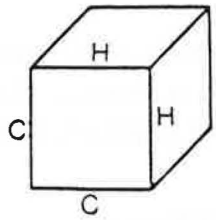	$Pr = 8.9 \times 10^4$ $2.29 \times 10^4 \leq Ra \leq 5.99 \times 10^4$ $A = 1$ $0 \leq \Omega \leq 6$	Fu and Ostrach [108]
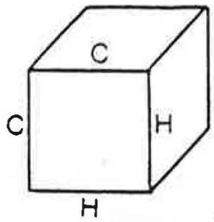 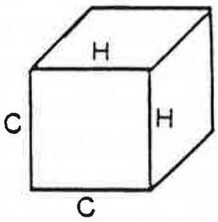 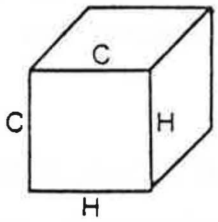	$Pr = 0.71$ $10^3 \leq Ra \leq 10^6$ $A = 1$ $-5 \leq \Omega \leq 5$	Shiralkar and Tien [109]
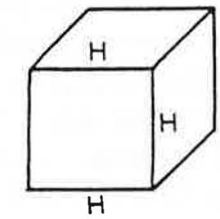 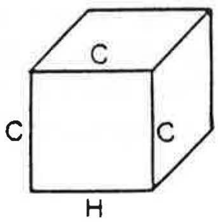	$Pr = 6.7$ $0.4 \times 10^{10} \leq Ra \leq 7 \times 10^{10}$ $A = 1$ $\Omega = 0, 1, \infty$	Kirkpatrick and Bohn [110, 111]

TABLE V *(Continued)*

Configuration	Parameters	Reference
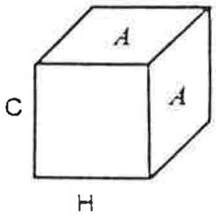	$\mathrm{Pr} = 0.7$ $\mathrm{Ra} = 10^6$ $\mathrm{AR} = 1$	Ozoe *et al.* [112]
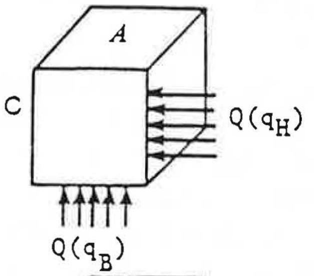	$\mathrm{Pr} = 6.7$ $1 \times 10^{11} \leq \mathrm{Ra}_H^* \leq 1 \times 10^{13}$ $\mathrm{AR} = 1$ $0 \leq \mathrm{PWR} \leq \infty$ $\mathrm{PWR} = q_B/q_H$	Anderson *et al.* [113]
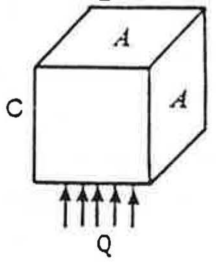	$0.7 \leq \mathrm{Pr} \leq 10$ $1 \times 10^6 \leq \mathrm{Ra}_H^* \leq 1 \times 10^{13}$ $\mathrm{AR} = 1$	Anderson and Lauriat [117]

mal cooled wall, Q signifying a constant flux heated wall and A signifying an adiabatic wall. The first letter in the sequence specifies the thermal boundary condition on the floor of the enclosure, followed by the thermal boundary condition on the right-hand-side wall, the ceiling, and finally left-hand-side wall of the enclosure. For example, the notation AHAC refers to the classical problem of an enclosure with heated and cooled vertical walls opposite to each other and adiabatic floor and ceiling surfaces.

Ostrach and Raghaven [107] and Fu and Ostrach [108] experimentally studied natural convection in enclosures with the configuration CHHC. They expected that the stable vertical temperature gradient caused by the cooled floor and heated ceiling would tend to damp out the natural convection flow in the enclosure. In both of these studies, the velocity distributions were measured by tracking the movement of particles suspended in large Prandtl number silicone oils. It was found that the imposition of a stable vertical temperature gradient caused a reduction in the velocity in the boundary layers next to the vertical walls and that small secondary circulation cells formed near the upper portion of the heated vertical wall and the lower portion of the cooled vertical wall.

Shiralkar and Tien [109] conducted numerical studies with stable and unstable vertical temperature gradients, corresponding to configurations HHCC and CHHC. Thermal instabilities such as Benard cells or thermal plumes were not observed when the enclosure was unstably heated. The temperature distribution in the core was found to be strongly dependent upon the heating configuration.

The controlling parameter that determines the relative strength of the vertical and horizontal temperature gradients is Ω, defined as the ratio of the two temperature differences $(T_T - T_B)$ and $(T_H - T_C)$, where $(T_T - T_B)$ is the difference between the temperature of the top surface T_T and the bottom surface T_B while $(T_H - T_C)$ is the difference between the thermally active sidewalls. Stable heating (CHHC) produced a motionless core with a high level of thermal stratification whereas unstable heating (HHCC) induced enough motion in the core to make it almost isothermal. Shiralkar and Tien found that the heat transfer from the vertical side walls increased with increasing Ω $\{= (T_T - T_B)/(T_H - T_C)\}$ in enclosures with stable vertical temperature gradient because of the preheating or precooling caused by the floor and ceiling. This result indicates that the increase in $(T_H - T_B)$ or $(T_T - T_C)$, which occurs with increasing Ω, more than compensates for any corresponding velocity reduction caused by the imposition of a stable vertical temperature gradient.

Kirkpatrick and Bohn [110, 111] conducted a series of experiments in a water-filled cubical enclosure that was heated from below, while the thermal boundary conditions for two side walls and the top were varied. They tested the configurations HACA, HHCC, HHHC, and HCCC at Rayleigh numbers four orders of magnitude higher than in previous studies. They found that the thermal boundary condition at the top of the enclosure strongly influenced the temperature distribution and flow structure. When the vertical temperature gradient was reduced to zero by heating the ceiling (configuration HHHC) the fluid in the core was highly stratified. Unstable heating generated turbulent thermal plumes at the top and bottom surfaces and destroyed the thermal stratification in the core of the enclosure.

Ozoe *et al.* [112] used numerical calculations with a two-equation model of turbulence to study the building configuration HAAC. Only 57% of the cooled wall was thermally active, to simulate a wall with a cold window. The remainder of the cooled wall was insulated. The calculations of Ozoe *et al.* [112] were carried out for only one Rayleigh number ($\mathrm{Ra}_L = 10^6$) and a Prandtl number of 0.7. They found the flow to be three dimensional with weak spiral flows near the side walls. A value of $Ra_L = 10^6$ placed their turbulent calculations intermediate to the onset of the turbulent regime at $Ra = 10^9$ in natural convection next to a vertical surface in an unconfined fluid, and at $Ra = 10^4$ for convection in an enclosure with a heated floor and a cooled ceiling. The calculations showed that the flow next to the floor consists of a horizontal boundary layer with no evidence of thermal instabilities.

Anderson *et al.* [113] experimentally examined the flow structure, heat transfer, thermal stratification, and temperature distributions in a closed cavity with the boundary condition QQAC. The ceiling and side walls of the cavity were insulated, the floor and one vertical wall were electrically heated, and the opposite vertical wall was cooled. They varied the level of heating provided to the floor and wall between $0 \leq PWR \leq \infty$. The parameter PWR is defined as the ratio of the energy per unit area convected from the floor divided by the energy per unit area convected from the vertical wall. The condition $PWR = 0$ corresponds to a closed cavity with differentially heated end walls. When $PWR = \infty$, the problem reduces to that of a cavity with a constant flux heated floor and a cooled vertical wall, similar to that studied by Ozoe *et al.* [112]. Anderson *et al.* [113] found that the level of the thermal stratification in the cavity is a strong function of the level of heating provided to the floor (see Fig. 46). The minimum level of

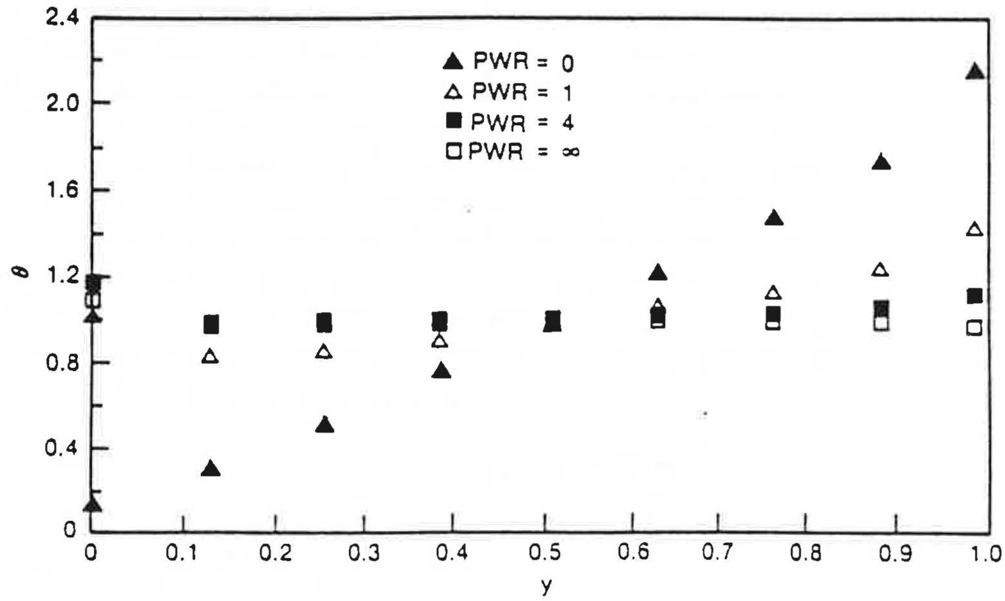

FIG. 46. Thermal stratification as a function of the relative levels of floor and wall heating in a direct gain zone (from Anderson *et al.* [113]).

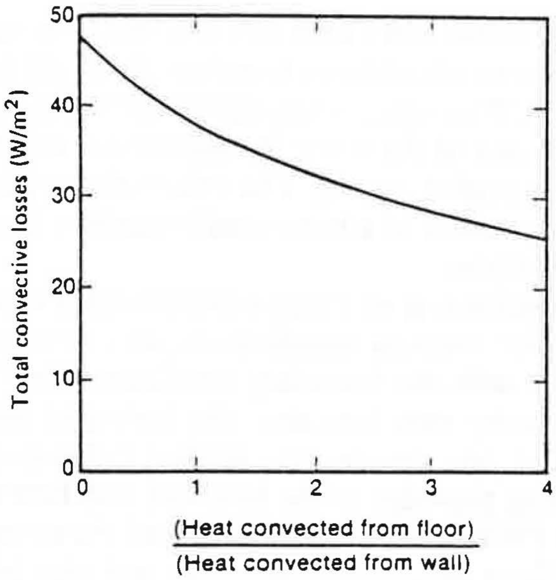

FIG. 47. Convective losses as a function of the relative levels of floor and wall heating in a direct gain zone (from Anderson *et al.* [113]).

thermal stratification occurred for pure floor heating (PWR $= \infty$). Anderson *et al.* [114] used these results to calculate the total convective losses from a direct gain zone over the range $0 \leq \mathrm{PWR} \leq 4$. Their results are plotted in Fig. 47. The convective losses for PWR $= 4$ were found to be less than half of the convective losses for PWR $= 0$. They concluded that floor heating is more effective than wall heating for maintaining room temperature in a single building zone because floor heating minimizes the level of thermal stratification. Side wall heating causes a high level of thermal stratification, which increases convective losses to the cold surface. The experiments of Anderson *et al.* [113] covered the range $10^{11} \leq \mathrm{Ra}_H^* \leq 10^{13}$ with $\mathrm{Pr} = 6.7$. The flow next to the floor was found to be an extremely stable horizontal boundary layer, indicating that natural convection in enclosures with adiabatic ceiling behaves entirely differently from natural convection in enclosures with cooled ceilings. The following correlation is proposed for the temperature in the core of the enclosure as a function of the heat convected from the floor and vertical wall.

$$\frac{(T'_{\mathrm{core}} - T_C)K}{q_H H} = 40.74\ \mathrm{Ra}_H^{*\,-0.304\left\{\frac{1}{2} + \frac{\mathrm{PWR}}{\mathrm{AR}}[0.454 + 0.001\ \mathrm{PWR}]\right\}} \tag{53}$$

This correlation can be used to calculate the combination of floor and wall heating required to maintain a given air temperature in a single building zone with a vertical cold surface. Anderson *et al.* also provide correlations for surface temperatures, thermal stratification, and heat transfer.

The natural convection flow within an enclosure differs from an external natural convection flow in an unconfined medium because it recirculates and thus interacts with itself. It is difficult to model this interaction accurately by applying external flow results to internal flows. However, because results for internal flows did not exist until recently, the common practice has been to calculate building heat loads based upon external flow results. Bauman *et al.* [115] compared results for external and internal flows and found the heat transfer calculated from internal results to be 30–50% lower than results based upon external situations. Based upon these findings, Altmayer *et al.* [116] conducted a series of numerical experiments aimed at developing an improved set of correlations for use in rooms with isothermal heating and cooling of two vertical side walls. They succeeded, but the correlations are substantially more complicated to use then other methods.

Anderson and Lauriat [117] conducted a numerical study of natural convection in a closed cavity with an isothermal vertical wall and a heated floor. The heat transfer and flow patterns were calculated for cases where the floor was isothermal as well as for cases when the floor was a constant heat-flux surface (configurations HAAC and QAAC). A horizontal boundary layer was found to form adjacent to the heated floor, in agreement with numerical calculations by Ozoe *et al.* [112] and experimental observations by Anderson *et al.* [113]. The calculated structure of the horizontal boundary layer is shown in Fig. 48. A comparison of the heat-transfer results with correlations for horizontal and vertical surfaces in an unconfined medium, showed that the unconfined medium correlations overpredict heat transfer from the vertical wall by 13% and underpredict heat transfer from the floor by 40%. The primary reason for the difference between the unconfined medium results for external flow and enclosure results for internal flow is the temperature difference used to define the heat-transfer coefficient. In external flows this temperature difference is taken to be the temperature of the surface minus the temperature of the ambient fluid, whereas in an enclosure, the temperature difference that determines the heat transfer from a given surface is the temperature of the surface in question minus the temperature of the surface located in the upstream flow direction.

4. *Surface Roughness Effects*

Room surfaces can have uniformly distributed roughness elements, for example, a masonry wall, or they can have isolated projections due to

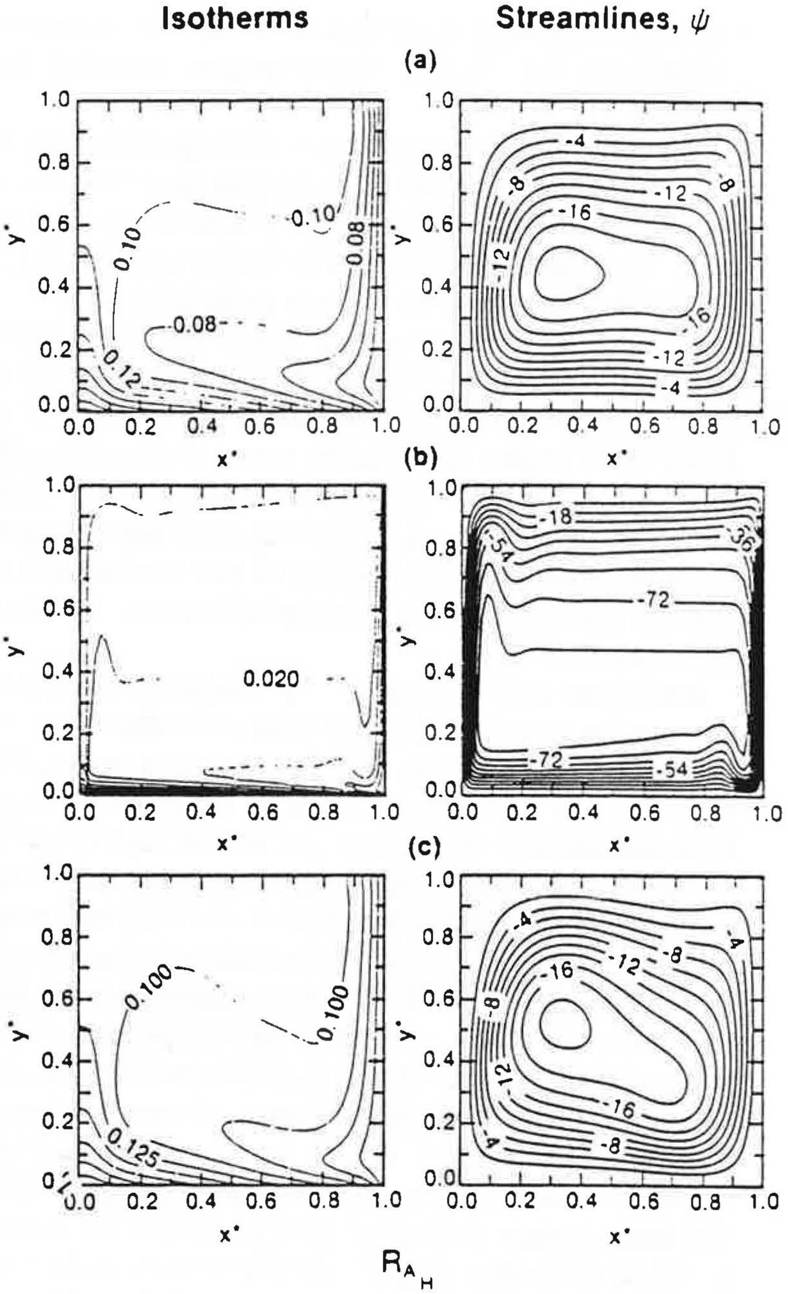

FIG. 48. Horizontal boundary layer structure in an enclosure (from Anderson *et al.* [114]).

windowsills, door soffits or ceiling beams. Anderson and Bohn [36] examined the effect on heat transfer of distributed roughness elements with the same length scale as the thermal boundary layer. They found that roughness was most effective for an isothermal wall, producing an average increase in total heat transfer of 10–15% and local increases of as much as 40%. The influence of the roughness elements upon the location of transition is shown in Fig. 49 for a constant-flux thermal boundary condition. The single solid line on Fig. 49 is the best fit curve demarking transition from laminar to turbulent flow in the absence of roughness. Transition in enclosures with heated and cooled vertical walls is delayed compared with transition for an isolated vertical surface (Fig. 49) [117a]. This delayed transition is caused by the strong thermal stratification in the core of the enclosure flow. The thermal stratification stabilizes the boundary layer by reducing the buoyancy force compared with an external flow in isothermal surroundings. Finite-size roughness elements in natural convection flows have been considered by Nansteel and Greif [118], ElSherbiny *et al.* [119], and Al-Arabi and El-Refaee [120]. Nansteel and Greif considered downward projections from the ceiling of an enclosure typical of door soffits. They found regions of intense turbulence downstream of the projections in a water-filled apparatus at $Ra_L = 10^{11}$. These turbulent regions did not exist if the projection extended across the entire width of the enclosure. ElSherbiny *et al.* [119] performed experiments in an enclosure with one V-corrugated and one flat surface. They found that the heat-transfer coefficient increased by up to 50% compared with an enclosure with two smooth surfaces. Al-Arabi and El-Rafaee [120] studied natural convection from an isolated V-corrugated plate. They also found this configuration provided higher heat transfer than a finned plate.

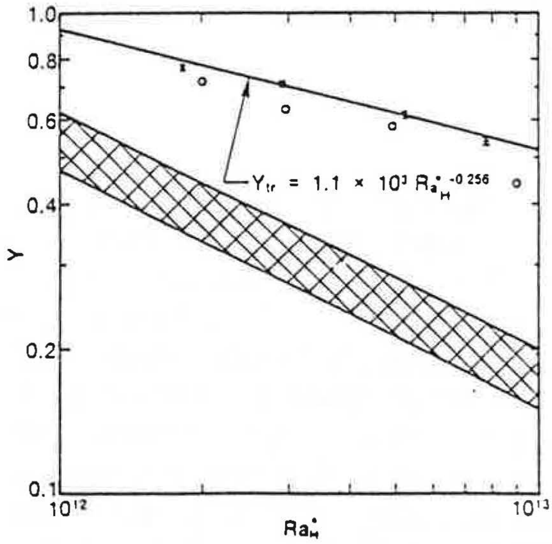

FIG. 49. Transition in an enclosure with a constant-flux heated surface. O, rough surface; +, smooth surface (from Anderson and Bohn [36]). The cross-hatched area is representative of the onset of transition for a heated plate in a semi-infinite medium as measured by Jaluria and Gebhart [117a].

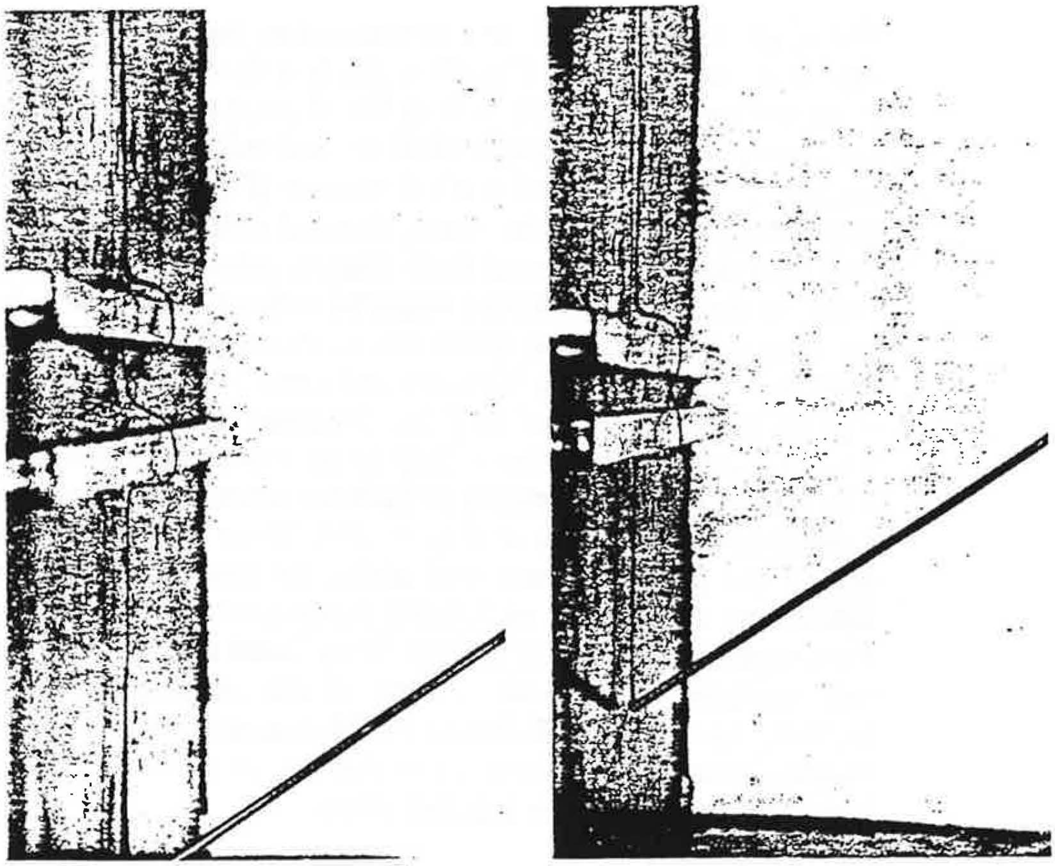

FIG. 50. Boundary-layer flow over horizontal roughness elements on a vertical surface (from Shakerin *et al.* [121]).

All of the studies mentioned above considered surface roughness in the context of heat-transfer enhancement. Surface roughness can also have the effect of blocking the natural convection flow and reducing heat transfer. Shakerin *et al.* [121] conducted a series of numerical and laboratory experiments with single and double roughness elements attached horizontally to a heated vertical surface in a rectangular enclosure. They found that if the spacing between the roughness elements was smaller than the height of the roughness element, then there was significant reduction in the ability of the natural convection flow to penetrate the space between the roughness elements. This effect is clearly shown in Fig. 50 for an experiment conducted in a water-filled enclosure. Dye was injected near the velocity maximum in the boundary layer next to the heated vertical wall. When the spacing between the roughness elements was reduced (Fig. 50b), the penetration depth of the dye was also reduced.

C. MULTIPLE BUILDING ZONES

Heat transfer between rooms separated by a partition in passive solar buildings occurs almost entirely by natural convection if the area of the flow aperture (e.g., doorway) is appreciably smaller than the overall cross-sectional area of the partition. Two approaches have been used to analyze interzonal convection in buildings. In one of these inviscid flow through a partition bounded by semi-infinite isothermal fluid reservoirs with different temperatures is assumed. This approach provides an accurate description of the flow through the partition under conditions of pure natural and forced/free convection when boundary layers are not important, but it predicts incorrect scaling for heat transfer when the flow is dominated by thermal boundary layers on the walls of the enclosure. The other approach recognizes the importance of the thermal boundary layers for interzone natural convection and thus heat-transfer results can be scaled correctly when thermal sources are present.

1. *Bulk Density Driven Flow*

Studies that have examined flow driven entirely by bulk density differences between zones include those of Emswiler [122], Brown and Solvason [123], Graf [124], Balcomb and Yamaguchi [125], and Kirkpatrick *et al.* [126]. Emswiler calculated the flow between zones with different density fluids for a partition with multiple openings by using Bernoulli's equation, but he did not treat the heat-transfer aspects of the problem. Brown and Solvason [123] conducted heat-transfer measurements in an air-filled enclosure that was divided into hot and cold regions by a single partition with a small variable-size opening. They developed an analytical expression for the heat transfer through the partition by the relation

$$\mathrm{Nu}_H = \frac{C}{3}\left(\frac{w}{W}\right)\left(\frac{l}{H}\right)^{3/2}(\mathrm{Ra}_H\,\mathrm{Pr})^{1/2} \tag{54}$$

The constant C appearing in Eq. (54) is the discharge coefficient for the aperture and can have values $C \leq 0.595$ [127]. The parameters l/H and w/W are the ratios of doorway height to total enclosure height and doorway width to total enclosure width, respectively. The temperature difference used in the definition of Nu_H and Ra_H in Eq. (54) is the temperature difference between the fluid in the hot and cold zones. Graf [124] examined invicid mixed forced and free convection by adding the pressure contribution from the forced flow to the pressure produced by the density differences between the fluid reservoirs. Examples of flow profiles resulting from the inviscid calculations are shown in Fig. 51. Balcomb and Yamaguchi [125] prepared a summary of velocity and temperature measurements taken in an occupied solar building. Kirkpatrick *et al.* [126] extended the model proposed by Brown and Solvason to include the effects of thermal stratification in the fluid reservoirs on either side of the partition. They measured thermal stratification levels in an unoccupied solar building and found that they could use their model to make accurate predictions of airflow and heat transfer that occurred as a result of the measured temperature differences between building zones.

2. *Boundary Layer Driven Flow*

In many building applications the heat transfer and fluid flow between zones are dominated by thin boundary layers that form next to heated and cooled surfaces. Studies of flow through two-dimensional partitions in the boundary layer region have been made by Janikowski *et al.* [128], Bejan

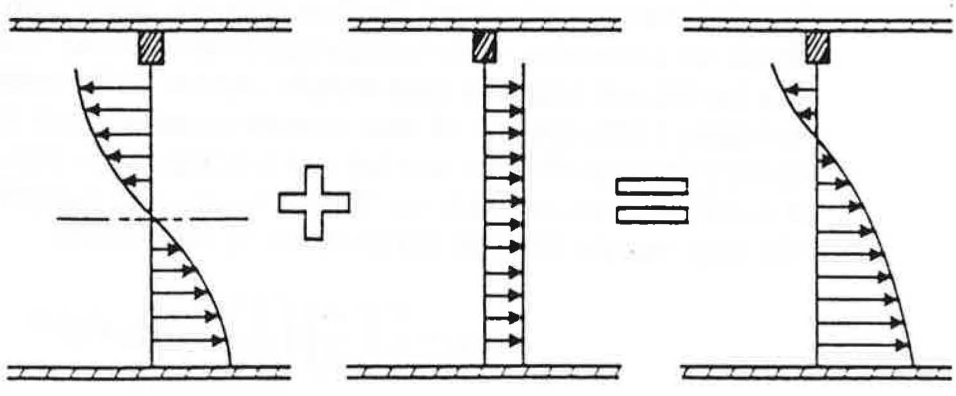

FIG. 51. Interzone flow profiles predicted by using Bernoulli's equation and assuming isothermal fluid reservoirs on either side of the partition; the skewed velocity profile is attributable to combined forcing pressure and density difference between the fluid reservoirs.

and Rossie [129], Nansteel and Greif [130], Bajorek and Lloyd [131], Chang *et al.* [132], Lin and Bejan [133], and Nansteel and Greif [118]. These studies were experimental, with the exception of Chang's, who used a finite-difference model for a geometry similar to that for the experimental work by Bajorek and Lloyd. Lin and Bejan, in addition to their experimental results, provided a perturbation solution valid in the limit $\mathrm{Ra} \rightarrow 0$. The only three-dimensional study is that by Nansteel and Greif [118] who considered a partition with a rectangular opening. A summary of the geometries and boundary conditions of these papers is shown in Table VI. Nansteel and Greif [130] and Lin and Bejan [133] demonstrated that the presence of a partition between zones tends to reduce the natural convection boundary-layer flow in subregions that are subjected to stable thermal boundary conditions. This effect reduces the wall area exposed to the primary boundary-layer flow and results in an overall reduction in the convective heat transfer between the hot and cold surfaces on either side of the partition. Nansteel and Greif [118] correlated their data to include this effect. Their correlation is

$$\mathrm{Nu}_H = 0.915(l/H)^{0.401}\,\mathrm{Ra}_H^{0.207} \tag{55}$$

The ranges of parameters for the above were

$$\tfrac{1}{4} \leq l/H \leq 1 \tag{56}$$

and

$$w/W = 0.093 \tag{57}$$

The temperature difference used in the evaluation of Nu_H and Ra_H in Eq. (55) is the temperature difference between the hot and cold end walls of the enclosure. Nansteel and Greif found that Eq. (55) can be used for width ratios w/W larger than 0.093 with a maximum error of 5–10%. The independence of heat transfer from doorway width in the boundary-layer regime is a result of the relative thinness of the boundary layer compared with the dimensions of the doorway.

If the area of the aperture is smaller than the area required for the passage of the boundary-layer flow, then the boundary-layer flow will have to accelerate to pass through the aperture. The additional driving force required to convect the flow through the aperture can only be provided by the creation of bulk density differences between the hot and cold zones of the enclosure. The flow area, A_{bl}, required by the boundary layers on heated and cooled surfaces can be calculated by summing the product of

TABLE VI

SUMMARY OF INTERZONE NATURAL CONVECTION STUDIES

Configuration	Type, parameters	Reference
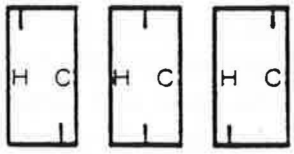	Air-filled $Gr_L = 1.1 \times 10^6$ $H/L_{enclosure} = 5$	Janikowski *et al.* [128]
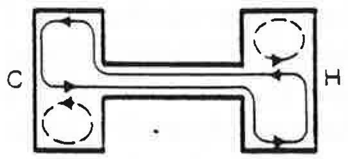	Water-filled $5 \times 10^6 \leq Ra_H \leq 5 \times 10^7$ $H/L_{duct} = \frac{1}{6}$	Bejan and Rossie [129]
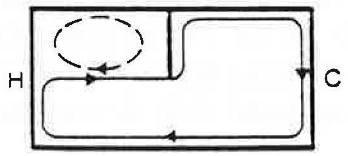	Water-filled $2 \times 10^{10} \leq Ra_L \leq 1 \times 10^{11}$ $H/L_{enclosure} = \frac{1}{2}$	Nansteel and Greif [130]
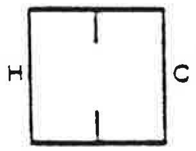	Air-filled, CO_2-filled $10^5 \leq Gr_L \leq 3 \times 10^6$ $H/L_{enclosure} = 1$	Bajorek and Lloyd [131]
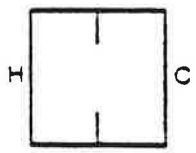	Air-filled $10^3 \leq Gr_L \leq 10^8$ $H/L_{enclosure} = 1$	Chang *et al.* [132]
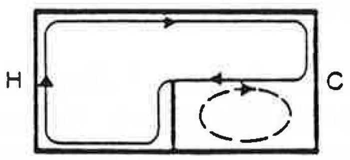	Water-filled $10^9 \leq Ra_H \leq 10^{10}$ $H/L_{enclosure} = 0.31$	Lin and Bejan [133]
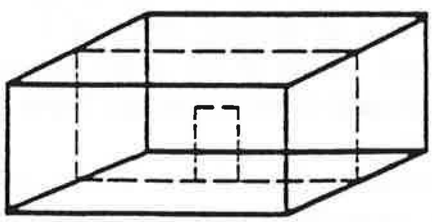	Water-filled $10^{10} \leq Ra_L \leq 10^{11}$ $H/L_{enclosure} = \frac{1}{2}$	Nansteel and Greif [118]
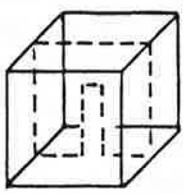	Water-filled $10^{11} \leq Ra_H \leq 10^{13}$ $H/L_{enclosure} = 1$	Scott *et al.* [135]

the thickness and width of each boundary layer in the enclosure, i.e.,

$$A_{bl} = \sum_{n=1}^{N} (\delta W)_n \tag{58}$$

According to the model described above, flow blockage will occur when

$$A_{bl}/lw = \sum_{n=1}^{N} (\delta W)_n/lw \sim 1 \tag{59}$$

For laminar flow it can be shown [134] that the natural convection boundary-layer thickness next to a vertical surface is scaled by the relationship

$$\delta/H \sim 1/\mathrm{Ra}_H^{*1/5} \tag{60}$$

If we assume that the height, width, and average heat flux from each active surface are H, W, and q'', respectively, then the flow blockage criteria expressed by Eq. (59) can be rearranged into the simple form

$$\frac{l}{W}\frac{w}{W} \sim \frac{N}{\mathrm{Ra}_H^{*1/5}} \tag{61}$$

The left-hand side of Eq. (61) is the ratio of the area of the aperture to the cross-sectional area of the enclosure and N is the number of active heat transfer surfaces in the enclosure. Equation (61) predicts that the onset of flow blockage is directly proportional to the number of active heat-transfer surfaces and is inversely proportional to the Rayleigh number that characterizes the natural convection flow.

A comparison between Eq. (54) and Eq. (55) demonstrates that the natural convection flow regime that governs the flow through the aperture (bulk density driven or boundary-layer driven) has a strong impact upon the geometric dependence of the heat-transfer coefficient. In the bulk density driven regime [Eq. (54)] the heat transfer between zones depends strongly upon both the aperture height ratio l/H and the aperture width ratio w/W. In the boundary-layer regime (Eq. 55) the heat transfer between zones depends weakly upon the aperture height ratio and appears to be independent of the aperture width ratio. Because of these differences, it is important to be able to predict when a multizone flow is in the bulk density driven or boundary layer driven regime. Scott, Anderson, and Figliola [135] conducted an experimental investigation to determine the onset of blockage of natural convection boundary-layer flow in a two-zone cavity with differentially heated end walls. They varied the width of the aperture between the zones while measuring the heat transfer and temperature distributions within the cavity. They found that flow blockage occurred when the area of the aperture was reduced below a critical value which was in qualitative agreement with Eq. (61). The temperature difference between the hot and cold zone reported by Scott *et al.* [135] is shown as a function of aperture width ratio in Fig. 52.

The data shown in Fig. 52 are for a constant zone-to-zone convective energy transport rate of 500 W. Also shown on Fig. 52 is the zone-to-zone temperature difference predicted by bulk density model of Brown and Solvason [123] [Eq. (54)]. As the width of the flow opening is reduced, the experimental data demonstrate that the zone-to-zone temperature difference required by the boundary-layer flow does not increase dramatically until $w/W \leq 0.10$. A flow driven by bulk density differences, on the other hand, requires a steady increase in zone-to-zone temperature difference as the width of the flow aperture is reduced. This result demonstrates that boundary-layer flows more than potential to transport energy without requiring large zone-to-zone temperatures particularly in critical flow applications where flow aperture areas are limited.

3. *Trombe Walls*

The two-zone studies described above assumed that the zones on either side of the dividing partition have the same aspect ratios. In a Trombe wall the width of the direct gain zone is reduced until it becomes a vertical duct bounded by the window surface and the absorbing wall surface (Fig. 5b). The first studies of natural convection between vertical parallel plates were performed by Elenbaas [136] and Ostrach [137] for fully developed flows. Studies with specific applications to solar buildings have been done by

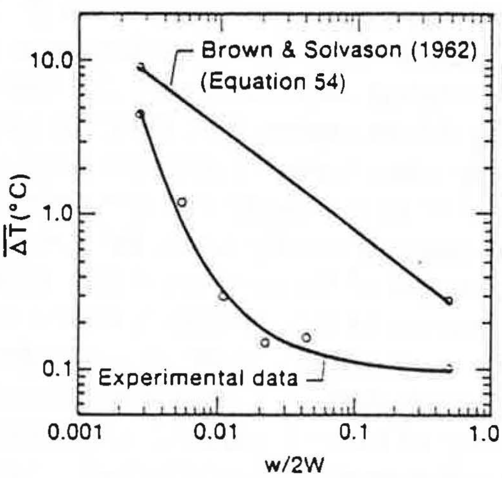

FIG. 52. Boundary-layer flow blockage in a two-zone enclosure (from Scott *et al.* [135]). $c = 0.6$.

Akbari and Borgers [138], Allen and Hayes [139], Tasdemiroglu *et al.* [140] and Ormiston, Raithby, and Hollands [141]. Bodoia and Osterle [142] considered the problem of developing flow between two isothermal plates with the same temperature. Miyatake and Fujii [143] and Miyatake *et al.* [144] calculated developing flow between two vertical plates when one plate was insulated and the other was an isothermal or constant flux surface. Aung *et al.* [145] conducted a numerical and experimental investigation of developing natural convection flow in a vertical duct with asymmetric side wall heating for both constant heat flux and constant temperature boundary conditions. Aung *et al.* [145] considered variable levels of the temperature or heat flux on the two side walls.

All of the studies referenced above that used numerical calculations assumed that the flow between the plates was parabolic and specified the velocity profile of the entering flow. Kettleborough [146] used an elliptic calculation method and found that regions of reverse flow could exist, particularly at high Rayleigh numbers. Sparrow *et al.* [147] observed flow reversals near the exit of a vertical channel with one insulated side wall and one isothermal side wall, but found that the average Nusselt number was unaffected by the presence of the recirculating zone. Sparrow *et al.* [148] considered natural convection combined with radiation in a vertical channel with one insulated wall and one isothermal wall. They found that the radiative transport between the walls increased the convective heat transfer by 50–70% for $1.1 \leq T_W/T_\infty \leq 1.25$, where T_∞ is the temperature of the fluid entering the channel.

The effect of channel width upon natural convection heat transfer between vertical parallel plates was studied experimentally by Sparrow and Azevedo [149]. They found that heat transfer was reduced dramatically if the width of the channel had the same order of magnitude as the boundary-layer thickness. The reduction in convective heat transfer that was measured in their experiment is plotted for different channel spacing in Fig. 53. Sparrow and Azevedo were able to reduce all of their data to a single curve by plotting the data as shown in Fig. 54. Their final correlation for heat transfer over the entire range of plate spacing $0.011 \leq L/H \leq 0.5$ and $3 \leq \mathrm{Ra}_L(L/H) \leq 10^8$ is

$$\overline{\mathrm{Nu}_L} = \left\{\left(\frac{12}{(L/H\,\mathrm{Ra}_L)}\right)^2 + \left(\frac{1}{0.619(L/H\,\mathrm{Ra}_L)^{1/4}}\right)^2\right\}^{-1/2} \tag{62}$$

Based upon their results, the channel width should satisfy the following inequality to avoid flow blockage effects

$$(L/H)\mathrm{Ra}_H^{1/4} \geq 5 \tag{63}$$

For a typical building application with $\mathrm{Ra}_H \sim 10^{10}$ and $H \sim 3$ m, the

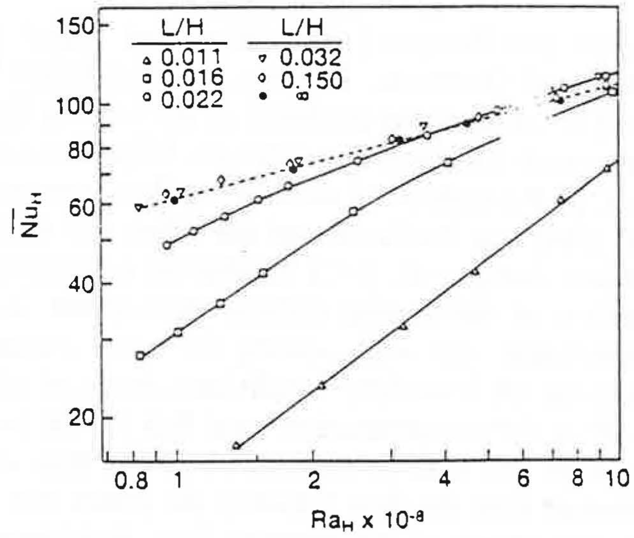

FIG. 53. Natural convection heat transfer as a function of channel with L (from Sparrow and Azevedo [149]).

channel width calculated from Eq. (62) is

$$L \geq 4.7 \quad \text{cm} \tag{64}$$

The equation assumes that there are no flow restrictions at the entrance and exit of the Trombe wall. In real applications that involve entrance and exit losses, the width of the duct at the entrance and exit should be increased beyond that recommended by Eqs. (63) and (64).

Ormiston *et al.* [141] completed a series of numerical calculations of

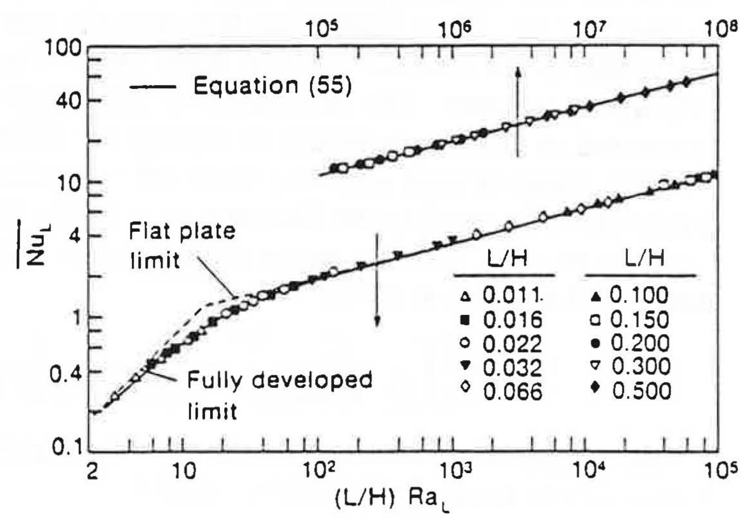

FIG. 54. Nusselt number correlation for natural convection in a parallel plate channel (from Sparrow *et al.* [149]).

natural convection for a Trombe wall channel that was coupled to a cold sink in a single-building zone. The problem was idealized by assuming that the cold sink was a perfect heat exchanger located in a trapezoidal volume near one end of the building zone. They found that their calculated heat-transfer results were 10% lower than the experimental results of Elenbaas [136] for parallel heated surfaces in an infinite medium. They attributed the difference to entrance and exit losses due to the turning of the flow at the top and bottom of the Trombe wall channel.

Tasdemiroglu *et al.* [140] conducted side-by-side tests of buildings, with and without a Trombe wall. They measured temperature distributions and incident solar radiation at intervals of 30 min and calculated the performance of the Trombe wall system. They found that the Trombe wall transmitted 15–35% of the incident solar radiation to the interior of the house.

IV. Summary and Conclusions

A. ACTIVE SOLAR COLLECTORS

There is a great deal of information available on natural convection phenomena under conditions and geometric configurations used in active solar collection systems. This information is adequate for calculating the heat loss by natural convection from flat-plate collectors at any orientation, but some of the scientific aspects of natural convection in small aspect ratio configurations used in convection suppression applications still elude complete explanations.

Available data on natural convection in line-focusing compound-parabolic configurations is adequate to estimate the heat loss in this type of collection system. Similarly, available information is adequate for estimating the heat loss in the annular space of line-focusing parabolic trough configurations, but most of the information is for uniform heat flux or uniform temperature boundary conditions. In real systems, the solar energy is reflected only onto a part of the receiver and there is relatively little information on the effect of nonuniform temperature or heat flux on the flow and heat loss in geometric configurations such as an annulus.

For point-focusing systems, there appears to be adequate information to calculate the heat loss from external-type central receivers. On the other hand our understanding of the mechanism and our ability to calculate natural convection losses from cavity-type central receivers is poor and additional work is required to clarify the situation. For parabolic dish receivers, relatively little experimental and analytic information exists. The situation is particularly complex because a receiver in such a system is in continuous motion, causing the orientation of the cavity with respect to the gravity vector to change during the day. In fact, only a single reference was found that deals specifically with natural convection loss from cavity receivers of point focusing parabolic dishes.

B. Solar Buildings

Natural convection is a primary heat transport mechanism in solar buildings. Geometries of buildings are usually complex and, until recently, information on natural convection was essentially confined to heating and cooling of the floor and ceiling or of opposite vertical walls in single-zone rectangular enclosures. Only in recent years has research been conducted on heat transfer by natural convection in enclosures with complex geometries and nonuniform thermal boundary conditions such as those found in real building applications. As a result of this research, it is now possible to predict thermal stratification and heat-transfer rates as a function of thermal boundary conditions in rectangular and triangular enclosures, as well as in simple single-level, multizone configurations. There are several numerical codes available to predict natural convection flow in enclosures and their range of applicability and reliability for solar building energy simulation could be improved dramatically by validating them with some current research results. Because of the wide range of geometries and thermal boundary conditions that are encountered in building design, there are a number of research areas that require further consideration. Some of the most important of these areas are summarized below.

Most buildings operate with Rayleigh numbers large enough that at least a portion of the boundary layer over the interior and exterior walls is turbulent. A good deal of work has been done on the transition to turbulent flow in enclosures with large aspect ratios (like flat-plate collectors), but there is a need for additional analytical and experimental studies of transition as well as turbulent natural convection in enclosures with aspect ratio of order 1, the geometry found in rooms of residential and commercial buildings. In particular, there is a need to determine the effect of Prandtl number upon heat transfer in the transitional and laminar regimes.

Real buildings consist of several rooms at different levels. Consequently, natural convection occurs in multiple flow paths, both in the horizontal and vertical direction. Most heat-transfer studies of interzonal flows driven by natural convection have been limited to single-level geometries. There exists a real need to extend available information to three-dimensional flows in complex geometries, particularly those encountered in rooms at different levels, or shafts and connecting spaces as encountered in commercial buildings and astria.

Most laboratory investigations have been conducted in enclosures that have relatively smooth surfaces. In real buildings, however, there are furnishings such as draperies, blinds, and furniture, as well as obstructions such as door soffits that can interfere with normal boundary-layer flow. Our understanding of the effects of such real world amenities in buildings on the predictions based on laboratory experiments is limited. It is important to quantify these effects in order to determine the extent to which results from idealized experiments can be applied to the real world.

In many building applications the natural convection flows described in this paper interact with forced flow generated by auxiliary space conditioning systems. Very little is known about the combination of Rayleigh–Reynolds number ranges over which forced flow appreciably affects the results of natural convection predictions in enclosures.

We believe that building heat transfer information can be more conveniently and more cheaply obtained with water or Freon in small-scale models, than with air in full-scale models. However, there is a reluctance among architects to accept results obtained in model studies. Therefore, a carefully controlled experimental program aimed at convincing potential users of the validity and usefulness of correlations obtained from small scale models would be important.

A number of the areas described above are the subject of ongoing research efforts and substantial additional information should be available in the next five or ten years. It may take longer, however, to integrate this information into the architectural design methodology, and we recommend that a serious effort continue to be made to package the results of research in the thermal sciences in a form that can easily be used by architects to reduce energy consumption without sacrificing human comfort.

NOMENCLATURE

A_a	aperture area	m^2	h	specific enthalpy	J/kg
A_r	receiver area	m^2	$\bar{h}_c$	average convective heat-transfer coefficient	W/m² °C
AR	aspect ratio, H/L		I_c	insolation on collector aperture	W/m²
C	concentration ratio A_a/A_r		I_b	beam insolation	W/m²
c_p	specific heat at constant pressure	J/kg °C	I_d	diffuse insolation	W/m²
Gr_L	Grashof number $(g\beta/L^3\,\Delta T)/\nu^2$		k	thermal conductivity	W/m °C
Gr_H	Grashof number $(g\beta H^3\,\Delta T)/\nu^2$		L	spacing between enclosure walls or characteristic length as defined in text	m
g	gravitational acceleration	m/sec²	l	doorway height	m
H	enclosure height	m			

$\dot{m}$	mass flow rate	kg/sec	T_f	mean fluid temperature $(T_{in} + T_{out})/2$	°C
Nu_H	Nusselt number $\bar{h}_c H/k$		T_H	average receiver temperature	°C
Nu_L	Nusselt number $\bar{h}_c L/k$		T_s	surface temperature	°C
Pr	Prandtl number, $c_p \mu/k$		ΔT	surface temperature difference	
PWR	$q_{sidewall}/q_{floor}$		$\overline{\Delta T}$	bulk fluid temperature difference	
q_c	rate of heat transfer by convection	W/m²	U	total thermal loss coefficient based on A_r	W/m² °C
q_u	rate of useful heat transfer	W/m²	V	velocity	m/sec
R	thermal resistance	m² °C/W	W	enclosure width	m
Re_f	film Reynolds number $V\delta/\nu$		w	doorway width	m
Ra_H	Rayleigh number $g\beta H^3 \Delta T/\nu\alpha$		x	distance from leading edge or coordinate	m
Ra_H^*	flux modified Rayleigh number $g\beta H^4 q_c \nu\alpha k$		y	vertical distance or coordinate	m
Re_L	Reynolds number $VL\rho/\mu$				
T_{amb}	ambient temperature	°C			

Greek Symbols

α	thermal diffusivity	m²/sec	μ	viscosity	kg/m sec
β	coefficient of expansion	K^{-1}	ν	μ/ρ	m²/sec
δ	boundary-layer thickness	m	ρ	density	kg/m³
δ	film thickness		ϕ	collector tilt angle	degrees
θ	dimensionless temperature, $(T_{core} - T_C)/(T'_{core} - T_C)$		Ω	$(T_T - T_B)/(T_H - T_C)$	

Subscripts

B	bottom wall	o	outlet or outside
C	cold	T	top wall
H	hot	w	wall
i	inlet or inside		

Superscripts

	midpoint	—	average

ACKNOWLEDGMENTS

The authors would like to thank several individuals for reviews and helpful comments during the preparation of the manuscript. In particular, Ms. Mary Linskens, Dr. M. Abrams, and J. B. Wright have been very helpful. The work was partially supported by the U.S. Department of Energy (DOE) Solar Buildings Program, and the DOE Solar Thermal Program. Portions of this chapter were originally presented as lectures at a NATO Advanced

Study Institute (ASI) in 1984 and published in the Advanced Study Institute Book *Natural Convection*, (S. Kakac, W. Aung, and R. Viskanta, eds.), Hemisphere Publishing Corp., 1985. We express our appreciation to the publisher for the permission to use a portion of this lecture material in the development of the present chapter.

Support for the preparation of the final manuscript was provided by the DOE Solar Technical Information Program.

REFERENCES

1. C. F. Chen and D. H. Johnson, Double diffusive convection: A report of an engineering foundation conference. *J. Fluid Mech.* **138**, 405–416 (1984).
2. R. Viskanta, T. L. Bergman, and F. P. Incropera, Double diffusive natural convection. *In* "Natural Convection: Fundamentals and Applications" (S. Kakac, W. Aung, and R. Viskanta, eds.), Hemisphere, New York, 1985.
3. F. Kreith and J. F. Kreider, "Principles of Solar Engineering." McGraw-Hill, New York, 1978.
4. F. Kreith, R. Davenport, and J. Feustel, Status review and prospects for solar industrial process heat. *J. Sol. Energy Eng.* **105**, 385–400 (1983).
5. A. Rabl, "Active Solar Collectors and Their Applications." Oxford Univ. Press, London and New York, 1985.
6. F. Kreith and M. Bohn, "Principles of Heat Transfer," 4th ed. Harper & Row, New York, 1986.
7. J. D. Balcomb, Passive solar energy systems for buildings. *In* "Solar Energy Handbook" (J. F. Kreider and F. Kreith, eds.), pp. 16–27. McGraw-Hill, New York, 1981.
8. H. Buchberg, I. Catton, and D. K. Edwards, Natural convection in enclosed spaces—A review of application to solar energy collection. *J. Heat Transfer* **98**, 182–188 (1976).
9. I. Catton, Natural convection in enclosures. *Heat Transfer Int. Heat Transfer Conf., 6th, 1978* (1978).
10. S. Ostrach, Natural convection in enclosures." *Adv. Heat Transfer* **8** (1972).
11. S. Ostrach, Natural convection heat transfer in cavities and cells. *Heat Transfer, Proc. Int. Heat Transfer Conf., 7th, 1982* (1983).
12. J. E. Hart, Stability of the flow in a differentially heated inclined box. *J. Fluid Mech.* **47**, 547–576 (1971).
13. H. Ozoe, H. Sayama, and S. W. Churchill, Natural convection in an inclined rectangular channel at various aspect ratios and angles—Experimental measurements. *Int. J. Heat Mass Transfer* **18**, 1425–1431 (1975); see also Natural convection patterns in a long-inclined rectangular box heated from below. Part I. Three dimensional photography. *ibid.* **20**, 123–129 (1977).
14. D. W. Ruth, K. G. T. Hollands, and G. D. Raithby, On free convection experiments in inclined air layers heated from below. *J. Fluid Mech.* **96**, 461–479 (1980).
15. S. J. M. Linthorst, W. M. Schinkel, and C. J. Hoogendoorn, Flow structure with natural convection in inclined air-filled enclosures. *J. Heat Transfer* **103**, 535–537 (1981).
16. H. Inaba, Experimental study of natural convection in an inclined air layer. *Int. J. Heat Mass Transfer* **27**, 1127–1139 (1984).
17. R. J. Goldstein and Q.-J. Wang, An interferometric study of the natural convection in an inclined water layer. *Int. J. Heat Mass Transfer* **27**, 1445–1453 (1984).
18. H. Ozoe, K. Fujii, N. Lior, and S. W. Churchill, Long rolls generated by natural convection in an inclined, rectangular enclosure. *Int. J. Heat Mass Transfer* **26**, 1427–1438 (1983).

18a. W. M. M. Schinkel, National convection in inclined air-filled enclosures. Ph.D Thesis. Delft University of Technology, The Netherlands (1980).

19. S. M. ElSherbiny, G. D. Raithby, and K. G. T. Hollands, Heat transfer by natural convection across vertical and inclined air layers. *J. Heat Transfer* **104**, 96–102 (1982).
19a. J. G. A. DeGraaf and E. F. M. Van Der Held, The relation between the heat transfer and convection phenomena in enclosed plane air layers. *Appl. Sci. Res.* 3, 393–409 (1953).
19b. E. R. G. Eckert and W. O. Carlson, Natural convection in an air layer enclosed between two vertical plates with different temperatures. *Int. J. Heat Mass Transfer* **2**, 106–120 (1961).
19c. W. M. M. Schinkel and C. J. Hoogendoorn, An Interferometric study of the local heat transfer by natural convection in inclined air-filled enclosures. *Heat Transfer, Int. Heat Transfer Conf., 6th, 1978*, Pap. NC-18 (1978).
19d. K. R. Randall, J. W. Mitchell, and M. M. El-Wakil, Natural convection heat transfer characteristics of flat-plate enclosures. *J. Heat Transfer* **101**, 120–125 (1979).
20. K. G. T. Hollands, L. Konicek, T. E. Unny, and G. D. Raithby, Free convection heat transfer across inclined air layers. *J. Heat Transfer* **98**, 189–193 (1976).
21. H. Buchberg and D. K. Edwards, Design considerations for solar collectors with cylindrical glass honeycombs. *Sol. Energy* **18**, 193–204 (1976).
22. H. Buchberg, O. A. Lalude, and D. K. Edwards, Performance characteristics of rectangular honeycomb solar-thermal converters. *Sol. Energy* **13**, 193–221 (1971).
23. K. G. T. Hollands, Honeycomb devices in flat-plate solar collectors. *Sol. Energy* **9**, 159 (1965).
24. K. L. D. Cane, K. G. T. Hollands, G. D. Raithby, and T. E. Unny, Free convection heat transfer across inclined honeycombed panels. *J. Heat Transfer* **99**, 86–91 (1977).
25. K. G. T. Hollands, G. D. Raithby, and T. E. Unny, "Studies on Methods of Reducing Heat Losses from Flat-Plate Collectors," Final Rep., ERDA Contract E(11-1)-2597. University of Waterloo, Ontario, Canada, 1976.
26. K. G. T. Hollands, G. D. Raithby, F. B. Russell, and R. G. Wilkinson, Coupled radiative and conductive heat transfer across honeycomb panels and through single cells. *Int. J. Heat Mass Transfer* **27**, 2119–2131 (1984).
27. C. J. Hoogendoorn, Natural convection suppression in solar collectors. *In* "Natural Convection: Fundamentals and Applications" (S. Kakac, W. Aung, and R. Viskanta, eds.). Hemisphere, New York, 1985.
28. K. G. T. Hollands and K. Iynkaran, Proposal for a compound-honeycomb collector. *Sol. Energy* **34**, 309–316 (1985).
29. J. N. Arnold, I. Catton, and D. K. Edwards, Experimental investigation of natural convection in inclined rectangular regions of differing aspect ratios. *J. Heat Transfer* **98**, 67–71 (1976).
30. J. N. Arnold, D. K. Edwards, and I. Cattan, Effects of tilt and horizontal aspect ratio on natural convection in rectangular honeycomb solar collectors. *J. Heat Transfer* **19**, 120–122 (1977).
31. P. A. Meyer, J. W. Mitchell, and M. M. El-Wakil, Natural convection heat transfer in moderate aspect ratio enclosures. *J. Heat Transfer* **101**, 655–659 (1979).
32. D. R. Smart, K. G. T. Hollands, and G. D. Raithby, Free convection heat transfer across rectangular-celled diathermanous honeycombs. *J. Heat Transfer* **102**, 75–80 (1980).
33. J. G. Symons and M. K. Peck, Natural convection heat transfer through inclined longitudinal slots. *J. Heat Transfer* **106**, 824–829 (1984).
34. J. G. Symons, Natural convection in inclined cavities with half and full partitions. *Proc. Australas. Conf. Heat Mass Transfer, 3rd*, pp. 69–76 (1985).

35. J. L. Balvanz and T. H. Kuehn, Effect of wall conduction and radiation on natural convection in a vertical slot with uniform heat generation on the heated wall. *HTD* [Publ.] *(Am. Soc. Mech. Eng.)* **8**, 55–62 (1980).
36. R. Anderson and M. Bohn, Heat transfer enhancement in natural convection enclosure flow. *HTD* [Publ.] *(Am. Soc. Mech. Eng.)* **39**, 29–38 (1985). Also *J. Heat Transfer* **108**, 330–337 (1986).
37. R. K. MacGregor and A. F. Emery, Free convection through vertical plane layers—Moderate and high prandtl number fluids. *J. Heat Transfer* **91**, 391–403 (1969).
38. W. M. M. Schinkel and C. J. Hoogendoorn, Natural convection in collector cavities with an isoflax absorber plate. *J. Sol. Energy Eng.* **105**, 19–22 (1983).
39. P. K. B. Chao, H. Ozoe, and S. W. Churchill, The effect of nonuniform surface temperature on laminar natural convection in a rectangular enclosure. *Chem. Eng. Commun.* **9**, 245–254 (1981).
40. G. S. H. Lock and R. S. Ko, Coupling through a wall between two free convective systems. *Int. J. Heat Mass Transfer* **16**, 2087–2096 (1973).
41. R. Anderson and A. Bejan, Natural convection on both sides of a vertical wall separating fluids at different temperatures. *J. Heat Transfer* **102**, 630–635 (1980).
42. R. Anderson and A. Bejan, Heat transfer through single and double vertical walls in natural convection: theory and experiment. *Int. J. Heat Mass Transfer* **24**, 1611–1620 (1981).
43. R. Viskanta and D. W. Lankford, Coupling of heat transfer between two natural convection systems separated by a vertical wall. *Int. J. Heat Mass Transfer* **24**, 1171–1177 (1981).
44. E. M. Sparrow and C. Prakash, Interaction between internal natural convection in an enclosure and an external natural convection boundary-layer flow. *Int. J. Heat Mass Transfer* **24**, 895–907 (1981).
45. F. Kreith, G. O. G. Lof, A. Rabl, and R. Winston, Solar collectors for low and intermediate temperature applications. *Prog. Eng. Cambridge Sci.* **6**, 1–34 (1980).
46. R. Winston, Principles of solar concentrators of a novel design. *Solar Energy* **16**, 89 (1974).
47. A. Rabl, Comparison of solar concentrators. *Sol. Energy* **18**, 93 (1976).
48. J. J. O'Gallagher, K. Snail, R. Winston, C. Peek, and J. D. Garrison, A new evacuated CPC collector tube. *Sol. Energy* **29**, 575–577 (1982).
49. U. Ortabasi and F. Fehlner, Cusp Mirror-heat pipe evacuated tubular solar thermal collector. *Sol. Energy* **24**, 477–489 (1980).
50. T. S. Lee, N. E. Wijeysundera, and K. S. Yeo, Free convection fluid motion and heat transfer in horizontal concentric and eccentric cylindrical collector systems. *In* "Solar Engineering 1984" (D. Y. Lowani, ed.), pp. 194–200. Am. Soc. Mech Eng., New York, 1984.
51. C. K. Hsieh, Thermal analysis of CPC collectors. *Sol. Energy* **27**, 19–29 (1981).
52. C. K. Hsieh and F. M. Mei, Empirical equations for calculation of CPC collector loss coefficient. *Sol. Energy* **30**, 487–470 (1970).
53. S. I. Abdel-Khalik, H.-W. Li, and K. R. Randall, Natural convection in compound parabolic concentrators—A finite element solution. *J. Heat Transfer* **100**, 199–204 (1978).
54. B. A. Meyer, J. W. Mitchell, and M. M. El-Wakil, Convective heat transfer in trough and C.P.C. collectors. *Proc. Annu. Meet., Am. Sect. ISES*, Vol. 3.1, pp. 437–440 (1980).
55. M. Collares Pereira, J. Dugue, A. Joyce, M. Delgado, G. Serrudo, and A. Rego-Teixeira, A 3X CPC-type concentrator with tubular receiver and tubular glass envelope to reduce

convective losses: Description and performance. *Proc. Int. Sol. Energy Cong., Sol. World Forum*, pp. 1718–1723 (1981).
56. K. N. Woo, Performance of the compound cylindrical concentrator. *Proc. Annu. Meet. Am. Soc. Eng. Sci.*, Vol. 6, pp. 465–470 (1983).
56a. A. Rabl, J. O'Gallagher, and R. Winston, Design and test of nonevacuated solar collectors with compound parabolic concentrators. *Sol. Energy* **25**, 335–351 (1980).
56b. R. Patton, Design considerations for a stationary concentrating collector. *Conc. Sol. Collect., Proc. ERDA Conf., 1977*, pp. 3–37 (1977).
56c. D. E. Prapas, B. Norton, and S. D. Probert, Design of compound concentrating solar energy collectors. *J. Sol. Energy Eng.* (1985).
57. A. Rabl, P. Bendt, and W. W. Gaul, Optimization of parabolic trough solar collectors. *Sol. Energy* **29**, 407–417 (1982).
58. T. H. Kuehn and R. J. Goldstein, An experimental and theoretical study of natural convection in the annulus between horizontal concentric cylinders. *J. Fluid Mech.* **74**, 695–719 (1976).
59. T. H. Kuehn and R. J. Goldstein, Correlating equations for natural convection heat transfer between horizontal circular cylinders. *Int. J. Heat Mass Transfer* **19**, 1127–1134 (1976).
60. T. H. Kuehn and R. J. Goldstein, An experimental study of natural convection heat transfer in concentric and eccentric horizontal cylinders. *J. Heat Transfer* **100**, 535–540 (1978).
61. T. H. Kuehn and R. J. Goldstein, A parametric study of prandtl number and diameter ratio effects on natural convection heat transfer in horizontal cylindrical annuli. *J. Heat Transfer* **102**, 768–770 (1980).
62. K. Butti and J. Perlin, "A Golden Thread." Van Nostrand-Reinhold, Princeton, New Jersey, 1980.
63. F. Kreith and R. T. Meyer, Large-scale use of solar energy with central receivers. *Am. Sci.* **71**, 518–605 (1983).
64. M. Abrams, The status of research on convective losses from solar central receivers. SAND **83–8224**, Sandia National Laboratory, Livermore, CA (1983).
65. D. L. Siebers, R. J. Moffat, and R. G. Schwind, Experimental mixed convection from a large, vertical plate in a horizontal flow. *Heat Transfer Proc. Int. Heat Transfer Conf., 7th 1982*, MC 13,1 (1983) (see also SAND **83–8225**); Experimental, variable properties natural convection from a large, vertical flat surface. *Proc. ASME-JSME Therm. Eng. J. Conf., 1983*, Vol. 3, pp. 269–275 (1983).
66. A. M. Clausing, Advantages of a cryogenic environment for experimental investigations of convective heat transfer. *Int. J. Heat Mass Transfer* **25**, 1255–1257 (1982).
67. A. M. Clausing, Convective losses from cavity solar receivers—Comparisons between analytical predictions and experimental results. *J. Sol. Energy Eng.* **105**, 29–33 (1983).
68. B. Afshari and J. H. Ferziger, Computation of orthogonal mixed-convection heat transfer. *Proc.—ASME-JSME Therm. Eng. Jt. Conf., 1983*, Vol. 3, pp. 169–173 (1983).
69. E. Achenbach, The effect of surface roughness on the heat transfer from a circular cylinder to the cross flow of air. *Int. J. Heat Mass Transfer* **20**, 359–369 (1977).
69a. K. Y. Wang and R. J. Copeland, Heat transfer in a solar radiation absorbing molten salt film flowing over an insulated substrate. Am. Soc. Mech. Eng. paper 84-WA/SOL-22 (1984).
70. P. K. McMordie, Convection losses from a cavity receiver. *J. Sol. Energy Eng.* **106**, 98–100 (1984).
71. Mirenayat, Etude expérimentale du transfert de chaleur par convection naturalle dans

une Cavite isotherme ouverte. D. Eng. Thesis, University of Poitiers (1981); see also Experimental study of heat loss through national convection from an isothermal cubic open cavity. **SAND 81-8014**, Sandia National Laboratory, Livermore, CA 165–174 (1981).

72. V. Sernas and I. Kyriakidas, "Natural convection in an open cavity. *Heat Transfer, Proc. Int. Heat Transfer Conf., 7th, 1982,* Vol. 2, pp. 275–280 (1983).
73. Y. L. Chen and C. L. Tien, Laminar natural convection in shallow open cavities. *HTD [Publ.] (Am. Soc. Mech. Eng.)* **26**, 77–82 (1983).
74. C. F. Hess and R. H. Henze, Experimental investigation of natural convection losses from open cavities. *J. Heat Transfer* **106**, 333–338 (1984).
75. J. A. C. Humphrey, F. S. Sherman, and K. S. Chen, Experimental study of free and mixed convective flow of air in a heated cavity. **SAND84–8192,** Sandia National Laboratory, Livermore, CA (1985).
76. J. S. Kraabel, An experimental investigation of the natural convection from a side-facing cubical cavity. *Proc.—ASME-JSME Therm. Eng. Jt. Conf., 1983,* Vol. 1, pp. 299–306 (1983).
77. P. LeQuere, J. A. C. Humphrey, and F. S. Sherman, Numerical calculation of thermally driven two-dimensional unsteady laminar flow in cavities of rectangular cross section. *Numer. Heat Transfer* **4**, 249–283 (1981).
78. Y. L. Chen and C. L. Tien, A numerical study of two-dimensional natural convection in square open cavities. *Numer. Heat Transfer* **8**, 65–81 (1985).
79. J. A. C. Humphrey, F. S. Sherman, and W. M. To, "Numerical Simulation of Buoyant Turbulent Flow," Rep. FM-84-6. Dep. Mech. Eng., University of California, Berkeley, 1984.
80. R. F. Boehm, Review of thermal loss evaluations of solar central receivers," **SAND85–8019,** Sandia National Laboratory, Livermore, CA (1985): *J. Sol. Energy Eng.* (to be published).
81. R. Anderson, "Heat and Mass Transfer in Falling Film Receivers," SERI/PR-252-2822. Sol. Energy Res. Inst., Golden, Colorado, 1985.
82. R. T. Taussig, Aerowindows for Central solar receivers. *Proc. ASME Winter Annual Meeting* (1984).
83. J. A. C. Humphrey and E. W. Jacobs, Free-forced laminar flow convective heat transfer from a square cavity in a channel with variable junction. *Int. J. Heat Mass Transfer* **24**, 1584–1547 (1981).
84. A. R. Saydah, A. A. Koenig, R. H. Lambert, and D. A. Kugath, Final report on test of STEP, Shenandoah parabolic dish solar collector quadrant facility. **SAND82–7153,** Sandia National Laboratory, Albuquerque, NM (1983).
85. D. A. Kugath, G. Drenker, and A. A. Koenig, Design and development of a paraboloidal dish solar collector for intermediate temperature service. *Proc. ISES Silver Jubilee Congr.,* Vol. 1, p. 449–453 (1979).
86. A. A. Koenig and M. Marvin, "Convection Heat Loss Sensitivity in Open Cavity Solar Receivers," Final Rep. DOE Contract No. EG77-C-04-3985. Department of Energy, Oak Ridge, Tennessee, 1981.
87. J. A. Harris and T. G. Lenz, Thermal performance of solar concentrator/cavity receiver systems. *Sol. Energy* **34**, 135–142 (1985).
88. E. F. C. Somerscales and M. Kassemi, Electrochemical mass transfer studies in open cavities. *J. Appl. Electrochem.* **15**, 405–413 (1985).
89. J. D. Balcomb, R. W. Jones, R. D. McFarland, and W. O. Wray, "Passive Solar Heating Analysis: A Design Manual." ASHRAE, Atlanta, Georgia, 1984.
90. W. Jones and D. McFarland, "The Sunspace Primer: A Guide to Passive Solar Heating." Van Nostrand-Reinhold, Princeton, New Jersey, 1985.

91. A. E. Gill, The boundary-layer regime for convection in a rectangular cavity. *J. Fluid Mech.* **26**, 515–536 (1966).
92. A. Bejan, On the boundary layer region in a vertical enclosure filled with a porous medium. *Lett. Heat Mass Transfer* **6**, 93 (1979).
93. S. A. Korpela, Y. Lee, and J. E. Drummond, Heat transfer through a double-pane window. *J. Heat Transfer* **104**, 539–544 (1982).
94. A. Bejan, A synthesis of analytical results for natural convection heat transfer across rectangular enclosures. *Int. J. Heat Mass Transfer* **23**, 723–726 (1980).
95. R. D. Flack, T. T. Konopnicki, and J. H. Rooke, The measurement of natural convective heat transfer in triangular enclosures. *J. Heat Transfer* **101**, 648–654 (1979).
96. R. D. Flack, The experimental measurement of natural convection heat transfer in triangular enclosures heated or cooled from below. *J. Heat Transfer* **102**, 770–772 (1980).
97. D. Poulikakos and A. Bejan, Natural convection experiments in a triangular enclosure. *J. Heat Transfer* **105**, 652–655 (1983).
98. V. A. Akinsete and T. A. Coleman, Heat transfer by steady laminar free convection in triangular enclosures. *Int. J. Heat Mass Transfer* **25**, 991–998 (1982).
99. D. Poulikakos and A. Bejan, Fluid dynamics of an attic space. *J. Fluid Mech.* **131**, 251–269 (1983).
100. E. M. Sparrow and F. A. Azevedo, Lateral-edge effects on natural convection heat transfer from an isothermal vertical plate. *J. Heat Transfer* **107**, 977–979 (1985).
101. M. S. Bohn, A. T. Kirkpatrick, and D. A. Olsen, Experimental study of three-dimensional natural convection at high Rayleigh number. *J. Heat Transfer* **106**, 339–345 (1984).
102. M. S. Bohn and R. Anderson, "Temperature and Heat Flux Distributing in a Natural Convection Enclosure Flow," SERI/TR-252-2189. Sol. Energy Res. Inst., Golden, Colorado, 1984. Also *J. Heat Transfer* **108**, 471–475 (1986).
103. Y. Jaluria, Buoyancy-induced flow due to isolated thermal sources on a vertical surface. *J. Heat Transfer* **104**, 223–227 (1982).
104. K. Yamaguchi, Experimental Study of Natural Convection Heat Transfer through an Aperture in Passive Solar Heated Buildings, *Nat. Conf. Passive Solar, 9th, Columbus, Ohio,* 1984.
105. Olsen, D., Glicksman, L., and Yuan, X.-D., Natural convection modeling experiments of building interior spaces. *HTD* [Publ.] *(Am. Soc. Mech. Eng.)* **16/4** (1985). Also, personal communication, May 16, 1986.
106. S. W. Churchill and H. S. Chu, Correlating equations for laminar and turbulent-free convection from a vertical plate. *Int. J. Heat Mass Transfer* **18**, 1323–1329 (1975).
107. S. Ostrach and C. Raghaven, Effect of stabilizing thermal gradients on natural convection in rectangular enclosures. *J. Heat Transfer* **101**, 238–243 (1979).
108. B.-I. Fu and S. Ostrach, The effects of stabilizing thermal gradients on natural convection flows in a square enclosure. *HTD [Publ.] (Am. Soc. Mech. Eng.)* **16**, (1981).
109. G. S. Shiralkar and C. L. Tien, A numerical study of the effect of a vertical temperature difference imposed on a horizontal enclosure. *Numer. Heat Transfer* **5**, 185–197 (1982).
110. A. T. Kirkpatrick and M. S. Bohn, High Rayleigh number natural convection in an enclosure heated from below and from the sides. *ASME-AIChE Natl. Heat Transfer Conf.* (1983).
111. A. T. Kirkpatrick and M. Bohn, An experimental investigation of mixed cavity natural convection in the high Rayleigh number regime. To appear in *Int. J. Heat Mass Transfer* (1985).

112. H. Ozoe, A. Mouri, M. Hiramitsu, S. W. Churchill, and N. Lior, Numerical calculation of three-dimensional turbulent natural convection in a cubical enclosure using a two equation model. *HTD [Publ.] (Am. Soc. Mech. Eng.)* **32**, 25–32 (1984).
113. R. Anderson, E. M. Fisher, and M. Bohn, "Thermal Stratification in a Closed Cavity with Variable Heating of the Floor and One Vertical Wall," SERI/J-252-0146. Sol. Energy Res. Inst., Golden, Colorado, 1985.
114. R. Anderson, E. Fisher, and M. Bohn, "Thermal Stratification in Direct Gain Passive Heating Systems with Variable Heating of the Floor and One Vertical Wall," SERI/TP-252-2767. Sol. Energy Res. Inst., Golden, Colorado, 1985.
115. F. Bauman, A. Gadgil, R. Kammerud, E. Altmayer, and M. Nansteel, Convective heat transfer in buildings: Recent research results. *ASHRAE Trans.* **89**, Part 1A, 215–230 (1983).
116. E. F. Altmayer, A. J. Gadgil, F. S. Bauman, and R. L. Kammerud Correlations for convective heat transfer from room surfaces. *ASHRAE Trans.* **89**, Part 2A, 61–77 (1983).
117. R. Anderson and G. Lauriat, The horizontal natural convection boundary layer regime in a closed cavity. SERI/TP-252-2830, Sol. Energy Res. Inst., Golden, Colorado (1985). Also in *Proc. Int. Conf. Heat Transfer* **4**, 1453–1458 (1986).
117a. Y. Jaluria and B. Gebhart, On transition mechanisms in vertical natural convection flow. *J. Fluid Mech.* **66**, 309–339 (1974).
118. M. W. Nansteel and R. Greif, An investigation of natural convection in enclosures with two- and three-dimensional partitions. *Int. J. Heat Mass Transfer* **27**, 561–571 (1984).
119. S. M. ElSherbiny, K. G. T. Hollands, and G. D. Raithby, Free convection across inclined air layers with one surface V-corrugated. *J. Heat Transfer* **100**, 410–415 (1980).
120. M. Al-Arabi and M. M. El-Refaee, Heat transfer by natural convection from corrugated plates to air. *Int. J. Heat Mass Transfer* **21**, 357–359 (1978).
121. S. Shakerin, M. Bohn, and R. I. Loehrke, Convection in an enclosure with discrete roughness elements on a vertical heated wall. *Heat Transfer, Proc. Int. Heat Transfer Conf., 8th, 1986* (1986).
122. J. E. Emswiler, The neutral zone in ventilation. *Trans. Am. Soc. Heat Vent. Eng.* **32**, 59–74 (1926).
123. W. G. Brown and K. R. Solvason, Natural convection through rectangular openings in partitions 1. *Int. J. Heat Mass Transfer* **5**, 859–868 (1962).
124. A. Graf, Theoretische Betrachtung über den Luftaustausch zwischen zwei Räumen. *Schweiz. Bl. Heiz. Lueft.* **31**, 22–25 (1964).
125. J. D. Balcomb and K. Yamaguchi, Heat distribution by natural convection. *Natl. Passive Sol. Conf., 8th, 1983* (1983); see also J. D. Balcomb, "Heat Distribution by Natural Convection: Interim Report." Los Alamos Natl. Lab., New Mexico, 1985.
126. A. Kirkpatrick, D. Hill, and P. Burns, Interzonal natural and forced convection heat transfer in a passive solar building. *J. Sol. Energy Eng.* (to be published).
127. J. H. Lienhard, V and J. H. Lienhard, IV, Velocity coefficients for free jets from sharp-edged orifices. *J. Fluid Eng.* **106**, 13–17 (1984).
128. H. E. Janikowski, J. Ward, and S. D. Probert, Free convection in vertical, air-filled rectangular counties fitted with baffles. *Heat Transfer, Int. Heat Transfer Conf., 6th, 1978* (1978).
129. A. Bejan and A. N. Rossie, Natural convection in horizontal duct connecting two fluid reservoirs. *J. Heat Transfer* **103**, 108–113 (1981).
130. M. W. Nansteel and R. Greif, Natural convection in undivided and partially divided rectangular enclosures. *J. Heat Transfer* **103**, 623–629 (1981).

131. S. M. Bajorek and J. R. Lloyd, Experimental investigation of natural convection in partitioned enclosures. *J. Heat Transfer* **104**, 527–532 (1982).
132. L. C. Chang, J. R. Lloyd, and K. T. Yang, A finite difference study of natural convection in complex enclosures. *Heat Transfer, Proc. Int. Heat Transfer Conf., 7th, 1982* (1983).
133. N. N. Lin and A. Bejan, Natural convection in a partially divided enclosure. *Int. J. Heat Mass Transfer* **26**, 1867–1878 (1983).
134. A. Bejan, "Convection Heat Transfer," p. 116. Wiley, New York (1984).
135. D. Scott, R. Anderson, and R. Figliola, "Blockage of Natural Convection Boundary Layer Flow in a Multizone Enclosure," SERI/TP252-2847. Sol. Energy Res. Inst., Golden, Colorado, 1985. Also ASME paper **86-HT-390.**
136. W. Elenbaas, Heat dissipation of parallel plates by free convection. *Physica (Amsterdam)* **9**, 1 (1942).
137. S. Ostrach, "Laminar Natural Convection Flow and Heat Transfer of Fluids with and without Heat Sources in Channels with Constant Wall Temperature," NACA TN2863. (Nat. Advis. Comm. Aeronaut., Washington, D.C., 1952).
138. H. Akbari and T. R. Borgers, Free convective laminar flow within the Trombe wall channel. *Sol. Energy* **22**, 165–174 (1979).
139. T. Allen and J. Hayes, Measured performance of thermosiphon air panels. *ASES Natl. Passive Conf. Proc., 10th*, pp. 442–447 (1985).
140. E. Tasdemiroglu, F. Ramos Berjano, and D. Tinaut, The performance results of Trombe-wall passive systems under Aegean Sea climatic conditions. *Sol. Energy* **30**, 181–189 (1985),
141. S. J. Ormiston, G. D. Raithby, and K. G. T. Hollands, Numerical predictions of natural convection in a Trombe wall system. *Am. Soc. Mech. Eng. [Pap.]* **85-HT-36** (1985).
142. J. R. Bodoia and J. F. Osterle, The development of free convection between heated vertical plates. *J. Heat Transfer* **84**, 40–44 (1962).
143. O. Miyatake and T. Fujii, Free convection heat transfer between vertical parallel plates — One plate isothermally heated and the other thermally insulated. *Heat Transfer—Jpn. Res.* **1**, 30–38 (1972).
144. O. Miyatake, T. Fujii, M. Fujii, and H. Tanaka, Natural convection heat transfer between vertical parallel plates—One plate with a uniform heat flux and the other thermally insulated. *Heat Transfer—Jpn. Res.* **2**, 25–33 (1973).
145. W. Aung, L. S. Fletcher, and V. Sernas, Developing laminar free convection between vertical flat plate with asymmetric heating. *Int. J. Heat Mass Transfer* **15**, 2293–2308 (1972).
146. C. F. Kettleborough, Transient laminar free convection between heated vertical plates including entrance effects. *Int. J. Heat Mass Transfer* **15**, 883–896 (1972).
147. E. M. Sparrow, G. M. Chrysler, and L. F. Azevedo, Observed flow reversals and measured-predicted Nusselt numbers for natural convection in a one-sided heated vertical channel. *J. Heat Transfer* **106**, 325–332 (1984).
148. E. M. Sparrow, S. Shah, and C. Prakash, Natural convection in a vertical channel. I. Interacting convection and radiation. II. The vertical plate with and without shrouding, *Numer. Heat Transfer* **3**, 297–314 (1980).
149. E. M. Sparrow and L. F. A. Azevedo, Vertical channel natural convection spanning between the fully-developed limit and the single-plate boundary-layer limit. *Int. J. Heat Mass Transfer* **28**, 1847–1857 (1985).